TRIANGULAR TRUSSES FABRICATED FROM RECTANGULAR HOLLOW SECTIONS

by

Dominique Bauer

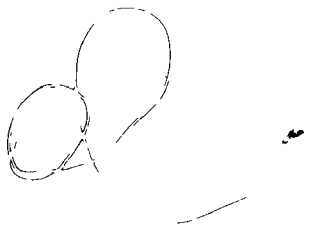

A Thesis submitted to the Faculty of Graduate Studies and Research in partial fulfillment of the requirements for the Degree of Doctor of Philosophy

Department of Civil Engineering
and Applied Mechanics

McGill University

Montreal, Quebec, Canada

February 1987

TRIANGULAR TRUSSES FABRICATED FROM RECTANGULAR HOLLOW SECTIONS

by
Dominique Bauer

Department of Civil Engineering
and Applied Mechanics

McGill University
Montreal, Canada

Ph.D. Thesis
February 1987

ABSTRACT

This thesis deals with the behaviour and design of triangular trusses fabricated from Hollow Structural Sections (HSS), with two Warren-type web planes and a single tension chord. Experimental programs are described in which triangular truss segments and simplified joints were tested in order to investigate the behaviour of compression web members and tension-chord welded joints. The mechanics of joint deformations are analysed in relation to the yield line theory, and simple models are shown to give a good prediction of the joint stiffnesses and strengths. Complex yield line models are investigated, but are at best only slightly superior to the simple models Recommendations are established covering the design of tension and compression chord joints, as well as chord and web members. The design of a 22 m span triangular truss is outlined.

POUTRES À TREILLIS TRIANGULAIRES FABRIQUÉES DE PROFILS CREUX RECTANGULAIRES

par
Dominique Bauer

Département de génie civil
et mécanique appliquée

Université McGill
Montréal, Canada

Thèse de Doctorat
Février 1987

RÉSUMÉ

Cette thèse traite du comportement et de la conception de poutres à treillis triangulaires fabriquées de profils creux rectangulaires (PCR), avec deux plans de barres de treillis à disposition Warren et une seule membrure tendue. Des études expérimentales sont décrites dans lesquelles des segments de poutres triangulaires et des joints simplifiés ont été mis à l'essai afin d'étudier le comportement des barres de treillis comprimées et des joints soudés sur la membrure en tension. Les mécanismes de déformation des joints sont analysés en relation avec la théorie des lignes de rupture, et on démontre que des modèles simples donnent une bonne prédiction de la rigidité et de la résistance des joints. Des modèles complexes sont étudiés, mais sont peu ou pas supérieurs aux modèles simples. Des recommendations pour la conception sont établies couvrant le dimensionnement des joints aux membrures tendues et comprimées, ainsi que des membrures et des barres de treillis. Le calcul d'une poutre à treillis d'une porté de 22 m est ebauché.

Je dédie cette thèse à ma famille qui m'a encouragé pendant ces longues études de doctorat Je fais hommage de mon travail en particulier à ma mère Geneviève que j'aime très fort et à mon père Max, récessement décédé, qui restera toujours dans mon coeur et mon souvenir une source d'inspiration et de courage J'adresse aussi cette dédicace spécialement à ma compagne Micheline qui m'a supporté avec amour et avec force, et qui a su partager aussi bien les durs moments que les joies de mon travail.

PREFACE

This thesis is concerned with the behaviour of triangular trusses fabricated from Rectangular Hollow Sections (RHS). The trusses considered have welded gap joints and are submitted to static loading.

The work reported herein is part of a research program which included tests and analytical studies of RHS triangular trusses. The research program is the only one known to the author which is concerned with such trusses. The research program was initiated by CIDECT (the International Committee for the Development and the Study of Tubular Construction), and was carried out at McGill University initially under the supervision of Professors P. J. Harris and R. G. Redwood, and subsequently by Professor R. G. Redwood.

Numerous studies on planar trusses using RHS have been made in the past two decades and empirically based design recommendations for these trusses have been published. These provided the only information available as a basis for the design of triangular trusses. The present research program was undertaken to study the aspects of behaviour and design particular to triangular trusses. The applicability of planar truss recommendations to the triangular trusses was also studied.

Results of seven truss segment tests are summarized herein which were carried out by M. Glebe and the author during their Master of Engineering degree programs. The tests of twenty-four simplified joints, which are described in detail herein, were part of the author's Ph.D. work. The theoretical analyses and the design recommendations proposed in this thesis are also based on original work done by the author.

In general, the problems associated with the triangular trusses are more complicated than with planar trusses. For example the geometry,

including joint eccentricities and load components, is 3-dimensional; the chord face failure involves web members connected at an angle and off-centered on the chord face; the gap failure involves stress distributions in chord walls inclined at 45° to the plane of loading; web member buckling involves buckling in and out of the plane of the webs These aspects are treated herein.

The research work described in this thesis provides a basis for the design of RHS triangular trusses. This includes analytical methods and recommendations for the design of the tension- and compression-chord joints in relation with chord face and gap strengths, and for the design of chord and web members.

This thesis is presented in a traditional format in an attempt to constitute a coherent document. It should be noted, however, that parts of the thesis have been adapted from two publications (Redwood and Bauer 1983, Bauer and Redwood 1984). While Chapter 5 and Appendix C treat new material, other chapters are based, to a greater or lesser extent, on the two references. The material used from these references has been rearranged and revised where necessary in the light of recent results. It is emphasized that the two publications were based on the author's Ph.D. work, and that his contribution in the two publications was major.

During his Ph D. work, the author has participated in the supervision of several students who worked on projects related to the research program on triangular trusses. These projects are referred to in this thesis, and are described in detail in the undergraduate Technical Papers and Project Reports of Santagata (1982), Skold (1986), Minicucci and Zafrani (1986), and the Master of Engineering Project Report of Kawczak (1983).

ACKNOWLEDGEMENTS

Acknowledgement is made to the following for support of this research program: CIDECT (the International Committee for the Development and Study of Tubular Construction) under Projects 5W/1 and 5W/2, The Steel Company of Canada Inc. (Stelco), The Natural Sciences and Engineering Research Council of Canada (NSERC) under Grant A-3366, and McGill University.

Special thanks are due to Professor R. G. Redwood for supervising the author's research project. The efficient guidance, advice and encouragements of Professor R. G. Redwood are gratefully acknowledged.

The author wishes to thank the following people: Messrs. Przykorski, Cockayne and Sheppard of the Jamieson Structures Laboratory for their help during the experiments; Mr. Renaud Cossette, Ing., for his suggestions for the design recommendations; Mr. Martin Glebe, for testing some of the truss segments.

Acknowledgement is also made to: Lord and Co. Ltd, who built the joint specimens; I.C.T. Tools Ltd, who built the base supports for the joint tests.

TABLE OF CONTENTS

LIST OF FIGURES

LIST OF TABLES

NOTATION

a	distance from corner of chord to side of web member
A	cross-section area of member
A, B	constants - yield line mechanisms with fans
b	width of RHS member
c	distance from upper corner of chord to side of web member
c.w.m.	compression web member
C	compressive load
C_r	web member compressive resistance
COV	coefficient of variation
d	overall depth of triangular truss or dimension - yield line mechanisms of chord face
D	energy dissipated by yield lines
e	eccentricity of joint to tension chord or dimension - yield line mechanisms with normal stresses in chord corners
e'	vertical eccentricity in joint to compression chord
e"	horizontal eccentricity in joint to compression chord
E	work done by loads
f	dimension - yield line mechanisms with normal stresses in chord corners or dimension - yield line mechanisms with inclined end lines
F_y, F_u	material yield stress, ultimate stress
g	gap dimension or dimension - yield line mechanisms with normal stresses in chord corners
h	depth of RHS member
HSS	Hollow Structural Section

K	effective length factor of a compression member
K_1 to K_5	constants - yield line mechanisms with normal stresses in chord corners
K	constant - yield line mechanisms with normal stresses in chord corners
K, L, M, N	constants - yield line analysis of DK joints
l, l_c, l_w (l, l_c, l_w)	length of member, chord member, web member
L_0	length of chord member
L_w	length measured from center of web member end ball to center of chord member
L_w'	length measured from center of web member end ball to face of chord member
m_p	plastic moment per unit width of chord wall
m_p'	plastic moment per unit width, reduced due to normal stresses
M	bending moment
M_t	twisting moment
n, n_p	normal stress, squash stress (also normal load per unit length of chord wall)
N	axial force
p	projection of web member parallel to chord
p, q, r	constants - yield line analysis of DK joints or constants - yield line mechanisms with normal stresses in chord corners
P	applied load
r	radius of gyration
R_{out}	outside radius of chord corners
RHS	Rectangular Hollow Section
s	web height of triangular truss, measured in web plane
S	fillet weld leg size
S_1 to S_6	constants - yield line mechanisms with normal stresses in chord corners

t	thickness of HSS member
T	tension force
T_1, T_2	tension force in chord on side of compression, tension web members
V	shearing force
w	width of triangular truss
W	external load applied to chord
x	dimension - yield line mechanisms of chord face or dimension - yield line mechanisms with normal stresses in chord corners
X	component of web member load applied to chord wall
Y	component of web member load in direction normal to chord wall
z	dimension - yield line mechanisms with normal stresses in chord corners
Z	component of web member load applied to chord wall
Z_x, Z_y, Z_z	plastic moduli about appropriate axes
α	angle between web planes in triangular truss or load factor used in limit state design
β	ratio of web member width to chord width, defined in text for different applications
γ	ratio of gap dimension to chord width
δ	ratio of dimension d to chord width - yield line mechanisms of chord face or virtual displacement
Δ	virtual displacement
η	ratio of web member size to chord width or angle between chord and plane containing two compression (or tension) web members
θ	angle between web member and chord or virtual rotation of yield line

λ	distance of web member centreline from corner of chord wall, expressed as unit fraction of chord wall width
Λ	ratio of force component normal to chord face of tension web member to that of compression web member
ξ	distance from chord corner to side of web member, expressed as fraction of chord wall width
ρ	normal load in chord corners, expressed as ratio of total load on the chord face
τ	shear stress
$\bar{\tau}$	ratio of shear stress to yield stress in shear
ϕ	performance factor
ψ	distance of web member centreline from corner of chord wall, expressed as fraction of chord wall width
Ω	dimension (angle) - yield line mechanisms with inclined end lines

Subscripts

cr	critical buckling load
f	factored load
g	refers to gap
i	member identification: 0 = chord 1 = compression web member 2 = tension web member 3 = tie member
r	resistance of member
s	service load
y	yield load
u	ultimate load
max	maximum load
1, 2	Side 1, Side 2. Refers to outside and upper corners, respectively, of tension chord cross-section

Superscripts

'(prime)	joint dimension adjusted for weld size and curvature at corners of chord
¯(bar)	contact dimension of web member on chord face

Types of Joints

DK	double Warren
DN	double Pratt
DT	double Vierendeel
K	planar Warren
N	planar Pratt
T	planar Vierendeel

CHAPTER 1 INTRODUCTION

Triangular sectioned trusses fabricated from hollow structural sections have been used in a number of applications both in Canada and Europe. The usual form adopted consists of a single tension chord and two compression chords, with the two web planes separated by an angle in the range 45° to 90°. These trusses have considerable visual appeal, particularly when a Warren arrangement of members is used, and in many cases appearance has been a significant factor in their selection. Their inherent lateral and torsional stiffness results in minimal lateral bracing, further enhancing their appearance (Fig. 1.1).

Some examples of triangular trusses with rectangular HSS chords are as follows:

- Oak Bay Recreation Centre, B.C. 27 m long trusses span a curling ring and swimming pool. Compression chords are HSS 127.0 x 76.2 x 9.53 and the tension chords are HSS 127.0 x 127.0 x 11.1. Webs are round HSS 60.3 mm diameter. Over the ice arena spans are 32.3 m and the compression and tension chords are respectively HSS 152.4 x 101.6 x 11.1, HSS 152.4 x 152.4 x 11.1 and round HSS of 88.9 mm and 73.0 mm diameter.
- Sheridan College of Applied Arts and Technology, Oakville, Ontario. Exposed triangular trusses and a vivid colour scheme provide considerable visual impact in this building. The trusses span 9 m and tension and compression chords are HSS 101.6 x 101.6 and web members HSS 50.8 x 50.8.
- Military Base - St. Jean d'Iberville, Quebec. 33.75 m long triangular trusses span a gymnasium and comprise compression chords of HSS 152.4 x 101.6 varying from 6.35 mm to 4.78 mm wall thickness, and tension chords HSS 152.4 x 152.4 with wall thickness either 6.35 mm or 9.53 mm. Web members

vary from HSS 38.1 x 38.1 x 3.81 to HSS 76.2 x 76.2 x 3.81.

Trusses of this type have a number of features which differ from those of planar HSS trusses. Of particular importance are the joints to the tension chord, where typically four web members meet. The configuration of compression chord joints and the end fixity of web members will also be quite different in a triangular truss.

A research project was undertaken to investigate the behaviour of triangular trusses. The first phase comprised the testing of a number of segments of triangular trusses, with attention being directed primarily at the behaviour of the tension chord joint. While detailed results of these tests were presented by Bauer (1981), a summary of the main features is given herein (Chapter 2) for completeness. The second phase comprised the testing of simplified triangular truss tension chord joints, as well as the development of general recommendations for the analysis and design of triangular trusses made of rectangular HSS, and is the principal subject of this thesis. A detailed description of the second test series is given herein (Chapter 3). Results from both tests series are then discussed (Chapter 4), and theoretical analyses of tension chord joints are presented (Chapter 5). From the two test series and from the theoretical analyses, information relevant to design is established (Chapter 6). Using these tentative design recommendations examples of some aspects of the design of a 22 m span triangular truss are given (Chapter 7).

The type of tension chord joint considered in this research program comprised a square HSS chord with walls inclined at angles of 45° to horizontal and vertical planes, and web members attached to the two uppermost walls, as shown in Fig. 1.2a. This configuration is appropriate when the included angle between web planes is in the range of about 50° to 90°. For lower values of this angle, and providing the chord wall is sufficiently

wide, all web members can be attached to one wall of the chord as shown in Fig. 1.2b. This type of joint has similarities to HSS planar truss joints and is not considered herein.

Because gap joints cause more severe loading of the chord walls than overlap joints, and because of the fabrication advantages of the former, the emphasis in the research programs was on the behaviour of gap joints. Similar emphasis is given to the analysis and design considerations treated herein.

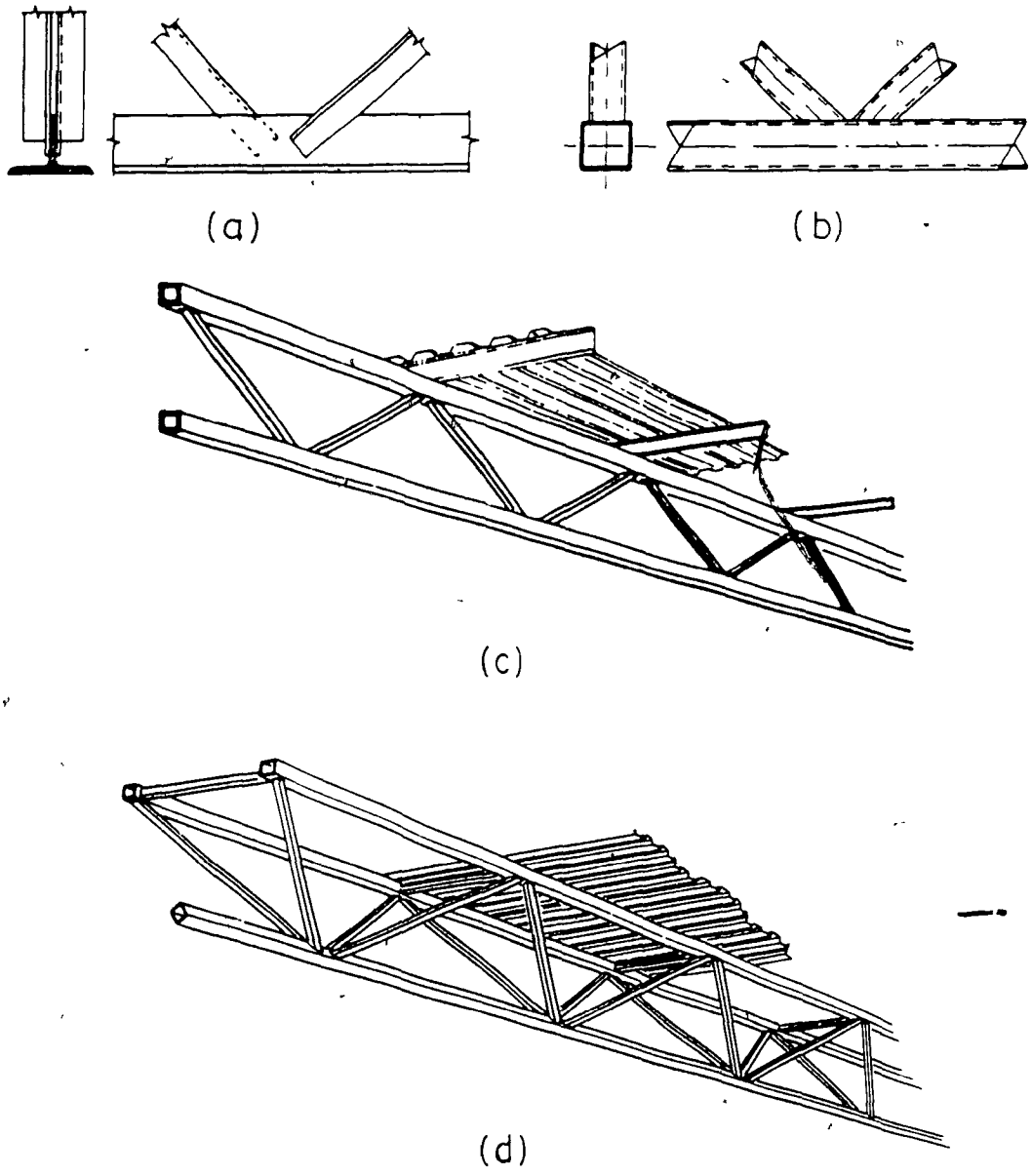

Fig. 1.1 Truss details and HSS trusses (a) Open section detail (b) Hollow section detail. (c) Plane truss. (d) Triangular truss

[(a), (b) and (d) adapted from Stelco 1981]

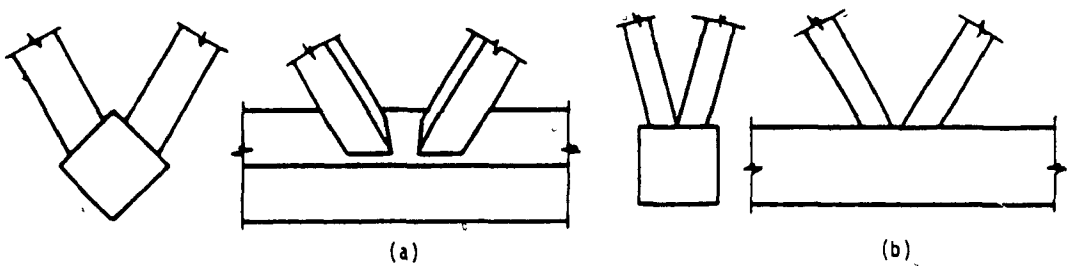

Fig. 1.2 Triangular truss tension chord connections.

CHAPTER 2 SUMMARY OF TRUSS TESTS

This chapter presents a brief summary of the truss tests which were carried out as the first part of the project Test results will be discussed further and referred to in the following chapters, and are included herein for completeness A full description and discussion of the tests is given by Bauer (1981)

2 1 SPECIMENS AND TEST DETAILS

Tests were carried out on seven short lengths of triangular truss, each representing one panel of a Warren type truss A truss segment of this type is shown schematically in Fig 2 1 in the inversed position in which the specimens were tested This truss panel was designed primarily to investigate the joint behaviour and at the same time study the behaviour of the web members All tension chords were HSS - 127 0 x 127 0 sections with wall thickness of either 4 78 mm or 7 95 mm. The principal variables, which are summarized in Table 2.1, were the width ratio, the angle between web planes, α, the gap dimension g, and the chord wall width-to-thickness ratio, b_0/t_0.

The truss segments were cantilevered from a massive rig which was bolted to the laboratory reaction floor Loads were applied vertically at the free end of the truss, as shown schematically in Fig 2 1 and illustrated in Fig. 2.2 For six trusses, this was the only load, and these therefore represent the end panel of a simply supported truss One truss, No 3, had an additional load consisting of uniform tension in the tension chord, applied by means of a second rig placed at the loaded end of the specimen

Instrumentation consisted of deflection and strain gauges. Overall truss deflections and lateral displacements within the length of compression web

members were recorded, and strains were measured at a number of cross sections of the members connected to the joint of interest Sufficient strains were recorded at each of these cross sections to enable the stress resultants to be determined Resultant forces (axial force and two moments) in the inelastic range were calculated on the assumptions of an elastic-perfectly-plastic material. Full details of the test specimens, instrumentation and loading are given elsewhere (Bauer 1981, Bauer et al 1983, Glebe 1980, Redwood and Harris 1981).

2.2 TEST OBSERVATIONS

In the elastic range of loading the member forces and truss deflections were compared with results of elastic analyses of the truss. Three analytical models were used the first treated the truss as a space truss (pinned joints), the second treated it as a space frame (rigid joints) with no eccentricities in the joints, and the third modelled it as a space frame with short fictitious members introduced to simulate joint eccentricities Predicted deflections and member axial forces were similar for all models, and agreed well with measures values. On the other hand, moments obtained from the latter two models differed significantly, and both underestimated the measured moments

The observed modes of failure and maximum test loads are summarized in Table 2.2 It can be seen that significant joint deformation occurred in four cases (Tests 1, 3, 4 and 6) and that web member buckling was associated with the attainment of the maximum load on the truss in three of these four cases In the fourth (Test 4), bending of the web members took place progressively during the test.

The joint region of this truss, No 4, is shown in Fig. 2.3, and in

Fig 2.4 the deformed chord cross section at the same joint is shown at the mid length of the compression web member connection to the chord wall Rotation of the chord walls, resulting in bending of the compression web members outward from the truss centreline, can be clearly seen This rotation arises both from the fact that one "side" wall supporting the deforming chord wall is stiffer than the other because of the second web member welds, and from geometrical considerations which lead to off-centre placement of the web members in order to minimize the offset between web member and chord axes

In the remaining three tests, small deformations only were observed at the joints (1 to 2 mm out-of-plane deflections of chord walls) Of these, in one case (Test 7) the truss resistance exceeded the safe load capacity of the rig, and the failure mode could not therefore be determined In the other two cases (Test 2 and 5) web member buckling occurred, although in Test 5 this took place after full yield of the cross sections of the tension web members

The choice of truss parameters, summarized in Table 2 1, allows a number of comparisons between truss pairs in which only one major parameter varied Minor differences in the values of the parameters existed because of section dimensions and material properties being different from their nominal values, and because gap dimensions varied as a result of fabrication procedures. However, these differences are known and their influence was minor, unless noted otherwise in the following.

The effect of a width ratio change from 0 4 to 0 6 was to increase the maximum strength in all three comparative cases The maximum loads with β = 0.6 compared with 0.4 were in the ratios 2 29 to 1 (Tests 3 and 1), >1.53 to 1 (Tests 7 and 5) and 1.13 to 1 (Tests 4 and 6). The lower value of this ratio for the latter pair, which were 60° trusses is probably due to the fact that the web member buckling resistances in Truss 4 were only 8% greater

than those in Truss 6, and web member buckling together with joint deformation occurred in both cases The axial loading on the chord of Truss 3, which unlike that on Truss 1 consisted of a high tensile load in addition to the tension resulting from the applied shearing load, did not produce any serious weakening effect on the joint, when compared with the other two truss pairs.

The effect of change of angle between web planes is partially obscured by buckling of web members Because of the different geometries with different α values, the comparison between strengths of the trusses is made on the basis of the maximum normal load on the chord wall. For 60° and 90° trusses respectively, these ultimate normal loads were in the ratios 1 61 to 1 (Tests 6 and 1) and 0.80 to 1 (Tests 4 and 3). These quite different results are related to the different web member buckling resistances which were in the ratios 2 to 1 (Tests 6 and 1) and 0.87 to 1 (Tests 4 and 3). It appears therefore that the web member buckling and its interaction with joint deformation, which is amplified by the off-centre attachment in the 60° trusses, is more dominant than differences in joint strength resulting from the change in angle between web planes.

Significantly greater strengths were exhibited in the trusses with thick chord walls than in those with thin walls. A decrease in b_0/t_0 from 26.6 to 16 resulted in ultimate strengths increasing in the ratios 1 to 2.29 (Tests 1 and 5) and 1 to >1 53 (Tests 3 and 7). Similarly the reduction of gap dimensions from $g/b_0 = 0.28$ to zero (Tests 1 and 2 respectively) corresponded to ultimate strengths increasing in the ratio 1 to 1.24.

Stronger joints were in most cases also stiffer. Joint deflections, measured in the direction and along the axis of the compression web members, are shown in Fig. 2.5.

In summary, it can be seen that a number of the test observations of the triangular truss joint behaviour show the same features as those exhibited by

planar truss joints. Thus the trends resulting from variations of β, b_0/t_0, g/b_0 are similar The magnitude of these effects will be compared in Chapter 4. Web member buckling occurred in many of the tests, and in most cases was associated with significant joint deformations

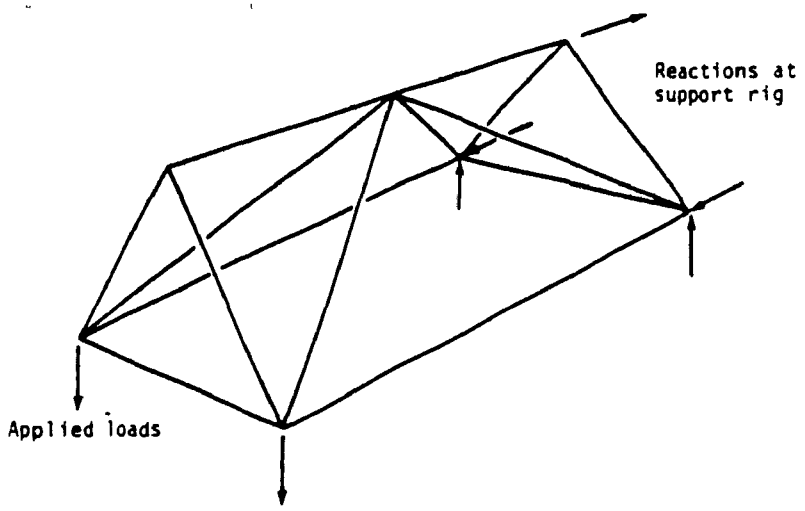

Fig. 2.1 Truss segment test arrangement.

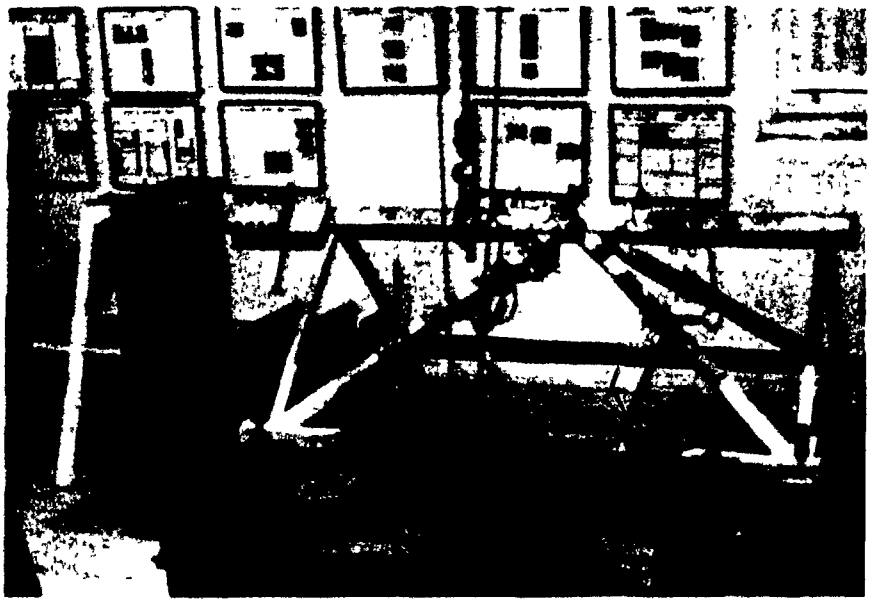

Fig. 2.2 Truss segment specimen in loading rig.

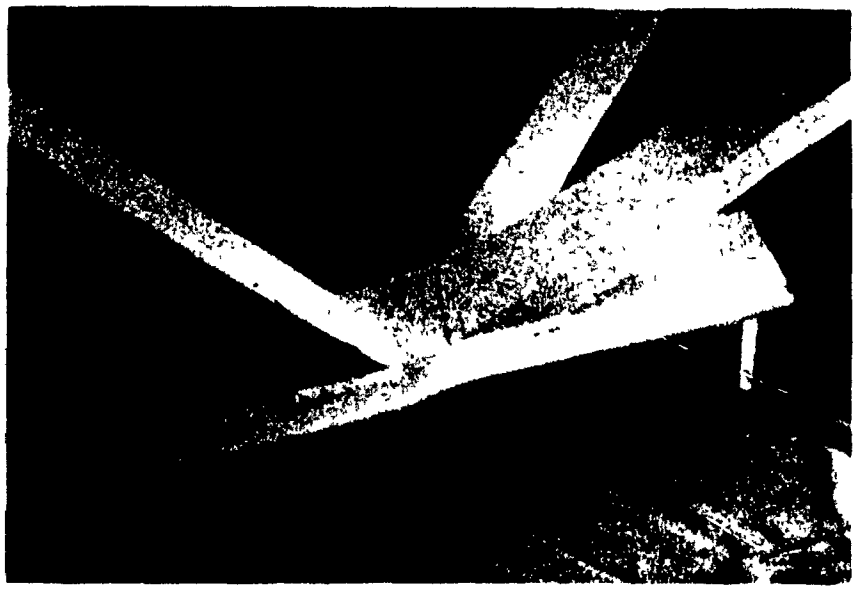

Fig. 2.3 Tension chord joint deformation. Truss 4

Fig. 2.4 Cross-section distortion. Truss 4.

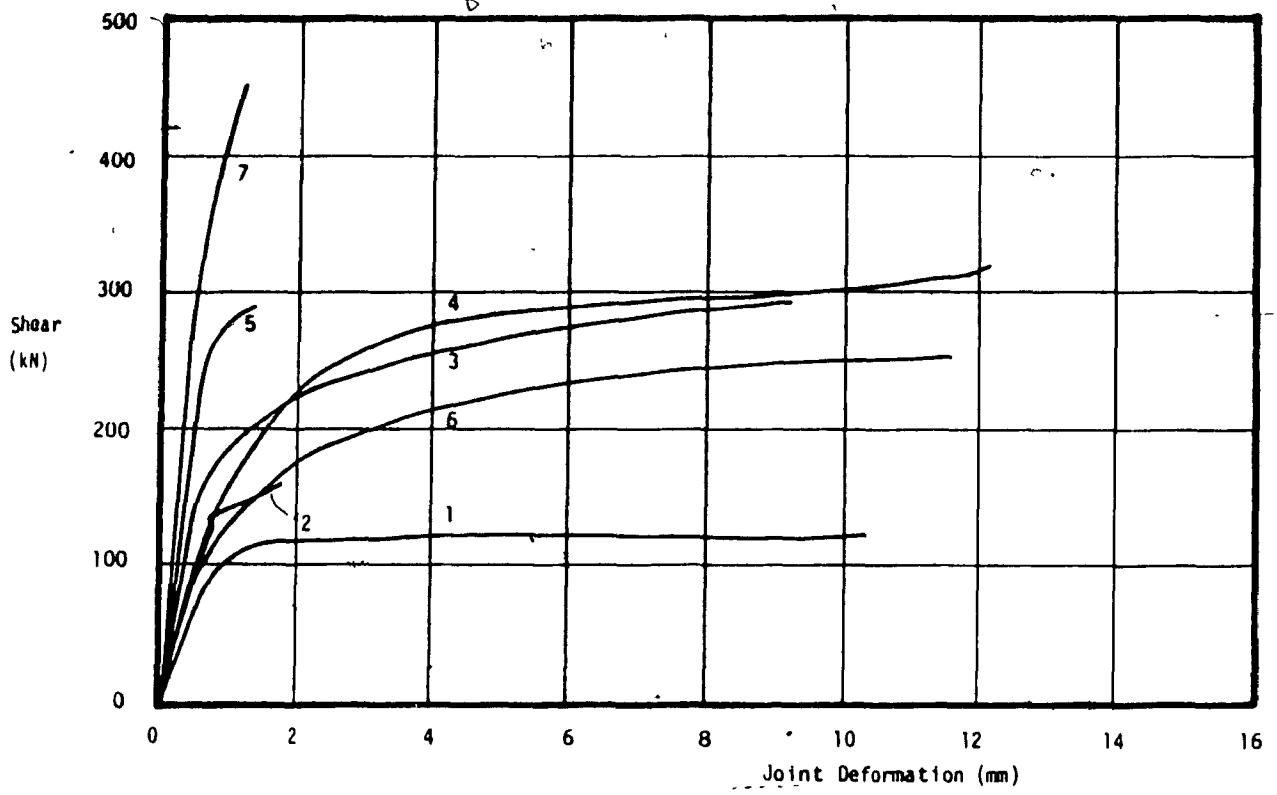

Fig. 2.5 Tension chord wall deflections on axis of web compression members. Truss tests.

Table 2.1 Principal joint parameters. Truss tests

Truss No	α (deg)	θ (deg)	β	$\frac{b_0}{t_0}$	$\frac{g}{b_0}$	e (mm)	ψ
DK-1	90	45	0 4	25 6	0 28	-7	0 50
DK-2	90	44	0.4	25 4	-	-22	0 50
DK-3	90	45	0 6	25 6	0 26	5	0 50
DK-4	60	39	0.62	25 2	0 47	18	0 60
DK-5	90	45	0 4	15 8	0 36	-3	0 50
DK-6	60	38	0 41	26 0	0 45	-3	0 62
DK-7	90	45	0 6	16·0	0 45	15	0 50

Notes. Values are based on measured dimensions

$$\beta = \frac{(b_1+b_2)}{2b_0} \sec(45^\circ-\alpha/2)$$

All chord members were nominall HSS - 127 0 x 127 0

Table 2 2 Summary of failure modes and maximum loads Truss tests

Failure Mode	Maximum Shear Force on Truss (kN)
Test 1 Significant chord wall deformation on side 1 The compression web member on side 1 buckled	125 9
Test 2-a Little joint deformation Local and overall buckling of the reinforced compression web member on side 2 Unconnected walls remained plane	155 6
Test 3 The chord wall on side 2 deformed significantly Unconnected walls deflected out of plane at joint Local and overall buckling of the compression web member on side 2	288 6
Test 4 Significant chord wall deformation on both sides Unconnected walls severely deflected out of plane at joint	281 5
Test 5 Little joint deformation The compression web member on side 1 buckled Tension web members yielded	288 6
Test 6 Significant chord wall deformation Both compression web members buckled	249 4
Test 7 Little joint deformation Test rig capacity reached prior to significant distress of test specimen	>441 8

CHAPTER 3 JOINT TESTS

3.1 INTRODUCTION

Following the tests of the seven segments of Double-K triangular trusses described in Chapter 2, further tests of 24 Double T joints (hereafter called DT joints), modeling in a simplified manner the Double-K joints (hereafter called DK joints), were carried out and are described in this chapter The first investigation was concerned with the behaviour of the joint in the tension chord of a DK triangular truss at which four web members are usually connected to the chord. In the second investigation, the configuration was simplified to consider the two compression web members only, and these were oriented normal to the chord. The instability of the compression web members was also considered.

3.1.1 Objectives

The following were the specific objectives of the second investigation:

(i) To determine, in as simple a manner as possible, the significance of the angle between web planes on both the joint strength, and the web member buckling strength. Angles between web planes varying from 90° to 30° were considered.

(ii) To analyse the simplified DT joint models described below.

(iii) To determine experimentally, using the same simplified DT joints, the significance, if any, of interaction between joint deformation and web member instability.

3.1.2 The DT Joint Model

A DT joint specimen is shown in the test rig in Fig. 3.1. The advantages of this experimental approach were the low cost of the test specimens, the

simple test arrangement, and the ability to choose web member lengths so as either to avoid buckling or to study it. By changing the angle between web members, some of the main effects of variations of this parameter could be determined. These effects included the deformation of the joint under the compression web member, and the compression strength of the web member.

Typical tension chord cross-section deformation at the connection, as observed in the DK truss tests (Chapter 2), is illustrated in Fig. 3.2 for DK Truss no.4. This indicates that the primary deformation was associated with the compression web members and also that the chord wall rotation resulted in bending of the compression web members away from the axis of symmetry of the truss. These are the main features which were simulated by the simplified DT configuration

It is clear that such a simple arrangement could not simulate all the conditions in a DK truss joint, and indeed some additional factors were introduced by the test arrangement. Principal among these were the bending stresses in the tension chord introduced by the way in which the loads were applied to the chord. The effect of these is discussed in Chapter 4, §4.1.5.

3.1.3 Test Program

The following primary parameters were investigated:

(a) The angle between web planes, α.

(b) The ratio of web member width to chord member width, β

(c) The chord wall width to thickness ratio, b_0/t_0.

(d) The slenderness ratio of the web members, L_w/r.

The program of tests, involving 24 specimens, is outlined in Table 3.1. In order to achieve the significant joint deformation which was the principal feature under investigation, it can be noted that the tests involved low

values of β (primarily a value of 0.4), and intermediate values of b_0/t_0 (most tests involved $b_0/t_0 = 26.6$). The planar T joints referred to in the Table were joints which corresponded to a planar truss with a single web member meeting the chord in the direction perpendicular to its axis. These tests were included for control reasons, in order to relate the behaviour with two chord walls loaded to the planar truss situation in which only one wall is loaded.

The test series comprised three categories:

(i) Joint Strength - Tests 1 to 12, 21 and 22:

In these, compression web member failure was avoided by employing a low slenderness ratio.

- tests 1,4,5,6,10 ; 7,8,12 ; 21,22 and 3,11 investigated the effect of the angle α.
- tests 4,7,22 ; 1,21 ; 5,8 and 10,12 investigated the effect of the width ratio $\beta = b_1/b_0$.
- tests 1,2,3,9 and 10,11 investigated the effect of the chord wall slenderness b_0/t_0.

Note that tests 10, 11 and 12 were of planar T joints.

(ii) Compression Web Member Strength - Tests 13 to 20:

The compression web member failure and its interaction with the joint deformation were investigated in these tests. Tests 13 to 20 involved low ratios of web member strength to joint strength, estimated at the time of design as 1.05 for tests 15 to 20 and 1.20 for tests 13 and 14. These tests involved similar joints to those of tests 1, 3, 4, 5, 7 and 10 but comprised web members with higher slendernesses L_w/r.

(iii) Comparison with DK Truss Tests - Tests 15, 17, 23 and 24:

These four test specimens were designed with chord and compression web members corresponding to those employed in four of the truss segment tests performed earlier. The four chosen were those which exhibited the most significant joint deformation.

Tests 7, 8, 12 and 19 investigated the rather extreme case of $\beta = 0.2$. It should be noted that β values in triangular trusses will in general be less than those in planar trusses. No tests were done for β values greater than 0.6.

3.1.4 Details of Specimens

Typical joint sections are shown in Fig. 3 3 Whenever possible, centre lines of web members intersected on the tension chord axis, although in some cases (as β became large and the angle between web planes became small) this was not possible if the web members were not to intersect, and were to be attached to adjacent faces of chord. In practice, for α less than 45°, it can be expected that the designer would attach both members to the same face of the chord. This however was not the type of joint being considered in this investigation.

3.2 TEST SPECIMENS

3.2.1 Specimens

Nominal values of the dimensions, member sizes, and joint parameters for all specimens are given in Table 3.2. Measured values, given in Table 3.3 were used in all calculations of member resistances and loads, etc. given herein.

3 2 2 Material Properties and Fabrication

All members were square HSS sections provided by Stelco Incorporated Anticipated material specifications were grade 350, type W (weldable steel), Class H (hot formed to final shape, or cold formed to final shape and stress relieved) according to CSA Standards G40 20-M and G40 21-M Nominal mechanical properties for this material include a minimum yield strength of 350 MPa, tensile strength in the range 450-620 MPa and minimum elongation in 50 mm of 22% One section size supplied conformed to Grade 300-W

Coupons were tested from each web and chord member, and were selected from tube walls other than the one containing the weld seam Average results for these tests are given in Table 3 4 for each member

The specimens were arc welded manually using low hydrogen electrodes of the E-48018 series (ultimate tensile strength = 480 MPa) Details of the fillet welds of the joints followed STELCO (1981), and are shown in Fig 3 4 The weld sizes are given in Table 3.3

3 3 EXPERIMENTAL METHOD

3 3.1 Test Arrangement

A specimen in its test position is shown in Figs 3 1 and 3 5 The specimen rested in special base supports on the ends of its web members, and was loaded by vertical loads applied to the chord member. The loads were applied through two loading caps on the chord and stiffeners were placed inside the chord directly under the caps to prevent distortion of the chord cross section at the loading points The spacing between the loading caps was determined according to the following equation

$$\text{spacing} = 2b_0 + b_1$$

which is the same equation as the one used by Kato (1979) for planar T joints based on the fact that the ratio of bending stresses to crippling stresses in the chord is the same whether or not the chord is inclined at 45° to the vertical

3 3 2 Base Supports

Details of the base supports are given in Figs 3 1 and 3 6 The ends of the web members were bolted to a short extension terminated in a ball which sat in a socket The ball was oiled to reduced friction and could rotate in any direction inside the socket The effective end of the web member was therefore the center of the ball and the end condition closely approximated a freely rotating hinge

The socket sat on two mutually perpendicular rockers concentric with the ball and was attached to a four arm frame by four link bars on each of which two strain gauges were fixed As transverse shears developed at the end of the web members, the ball pushed sideways on the socket which was restrained elastically by the link bars. The socket rolled on the rockers, which offered negligible rolling resistance, and the transverse shears were resisted therefore only by the link bars The strains in the links were measured in an attempt to obtain the transverse shear magnitudes

Below the frame, different abutments could be placed to accomodate the various angles and sizes of all specimens All elements of the base supports were designed to resist, at ultimate, an axial load of 250 kN in the web members and a transverse shear load of 30 kN at the end of the web members

3 3.3 Instrumentation

Instrumentation comprised LVDT's (Linearly Variable Differential Transformers), electric wire resistance strain gauges and mechanical (dial) deflection gauges.

LVDT and strain gauge readings were collected through a Digital MINC computer. During the tests, end shears and joint deformations were calculated at each load step by the computer and the joint deformations plotted on the screen terminal.

Details of the measurements taken and the quantities derived are given below

3 3 3 1 Joint Deformations

Joint deformations were measured parallel to the axes of the web members relative to plates supported at the top corner of the chord and hanging normal to the web members, as shown in Fig 3.7

Parallel to the web member axis, two LVDT's were used to measure both the axial deformation and the rotation in a plane normal to the chord axis. For the specimens with long web members, a third LVDT was used to measure the rotation due to bending of the web member about its other axis By correcting for these rotations, the joint deformations along the web member centreline were calculated, as shown in Fig. 3.8.

3 3.3.2 Web Member End Shears

Each base support had four link bars lying in one plane perpendicular to the web member and radiating in four perpendicular directions The strain in each link bar was measured by two electric wire resistance strain gauges and the force in the link bar calculated The link bars were prestressed and the differences between the loads in each pair of opposite link bars gave components of the web member end shears.

The attempt to measure end shears in the web members, and hence bending moments, proved a failure. Due to P-Δ effects the moments calculated from the end shears were meaningless (e.g. several times larger than the plastic

moment), and are not considered further

3 3 3 3 Other Deflection Measurements

Three dial gauges (nos 2, 3 and 4) were used to measure the chord bending deformations, and one dial gauge (no 1) was used to measure the overall specimen deflection, as shown in Fig 3 1 For slender web members, two dial gauges were positioned on each web member as shown on Fig 3 9 to measure the mid-length deflection in two perpendicular directions

3 3 4 Loading

Downward loads were applied on the chord of the specimens by a 2,000 kN hydraulic universal testing machine Loads were recorded using the hydraulic load cell integral with the machine

3 4 TEST RESULTS

3 4 1 Failure Modes

Three failure modes have been identified and are shown in Fig 3 10 These are.

Mode 1 . punching in failure of the chord connected walls with small outward out-of-plane deflection of the chord unconnected walls,

Mode 2 . punching in failure of the chord connected walls and crippling failure of the chord unconnected walls, and

Mode 3 . overall buckling failure of the web members

The mode of failure of each individual specimen is given in Table 3 5

3.4.2 Measured Loads

If the total load acting on the test specimen is P, the axial load in each web member, N, is

$$N = \frac{P}{2\cos(\alpha/2)} \qquad [3.1]$$

where α is the angle between web members. The component of this load acting in a direction normal to the chord wall, Y, is

$$Y = N\cos(45^\circ - 0.5\alpha) \qquad [3.2]$$

The maximum load carrying capacity of tubular joints is the widely used measure of resistance which is treated as corresponding to the ultimate limit state of strength In some types of joint between rectangular HSS members however, notably T, X and Y joints between members of different widths, the maximum load carrying capacity is attained only when very large deformations have occurred. Punching deformations in excess of 30% of the chord wall width are frequently reached before the ultimate strength is developed For such joints a practical deformation limit will usually govern the design, rather than the ultimate load carrying capacity. The joints considered in this test program exhibit similar characteristics, and a problem therefore exists in defining an appropriate load or deformation to represent the necessary limits of behaviour.

In all the tests where joint failure occurred (modes 1 and 2), loading was stopped after the joint had developed some arbitrarily large deformation (11 to 15% of the chord width) while the load was either constant or still slightly increasing Testing of one specimen (No. 9) beyond a point at which the joint had undergone large deformations showed that the joint then started to stiffen because of membrane action taking place between stiffeners under the loading points. The increased load then triggered a very ductile overall bending failure of the chord. This bending failure was induced by the test arrangement and could not be considered representative of triangular truss joint behaviour. Consequently, other tests were stopped after the joint had

undergone large deformations, but before this phenomenon occurred. The maximum loads sustained in those tests terminated in this way is therefore arbitrary, and alternative measures of joint strength are needed.

The following loads were derived from the test results, and are given in Table 3.5, in terms of Y, the normal load on the chord wall arising from the one member attached to it:

(a) The maximum load sustained in the test, Y_{max} For most tests this value is not considered further, for reasons outlined above. However for those cases where web member instability occurred (mode 3), this maximum corresponded directly to the primary failure mode and is a real measure of resistance in these cases

(b) A failure load Y_u is taken as the load corresponding to a chord wall deflection of 0 06 b_0. This limit was chosen because most joints achieved a constant or slowly increasing resistance at this deflection, and any increase in joint stiffness due, at least in part, to the test arrangement, had not yet commenced Only modes 1 and 2 permitted this deflection to be reached.

(c) A yield load Y_y was chosen to correspond to the region of the load-deflection curve where deflections started to increase rapidly This load is defined by the offset shown in Fig 3.11

(d) A load Y_s corresponding to a chord wall deflection of 0 01 b_0 is also given in Table 3 5 This deflection has been proposed as a suitable limit under service loads (Mouty 1977).

3 4.3 Joint Deformations

The joint deformations along the axis of the web members are shown in Fig 3.12 for the tests that failed in mode 1 or 2 (tests 1 to 12, 21 to 24).

Results of the tests described above (DT joints), as well as those described in Chapter 2 (DK truss segments), are discussed in the next chapter

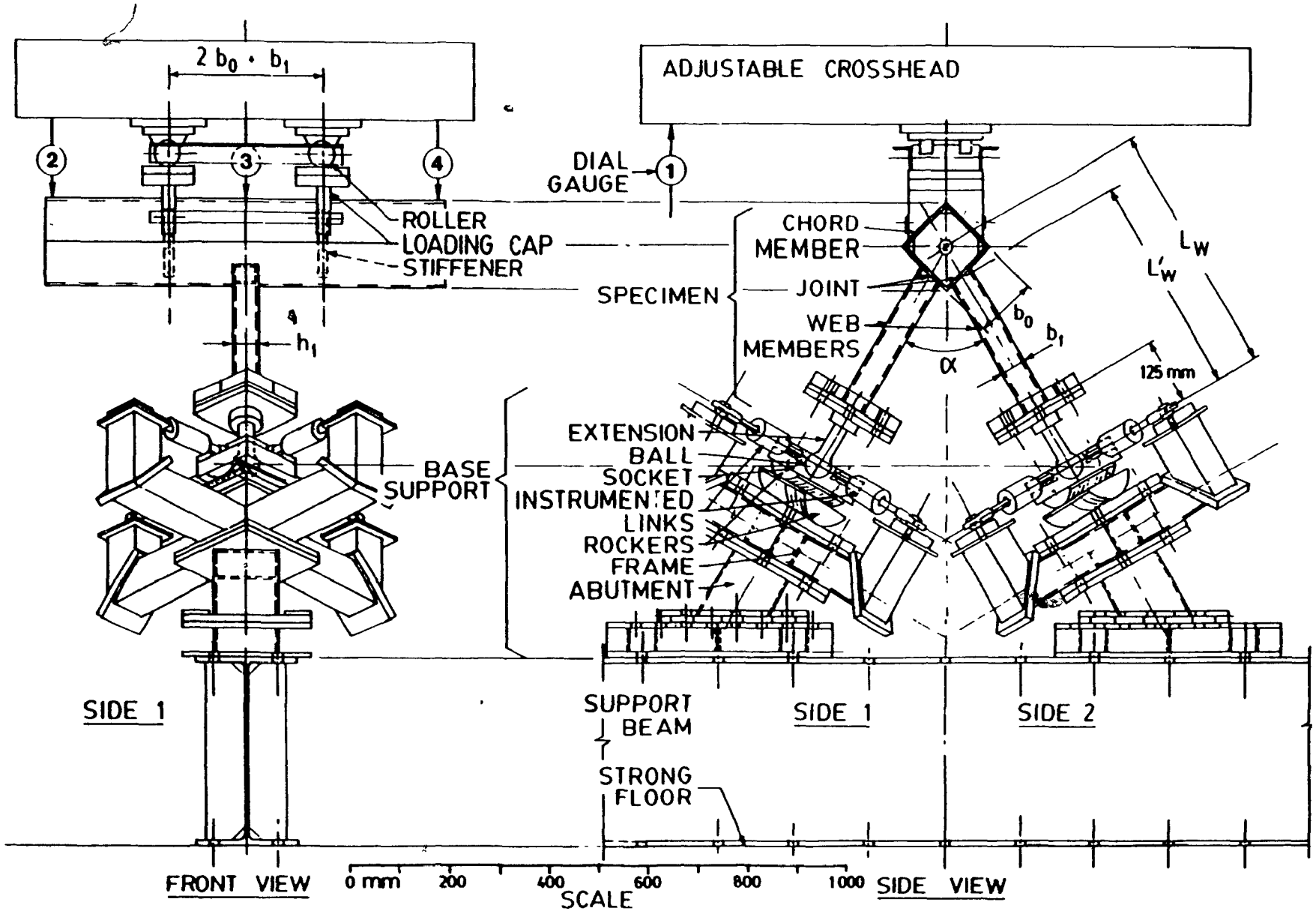

Fig. 3.1 Test arrangement. Joint tests.

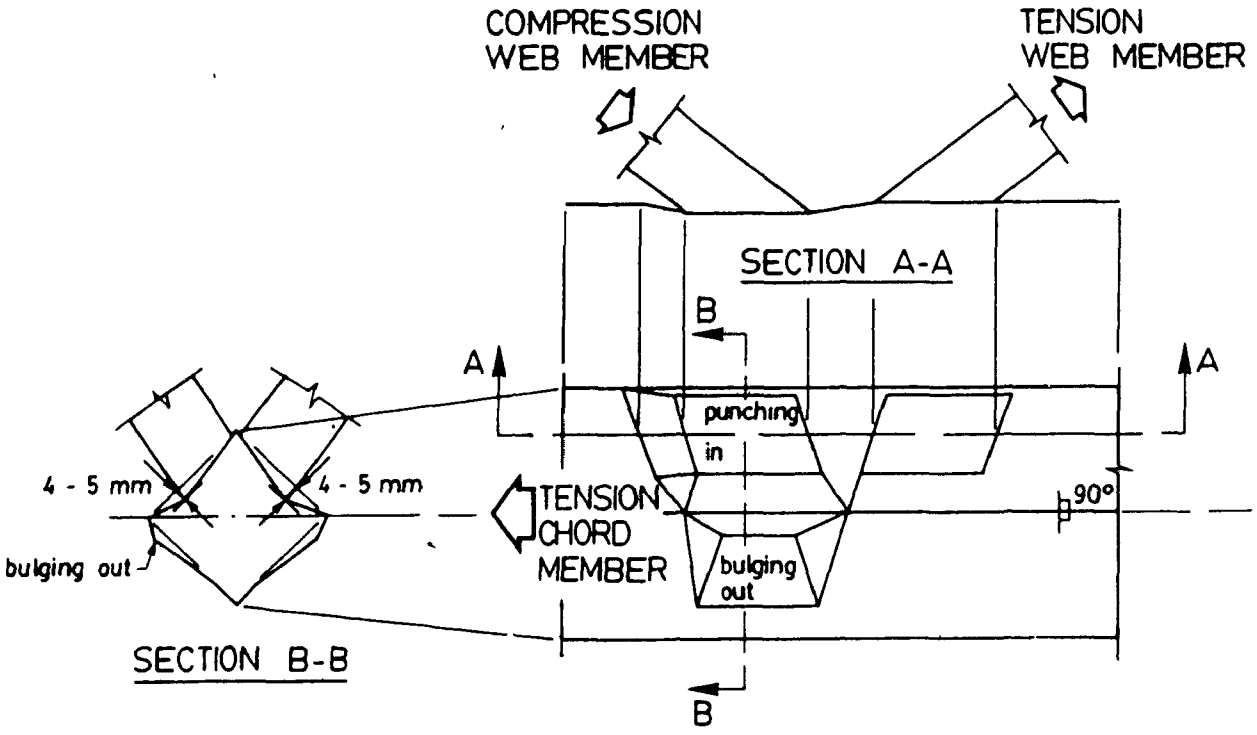

Fig. 3.2 Joint deformation in Truss 4. Truss tests.

$\beta = b_1/b_0$	b_0/t_0	α				
		T-	90°	60°	45°	30°
0.2	26.6	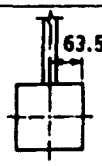 63.5 12 (Test No.)	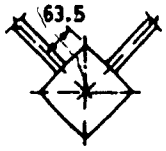 63.5 7, 19		 37.2 8	
0.4		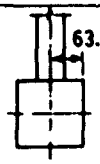 63.5	 63.5	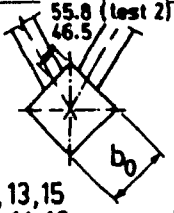 65.1 (test 9) 55.8 (test 2) 46.5 b_0	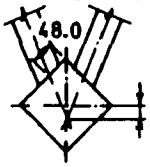 48.0 26.1	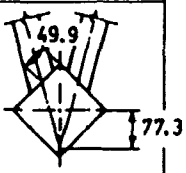 49.9 77.3
0.43	37.2			9		
0.42	31.9			2		
	26.6	10, 20	4, 17	1, 13, 15	5, 18	6
	20.0	11		3, 14, 16		
0.6	26.6		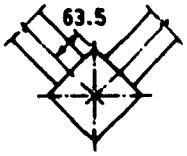 63.5 22, 24	 63.5 32.9 21, 23	b_0 = 177.8 in test 9 152.4 in test 2 127.0 in all other tests	

Fig. 3.3 Nominal test parameters. Joint tests.

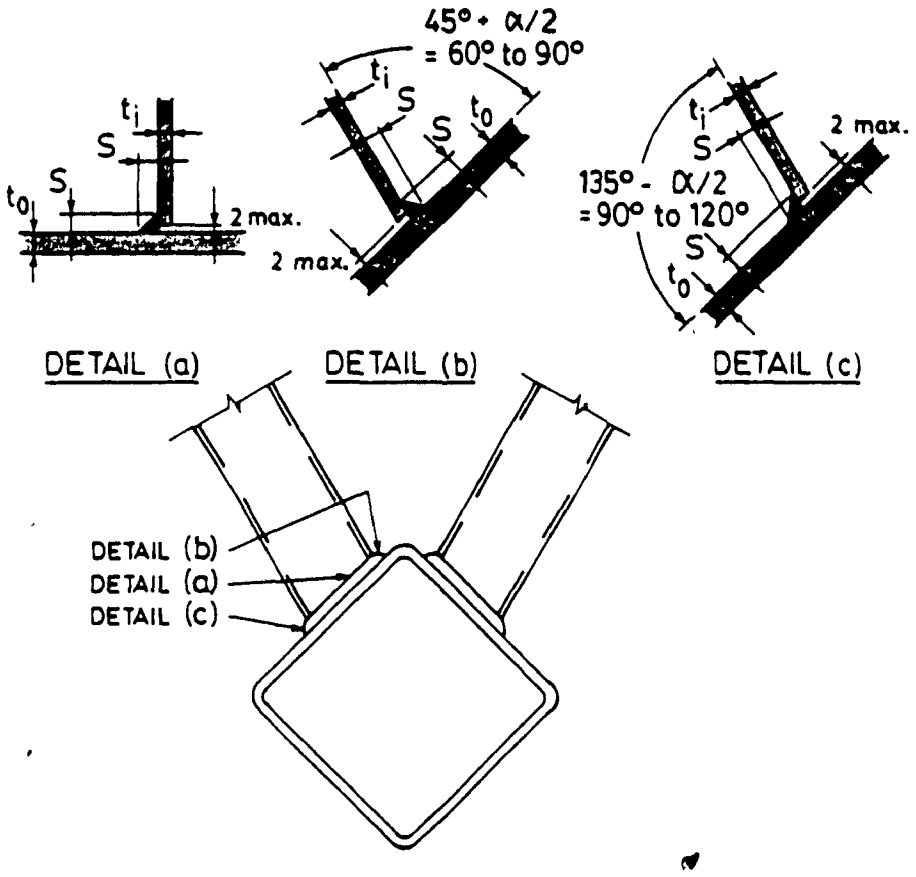

Fig 3.4 Fillet weld details. Joint tests

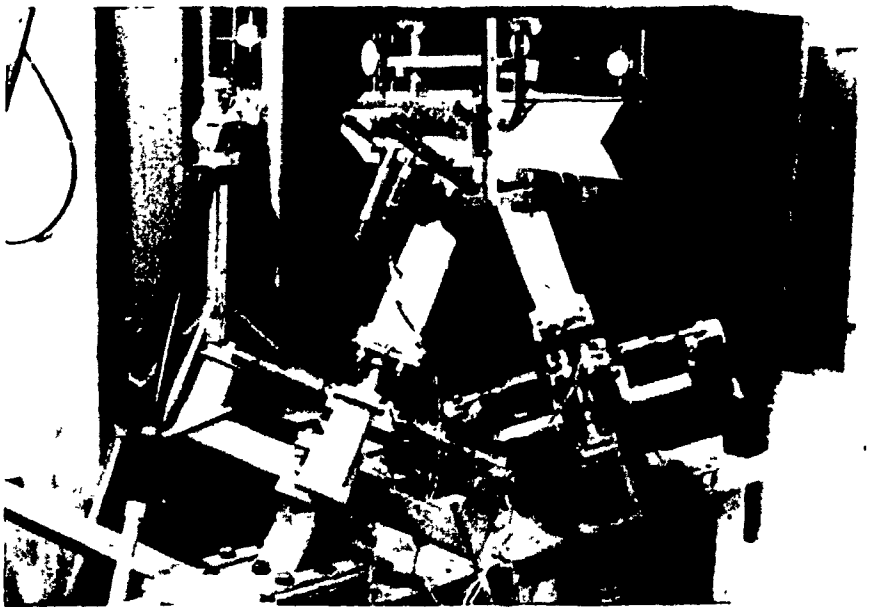

Fig. 3.5 Specimen in test position. Joint tests.

Fig. 3.6 Base support details Joint tests.

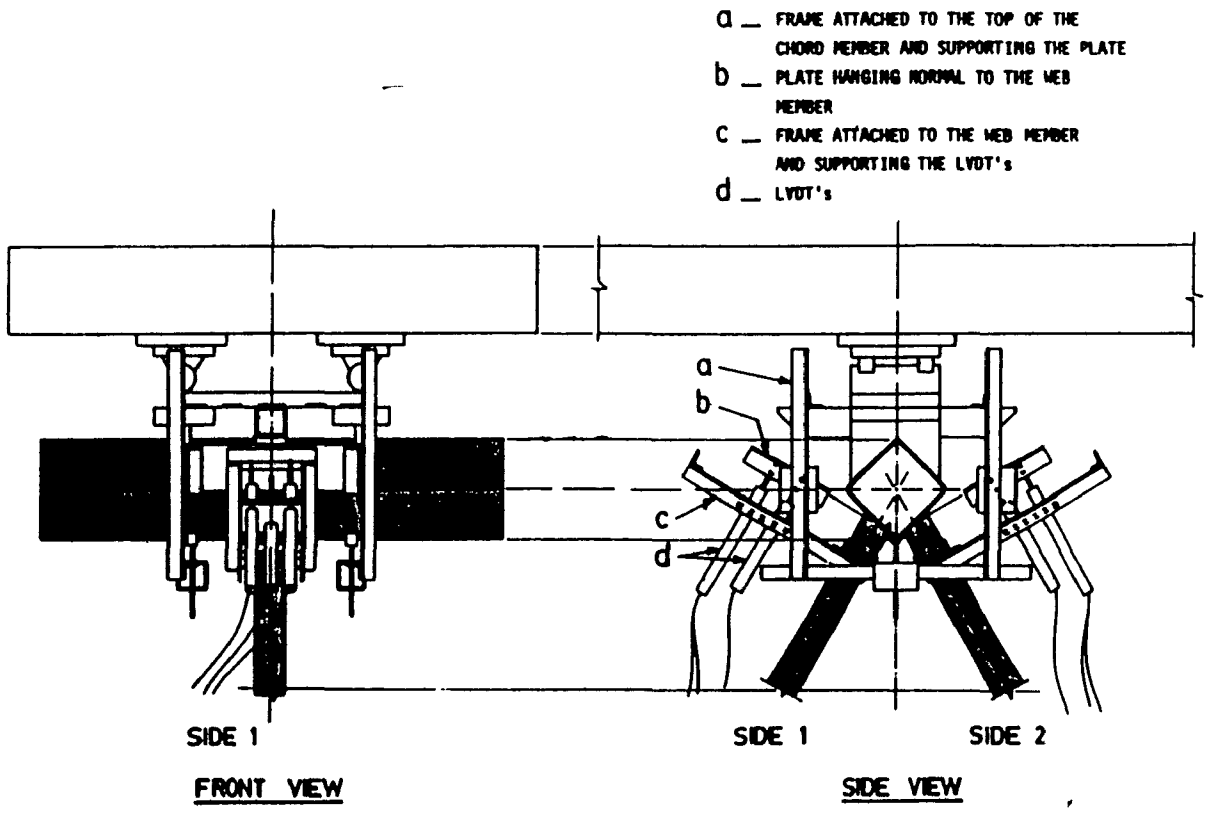

Fig. 3.7 LVDT arrangement for measuring the joint deformations. Joint tests.

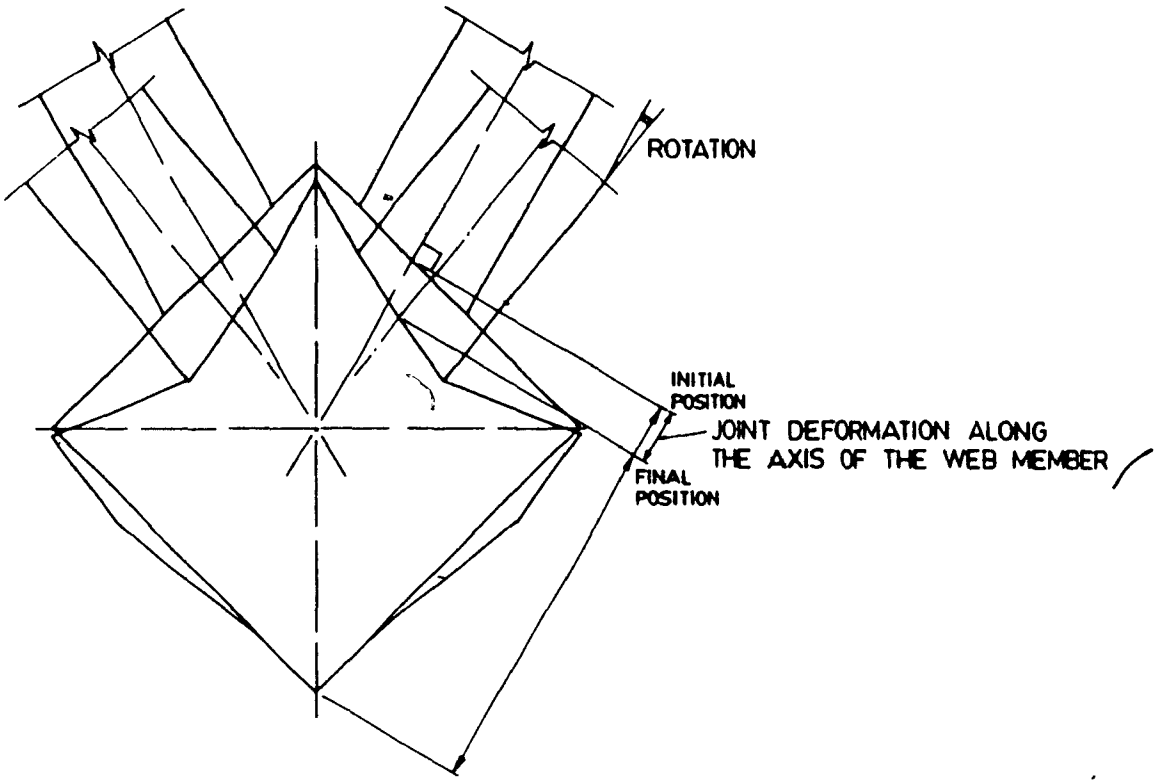

Fig. 3.8 Definition for the joint deformation along the axis of the web member.

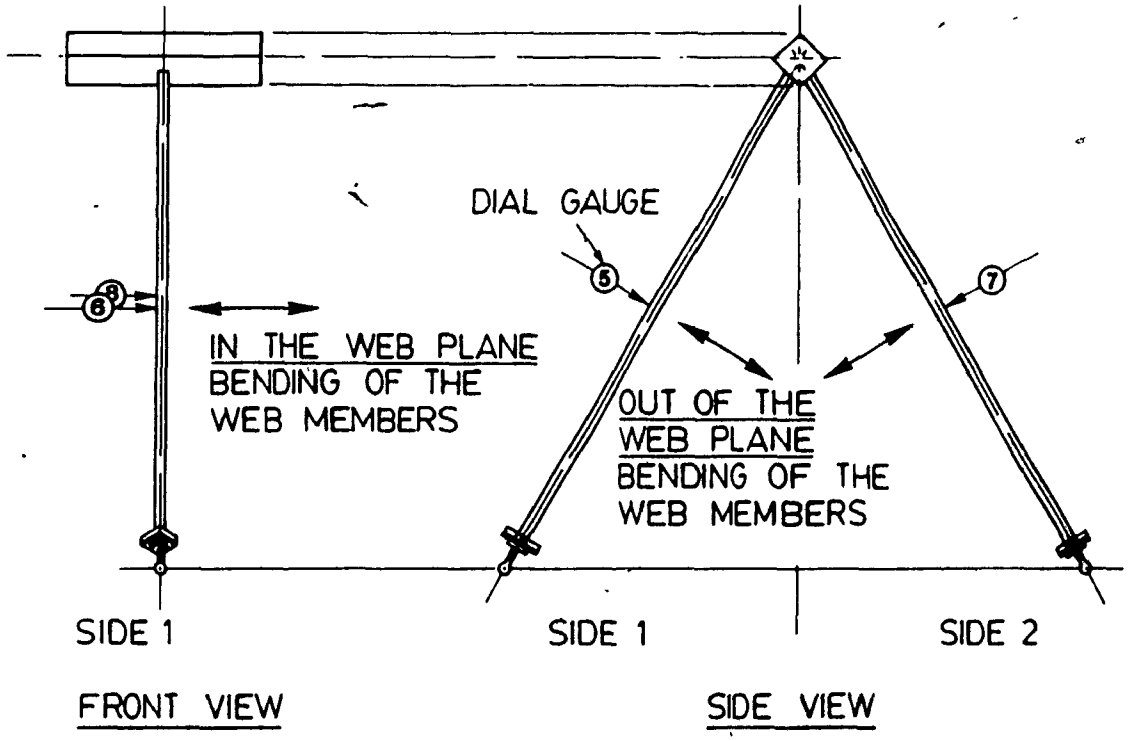

Fig. 3.9 Dial gauge arrangement for measuring the mid-length transverse deflections of the web members. Joint tests.

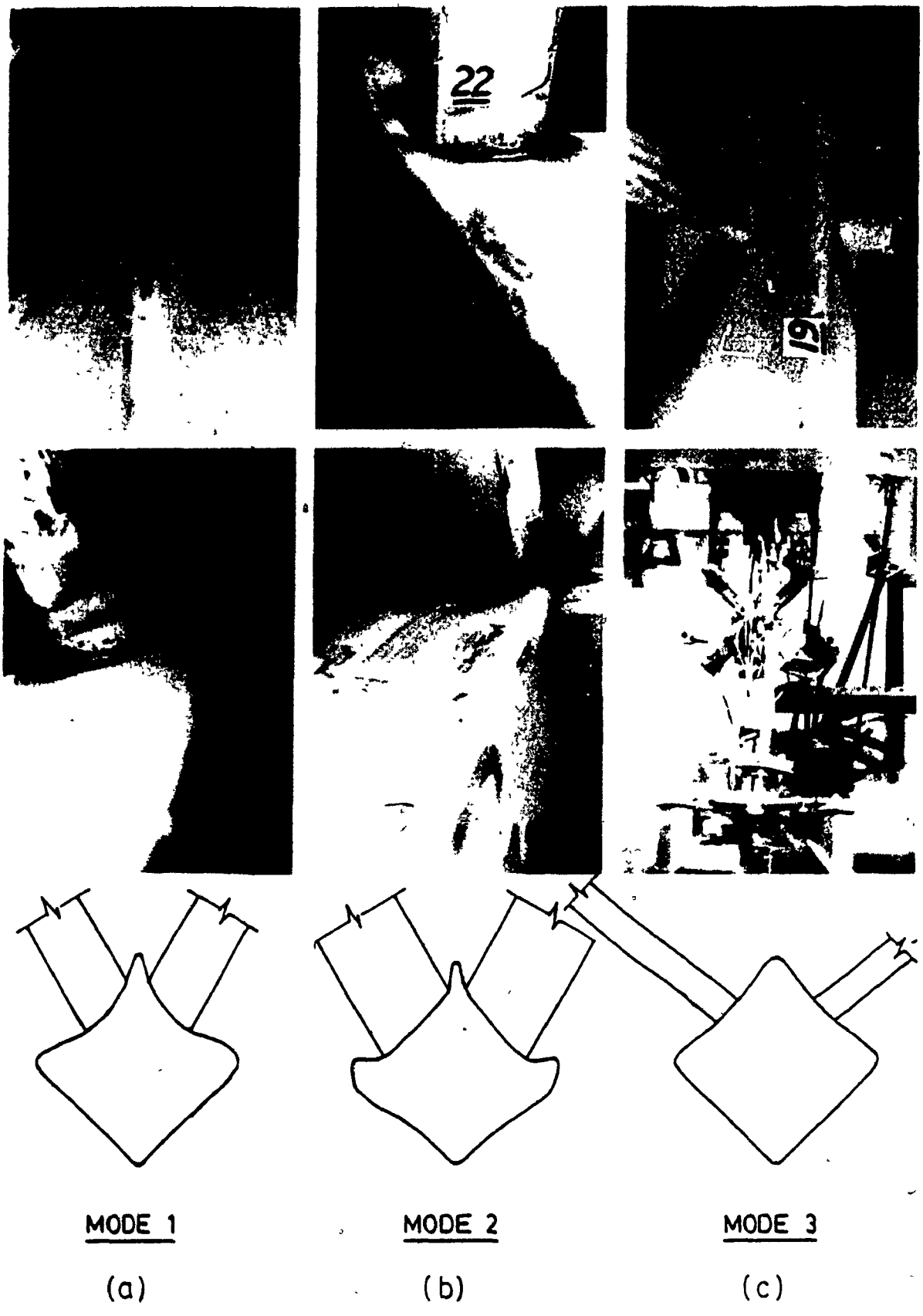

Fig. 3.10 - Failure modes.

Examples (joint test specimens):
(a) Mode 1: test no.2 (b) Mode 2: test no.22 (c) Mode 3: test no.19.

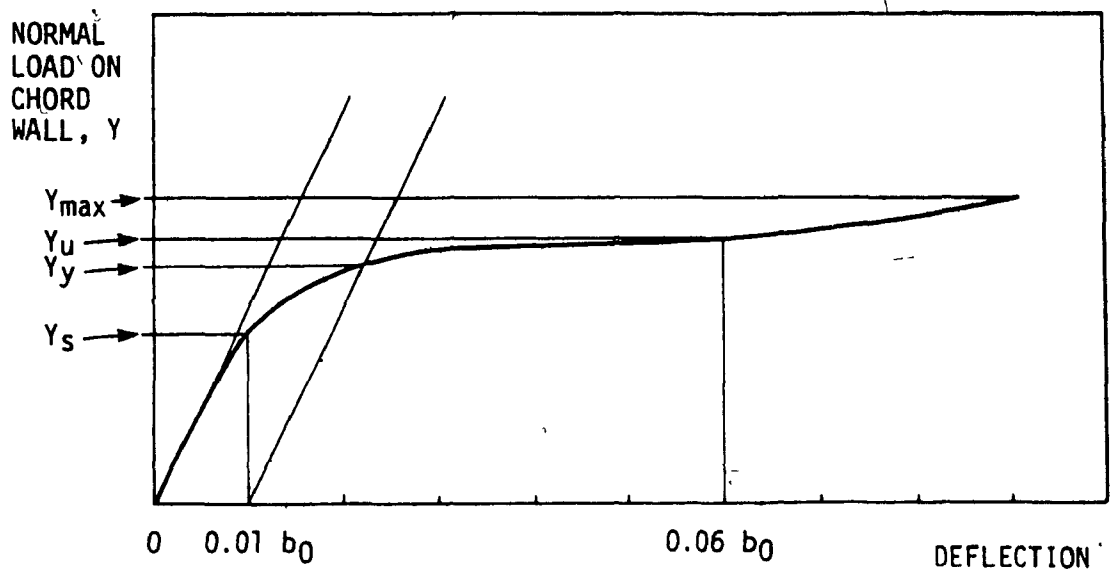

Fig. 3 11 Typical joint deformation.

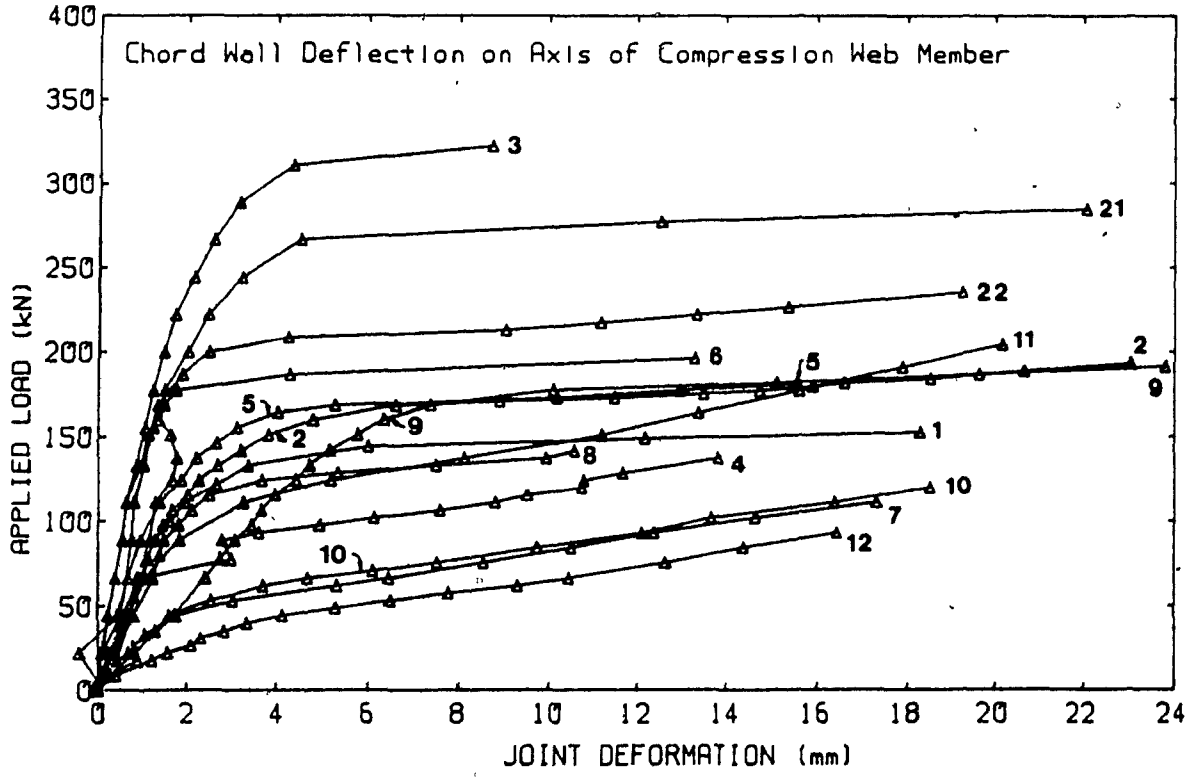

Fig. 3.12 Joint deformations. Joint tests.

Table 3 1 Program of tests (joint tests)

β exact	β approx	b_0/t_0	Chord Member Size mm	Compression Web Member Size mm	TEST no. T-Joint[1]	α = 90°	α = 60°	α = 45°	α = 30°
					L_w/r	L_w/r	L_w/r	L_w/r	L_w/r
					t_r[2] 20	t_r[2] 20	t_r[2] 20	t_r[2] 20	t_r[2] 20
					C_r/N_u	C_r/N_u	C_r/N_u	C_r/N_u	C_r/N_u
					1.05 1.20	1.05 1.20	1.05 1.20	1.05 1.20	1.05 1.20
.21	.2	37.2							
.21		31.9							
.2		26.6	127.0 x127.0 x4.78	25.4 x25.4 x3.18	12	19 7		8	
.2		20.0							
.2		16.0							
.43	.4	37.2	177.8 x177.8 x4.78	76.2 x76.2 x4.78			9		
.42		31.9	152.4 x152.4 x4.78	63.5 x63.5 x3.18[3]			2		
.4		26.6	127.0 x127.0 x4.78	50.8 x50.8 x2.79	20 10	T1,T2 17 4	T6 15 13 1	18 5	6
.4		20.0	127.0 x127.0 x6.35	50.8 x50.8 x4.78	11[4]	(90)	(90) 16 14 3		
.4		16.0				T5(100)			
.57	.6	37.2							
.58		31.9							
.6		26.6	127.0 x127.0 x4.78	76.2 x76.2 x4.78		T3(60) 24 22	T4(55) 23 21		
.6		20.0							
.6		16.0				T7(65)			

Notes:
(1) T-Joint refers to a single web member perpendicular to and centered on the chord wall, i.e. a planar T joint.
(2) This column indicates the test number of the truss test series and gives also the compression web member slenderness ratio.
(3) Size requested: 63.5 x63.5 x3.81, size supplied: 63.5 x 63.5 x 3.18.
(4) Web member size supplied: 50.8 x 50.8 x 2.79.

Table 3 2 Nominal sizes and dimensions Joint tests

Test	α deg	$\frac{b_1}{b_0}$	b_0 mm	t_0 mm	$\frac{b_0}{t_0}$	L_0 mm	b_1 mm	t_1 mm	$\frac{b_1}{t_1}$	L_w mm	r_1 mm	$\frac{L_w}{r_1}$	S* mm
1	60	.4	127.0	4.78	26.6	800	50.8	2.79	18.2	511	19.4	26.3	3
2	60	.42	152.4	4.78	31.9	950	63.5	3.18	20.0	614	24.4	25.2	4
3	60	.4	127.0	6.35	20.0	800	50.8	4.78	10.6	491	18.4	26.7	5
4	90	.4	127.0	4.78	26.6	800	50.8	2.79	18.2	514	19.4	26.5	3
5	45	.4	127.0	4.78	26.6	800	50.8	2.79	18.2	515	19.4	26.5	3
6	30	.4	127.0	4.78	26.6	800	50.8	2.79	18.2	511	19.4	26.3	3
7	90	.2	127.0	4.78	26.6	800	25.4	3.18	8.0	394	8.8	44.8	4
8	45	.2	127.0	4.78	26.6	800	25.4	3.18	8.0	394	8.8	44.8	4
9	60	.43	177.8	4.78	37.2	1100	76.2	4.78	15.9	702	28.8	24.4	5
10	T-	.4	127.0	4.78	26.6	800	50.8	2.79	18.2	514	19.4	26.5	3
11	T-	.4	127.0	6.35	20.0	800	50.8	2.79	18.2	494	19.4	25.5	5
12	T-	.2	127.0	4.78	26.6	800	25.4	3.18	8.0	394	8.8	44.8	4
13	60	.4	127.0	4.78	26.6	800	50.8	2.79	18.2	2396	19.4	123.5	3
14	60	.4	127.0	6.35	20.0	800	50.8	4.78	10.6	2136	18.4	116.1	5
15	60	.4	127.0	4.78	26.6	800	50.8	2.79	18.2	2616	19.4	134.8	3
16	60	.4	127.0	6.35	20.0	800	50.8	4.78	10.6	2316	18.4	125.9	5
17	90	.4	127.0	4.78	26.6	800	50.8	2.79	18.2	2669	19.4	137.6	3
18	45	.4	127.0	4.78	26.6	800	50.8	2.79	18.2	2535	19.4	130.7	3
19	90	.2	127.0	4.78	26.6	800	25.4	3.18	8.0	1049	8.8	119.2	4
20	T-	.4	127.0	4.78	26.6	800	50.8	2.79	18.2	2669	19.4	137.6	3
21	60	.6	127.0	4.78	26.6	800	76.2	4.78	15.9	702	28.8	24.4	5
22	90	.6	127.0	4.78	26.6	800	76.2	4.78	15.9	699	28.8	24.3	5
23	60	.6	127.0	4.78	26.6	800	76.2	4.78	15.9	2697	28.8	93.6	5
24	90	.6	127.0	4.78	26.6	800	76.2	4.78	15.9	2699	28.8	93.7	5

Notes:
* S: Fillet weld size.

Table 3 3 Measured sizes and dimensions Joint tests

Test	α	α	β	CHORD				WEB MEMBER - SIDE 1							WEB MEMBER - SIDE 2							
			$\frac{b_1}{b_0}$	b_0	t_0	$\frac{b_0}{t_0}$	L_0	b_1	t_1	$\frac{b_1}{t_1}$	L_w	L_w	r_1	$\frac{L_w}{r_1}$	b_1	t_1	$\frac{b_1}{t_1}$	L_w	L_w	r_1	$\frac{L_w}{r_1}$	S*
	+ deg	deg		mm	mm		+ mm	mm	mm		+ mm	mm	mm		mm	mm		+ mm	mm	mm		+ mm
1	60	60.4	.40	127.3	4.79	26.6	800	50.9	2.68	19.0	511	512	19.5	26.2	50.9	2.70	18.9	511	512	19.5	26.2	3
2	60	58.7	.42	152.1	4.81	31.6	950	63.8	3.24	19.7	614	613	24.5	25.1	63.8	3.22	19.8	614	613	24.5	25.1	4
3	60	60.1	.40	126.7	6.16	20.6	800	51.3	5.14	10.0	491	490	18.5	26.5	51.1	5.09	10.0	491	490	18.4	26.7	5
4	90	90.5	.40	127.4	4.73	26.9	800	50.7	2.65	19.1	514	512	19.4	26.5	50.8	2.67	19.0	514	512	19.4	26.5	3
5	45	42.7	.40	127.4	4.74	26.9	800	50.5	2.70	18.7	515	515	19.3	26.7	50.6	2.71	18.7	515	515	19.3	26.7	3
6	30	29.7	.40	127.4	4.73	26.9	800	50.6	2.69	18.8	511	512	19.3	26.5	50.4	2.71	18.6	511	512	19.3	26.5	3
7	90	90.	.20	127.4	4.74	26.9	800	26.0	3.56	7.3	394	392	8.9	44.3	26.0	3.54	7.3	394	392	8.9	44.3	4
8	45	48.4	.20	127.7	4.78	26.7	800	26.0	3.54	7.3	394	394	8.9	44.3	26.0	3.59	7.2	394	394	8.9	44.3	4
9	60	58.0	.43	178.6	4.62	38.7	1100	76.5	4.96	15.4	702	675	28.8	24.4	76.4	4.98	15.3	702	675	28.7	24 5	5
10	T-	T-	.40	127.4	4.76	26.8	800	50.9	2.69	18.9	514	514	19.5	26.4	-	-	-	-	-	-	-	3
11	T-	T-	.40	127.0	6.23	20.4	800	50.9	2.70	18.9	494	494	19.5	25.3	-	-	-	-	-	-	-	5
12	T-	T-	.20	127.6	4.76	26.8	800	25.9	3.53	7.3	394	394	8.9	44.3	-	-	-	-	-	-	-	4
13	60	56.2	.40	127.3	4.76	26.7	800	50.8	2.60	19.5	2396	2396	19.5	122.9	50.9	2.60	19.6	2396	2396	19.5	122.9	3
14	60	58.5	.40	126.9	6.23	20.4	800	51.2	5.31	9.6	2136	2136	18.4	116.1	51.3	5.36	9.6	2136	2136	18.4	116.1	5
15	60	57.7	.40	127.5	4.65	27.4	800	50.9	2.67	19.1	2616	2617	19.5	134.2	50.7	2.67	19.0	2616	2617	19.4	134.8	3
16	60	58.3	.40	126.8	6.19	20,5	800	50.7	5.11	9.9	2316	2315	18.3	126.6	50.8	5.09	10.0	2316	2315	18.3	126.6	5
17	90	89.3	.40	127.5	4.72	27.0	800	50.9	2.58	19.7	2669	2669	19.5	136.9	50.6	2.59	19.5	2669	2669	19.4	137.6	3
18	45	42.2	.40	127.7	4.70	27.2	800	50.8	2.67	19.0	2535	2536	19.4	130.7	50.9	2.68	19.0	2535	2536	19.5	130.0	3
19	90	90.	.20	127.6	4.76	26.8	800	26.0	3.54	7.3	1049	1050	8.9	117.9	26.0	3.55	7.3	1049	1050	8.9	117.9	4
20	T-	T-	.40	127.6	4.74	26.9	800	50.8	2.67	19.0	2669	2669	19.4	137.6	-	-	-	-	-	-	-	3
21	60	57.8	.60	127.5	4.64	27.5	800	76.3	4.96	15.4	702	702	28.7	24.5	76.3	4.93	15.5	702	702	28.7	24.5	5
22	90	90.	.60	127.6	4.75	26.9	800	76.4	4.70	16.3	699	699	28.8	24.3	76.3	4.71	16.2	699	699	28.8	24.3	5
23	60	58.8	.60	127.6	4.67	27.3	800	76.0	4.72	16.1	2697	2695	28.7	94.0	76.6	4.95	15.5	2697	2695	28.8	93.6	5
24	90	89.4	.60	127.5	4.76	26.8	800	76.7	5.07	15.1	2699	2696	28.8	93.7	76.7	4.93	15.6	2699	2696	28.9	93.4	5

Notes:
* S: Fillet weld size
+ Nominal values. Since measured values are close to nominal values, use nominal values in calculations.

Table 3.4 Average coupon results Joint tests

Test	Member Designation	Nominal Size (supplied)	Yield Strength at 0.2%	Ultimate Tensile Strength	Elongation % in 50.8 mm	Reduction of Area at Fracture
			MPa	MPa		%
1	Chord	127.0 x 127.0 x 4.78	354	483	32	56
	C.W.M.-S1	50.8 x 50.8 x 2.79	359	542	24	51
	C.W.M.-S2	50.8 x 50.8 x 2.79	359	542	24	51
2	Chord	152.4 x 152.4 x 4.78	380	473	30	59
	C.W.M.-S1	63.5 x 63.5 x 3.18	354	517	25	53
	C.W.M.-S2	63.5 x 63.5 x 3.18	354	517	25	53
3	Chord	127.0 x 127.0 x 6.35	425	510	29	63
	C.W.M.-S1	50.8 x 50.8 x 4.78	444	582	23	60
	C.W.M.-S2	50.8 x 50.8 x 4.78	444	582	23	60
4	Chord	127.0 x 127.0 x 4.78	354	483	32	56
	C.W.M.-S1	50.8 x 50.8 x 2.79	371	545	24	50
	C.W.M.-S2	50.8 x 50.8 x 2.79	371	545	24	50
5	Chord	127.0 x 127.0 x 4.78	354	483	32	56
	C.W.M.-S1	50.8 x 50.8 x 2.79	371	545	24	50
	C.W.M.-S2	50.8 x 50.8 x 2.79	371	545	24	50
6	Chord	127.0 x 127.0 x 4.78	354	483	32	56
	C.W.M.-S1	50.8 x 50.8 x 2.79	371	545	24	50
	C.W.M.-S2	50.8 x 50.8 x 2.79	371	545	24	50
7	Chord	127.0 x 127.0 x 4.78	354	483	32	56
	C.W.M.-S1	25.4 x 25.4 x 3.18	365	544	23	52
	C.W.M.-S2	25.4 x 25.4 x 3.18	365	544	23	52
8	Chord	127.0 x 127.0 x 4.78	437	542	27	57
	C.W.M.-S1	25.4 x 25.4 x 3.18	365	544	23	52
	C.W.M.-S2	25.4 x 25.4 x 3.18	365	544	23	52
9	Chord	177.8 x 177.8 x 4.78	380	503	32	56
	C.W.M.-S1	76.2 x 76.2 x 4.78	335	509	28	56
	C.W.M.-S2	76.2 x 76.2 x 4.78	335	509	28	56
10	Chord	127.0 x 127.0 x 4.78	354	483	32	56
	C.W.M.-T-	50.8 x 50.8 x 2.79	359	542	24	51
11	Chord	127.0 x 127.0 x 6.35	425	510	29	63
	C.W.M.-T-	50.8 x 50.8 x 2.79	359	542	24	51
12	Chord	127.0 x 127.0 x 4.78	411	521	28	55
	C.W.M.-T-	25.4 x 25.4 x 3.18	365	544	23	52
13	Chord	127.0 x 127.0 x 4.78	354	483	32	56
	C.W.M.-S1	50.8 x 50.8 x 2.79	349	517	25	52
	C.W.M.-S2	50.8 x 50.8 x 2.79	349	517	25	52
14	Chord	127.0 x 127.0 x 6.35	425	510	29	63
	C.W.M.-S1	50.8 x 50.8 x 4.78	423	573	25	61
	C.W.M.-S2	50.8 x 50.8 x 4.78	423	573	25	61
15	Chord	127.0 x 127.0 x 4.78	387	511	30	55
	C.W.M.-S1	50.8 x 50.8 x 2.79	369	542	23	49
	C.W.M.-S2	50.8 x 50.8 x 2.79	369	542	23	49
16	Chord	127.0 x 127.0 x 6.35	425	510	29	63
	C.W.M.-S1	50.8 x 50.8 x 4.78	444	582	23	60
	C.W.M.-S2	50.8 x 50.8 x 4.78	444	582	23	60
17	Chord	127.0 x 127.0 x 4.78	411	521	28	55
	C.W.M.-S1	50.8 x 50.8 x 2.79	359	520	25	52
	C.W.M.-S2	50.8 x 50.8 x 2.79	359	520	25	52
18	Chord	127.0 x 127.0 x 4.78	405	518	29	55
	C.W.M.-S1	50.8 x 50.8 x 2.79	370	544	24	49
	C.W.M.-S2	50.8 x 50.8 x 2.79	370	544	24	49
19	Chord	127.0 x 127.0 x 4.78	411	521	28	55
	C.W.M.-S1	25.4 x 25.4 x 3.18	365	544	23	52
	C.W.M.-S2	25.4 x 25.4 x 3.18	365	544	23	52
20	Chord	127.0 x 127.0 x 4.78	437	542	27	57
	C.W.M.-T-	50.8 x 50.8 x 2.79	380	541	28	49
21	Chord	127.0 x 127.0 x 4.78	405	518	29	55
	C.W.M.-S1	76.2 x 76.2 x 4.78	361	532	27	56
	C.W.M.-S2	76.2 x 76.2 x 4.78	361	532	27	56
22	Chord	127.0 x 127.0 x 4.78	411	521	28	55
	C.W.M.-S1	76.2 x 76.2 x 4.78	323	490	28	57
	C.W.M.-S2	76.2 x 76.2 x 4.78	323	490	28	57
23	Chord	127.0 x 127.0 x 4.78	424	532	27	57
	C.W.M.-S1	76.2 x 76.2 x 4.78	361	532	27	56
	C.W.M.-S2	76.2 x 76.2 x 4.78	361	532	27	56
24	Chord	127.0 x 127.0 x 4.78	437	542	27	57
	C.W.M.-S1	76.2 x 76.2 x 4.78	335	509	28	56
	C.W.M.-S2	76.2 x 76.2 x 4.78	335	509	28	56

Table 3.5 Test and theoretical values of chord wall normal loads
Joint tests

Test	Load at 0.01 b_0 defn.	Test Value Yield Load	Ultimate Load 0.06 b_0 defn.	Maximum Load	Failure Mode	Yield Line Theory	$\frac{Y_y(\text{test})}{Y_y(\text{theory})}$
	Y_s^+	Y_y^+	Y_u^+	Y_{max}		Y_y	
1	49.4	73.0	81.4	85.6	1	70.3	1.04
2	58.6	82.0	95.0	114.2	1	78.8	1.04
3	84.8	165.0	178.9	182.7	1	151.6	1.09
4	42.3	60.0	74.2	97.9	1	58.4	1.03
5	54.6	76.0	84.3	89.7	1	70.0	1.09
6	51.0	83.0	86.1	87.9	1	71.8	1.16
7	23.0	39.0	50.2	78.6	1	44.1	0.88
8	36.6	63.0	68.9	72.9	1	71.2	0.88
9	33.5	93.0	98.6	151.6	2	73.3	1.27
10	37.0	61.5	76.0	120.1	1	59.3	1.04
11	72.5	107.0	135.5	204.6	1	133.0	0.80
12	14.0	48.0	56.0	93.4	1	51.5	0.93
13	45.8	-	-	68.3	3	67.9	-
14	65.6	136.0	-	137.4	3	155.4	(0.88)
15	39.2	-	-	60.3	3	72.3	-
16	53.1	-	-	132.8	3	152.4	-
17	47.1	-	-	67.8	3	67.5	-
18	44.6	-	-	65.4	3	78.9	-
19	39.2	51.0	-	64.5	3	51.6	(0.99)
20	34.0	68.5	-	68.9	3	72.4	(0.95)
21	87.6	134.0	149.0	156.2	2	122.6	1.09
22	107.7	138.0	149.6	166.7	2	120.6	1.14
23	55.8	132.0	147.6	155.2	2	127.6	1.03
24	105.0	151.0	160.7	181.5	2	127.5	1.18

All loads given in kN.
+ The average of values obtained from each side is given.

CHAPTER 4 DISCUSSION OF TEST RESULTS

Results discussed in the following are treated in two categories In the first, those tests in which failure took place in either mode 1 or 2 are treated, that is, failure was primarily associated with joint deformation The second category comprises the tests in which web member overall instability was the primary cause of failure (mode 3 indicated in Table 3 5) Both the truss segment test series and the simplified joint test series are considered

4.1 JOINT BEHAVIOUR (DOUBLE-T JOINT TESTS)

4 1 1 Yield Line Theory

In a subsequent section the influence of the parameters α, β and b_0/t_0, as outlined in §3 1 3 will be examined Firstly however, test results are compared with the yield line method of analysis (Jubb and Redwood 1966, Kato and Nishiyama 1979, Mouty 1977, Wardenier 1982) This method is recommended for the design of T, Y and X joints with the web member(s) in one plane, and for which the web member width is no more than 80 to 85% of the chord member width The yield line approach has been justified both on the basis that it corresponds to a reasonable deflection magnitude at service load level (Mouty 1977, Wardenier 1982), and because it predicts a "yield load" which is in reasonable agreement with test loads at which the growth of joint deformations accelerate (Jubb and Redwood 1966, Kato and Nishiyama 1979) The yield line method, and its application to the test specimens, is summarized in Chapter 5, which includes the equation for the yield load of a T joint, and various modifications to that equation to account for the inclination of the web members to the chord wall, and for the off-

centre position of the web member for DT joints.

Test results, expressed as the normal loads on the chord walls Y_u and Y_y are compared with the yield line theory results on Fig. 4.1. This comparison includes all Mode 1 and 2 failures, and thus includes the full range of values of the parameters tested While there is some scatter, it can be seen that there is a considerable measure of agreement The mean value of the ratio of test and theoretical yield loads Y_y is 1 043 with coefficient of variation 11.8% For the ultimate loads (corresponding to 0 06 b_0 deflection) the corresponding figures are 1 184 and 8.2% The distributions of these results are shown in Fig. 4.2.

The discussion of joint strength in the following is based primarily upon the yield values of the test loads, i.e , Y_y or N_y. However, except where otherwise discussed, the effects of the various parameters on the ultimate loads, Y_u or N_u, follow identical trends.

4.1.2 Comparative Test Results

With a limited number of test specimens, and a limited range of section sizes to select from, it was not possible to isolate all of the principal test parameters when designing the experiments As an example, variation of the angle α will change the contact width of the web member on the chord face, so that with the same size of web member the value of the effective width ratio, β, will change with α The yield line theory predicts that this accompanying change in β will have a non-negligible effect on the yield load, and indeed the evidence suggests that the β effect is much greater than any effect of the corresponding variations in α. For this reason, and because the yield line theory has been shown to provide a good correlation with the test results, the ratio of test load to theoretical yield line load is used in the next section to investigate the effects of the principal parameters.

One major influence can, however, be investigated by direct comparison between test results, namely, the effect of loading on two adjacent chord walls, compared with the loading on one chord wall which occurs in planar trusses The latter has been the object of much of the joint testing carried out over the last two decades, and is the case to which the yield line theory has been compared in earlier research work

Such direct comparisons will nevertheless require normalization in view of the significant variation in yield stresses between specimens and because of dimensional variations Because of the correlation already observed between tests and yield line theory, the latter was used as a basis for normalization of the test results to nominal dimensions and nominal yield of 350 MPa Measured and adjusted values of the normal yield loads on the chord wall, Y_y, are given in Table 4.1 for the relevant test specimens These are the ones corresponding to planar T joints and to DT joints with 90° angles between web planes

Only two pairs of these specimens can be compared Nos 4 and 10 for which the ratio of normalized failure loads is 0 99 and Nos 7 and 12 for which the ratio is 0 95. These results, for which β was 0 2 and 0 4 and $b_0/t_0 = 26.6$, suggest that there is little interactive effect produced by identical loading on an adjacent wall of the chord

4.1 3 Effects of Principal Parameters

The ratio of test to theoretical yield load values for the range of angles between web planes, α, are shown in Fig. 4 3 Tests involving nominally identical values of other parameters are linked. This graph indicates no discernible trend with α, suggesting that the yield line theory adequately incorporates its effects.

Similar load ratios are shown as they vary with β, in Fig. 4.4a. Here

there appears to be a decrease in test to theoretical load ratio as β decreases. While low values of β are uncommon in planar trusses, they more frequently arise in triangular trusses The trend is however less consistent for the ultimate loads, shown in Fig. 4.4b.

The yield line theory does not incorporate any influence of the chord wall slenderness ratio b_0/t_0 High values of this ratio can lead to web crippling in T joint tests, especially when β is large, but may also allow membrane action to develop in K or N truss joints The ratio of test to theoretical yield load is plotted for the four slenderness ratios in Fig 4 5 Considerable scatter exists and no consistent variation of the load ratio with b_0/t_0 can be seen. In particular, no indication of loss of resistance with increasing b_0/t_0 is evident from the limited experimental data.

4.1.4 Joint Deformations

A joint deformation of 1% of the chord width b_0 has been suggested as an appropriate deflection limit at service load level for planar HSS truss joints (Mouty 1977). The test loads at which this deformation was recorded are listed in Table 3.5, and are also compared in Fig. 4.6 with the yield load predicted by the yield line theory. The mean value of the ratio of these measured loads to the theoretical yield line value is 0.625, with standard deviation 16 3%. A line corresponding to this mean is shown on Fig. 4 6 This indicates that the joints considered are rather more flexible than planar T joints and have similar flexibility to planar X joints (Mouty 1977, Wardenier 1981, 1982). It should be noted that the interpretation of the yield line geometry (in connection with taking into account the weld size and the chord corner curvature when calculating the β ratio), following Chapter 5, leads to a slightly higher theoretical yield strength than the interpretation of Mouty (1977). In any case, as for the planar joints, the

yield line theory does demonstrate some correlation with the specified deformation at service load levels, for the triangular joint considered here

4.1 5 Effect of Longitudinal Chord Stresses

The longitudinal stresses in the chord due to bending, induced by the loading system, were calculated for the joints that failed in mode 1 or 2 At the applied load P_y, causing yield of the joint, compression bending stresses in the chord at the web member level varied between 8% and 42% of the chord yield stress, with an average of 25.8%

To account for the effect of the longitudinal stresses on the chord face strength, the reduced plastic moment

$$M_{p,reduced} = \left[1 - \left(\frac{N}{N_p}\right)^2 \right] M_p \qquad [4\ 1]$$

must be calculated for every yield line of the failure mechanism For the DT joints considered herein, this would be done by considering the variation of the longitudinal stress components normal to every yield line Based on these reduced plastic moments, a slightly different yield line mechanism would be obtained and the chord face strength would be recalculated This sequence of calculations would be iterated until convergence occurred

For planar K joints, an approximation of the chord loading influence assumes the same maximum reduction of the plastic moment for all yield lines and no iterations are done. Hence the reduced chord face strength is calculated by multiplying by a chord loading influence function (Wardenier 1982), given as $f(n) = 1-(n)^2$. Alternatively, an empirical chord loading influence function (Wardenier 1982) is proposed as $f(n) = 1\ 3 - \frac{0.4\ |n|}{\beta}$

For the DT joints, the same simplifying approaches can be used A uniform longitudinal stress distribution in the chord, equal to the bending stress at the web member level, is conservatively assumed to have the same

effect as the actual linearly varying bending stress distribution Using $f(n) = 1-(n)^2$, the reduction of the chord face joint strength due to the longitudinal stresses varies from 1% to 18%, with an average of 8.7%, and the mean value of the ratio of test and theoretical yield loads Y_y becomes 1.143 with coefficient of variation 15.7%. Using $f(n) = 1.3 - \frac{0\ 4\ |n|}{\beta}$, the reduction varies from 0% to 16%, with an average of 2 5%, and the mean value of the ratio of test and theoretical yield loads becomes 1 072 with coefficient of variation 12.4%

4.1.6 Conclusions

Specific conclusions based on the results presented are listed below·

1 The strength of DT joints with two web members separated by 90° is indistinguishable from that of planar T joints with one web member perpendicular to the chord wall. This has been observed by direct comparison for width ratios up to 0.4 and values of b_0/t_0 of 26.6.

2. The yield line theory, as developed and interpreted in Chapter 5, correlates well with the measured yield loads The mean of test load to theoretical load for all 16 specimens failing in modes 1 or 2 is 1.043, with coefficient of variation of 11.8% The correlation with the test load corresponding to a chord wall deflection of 6% of its width is also good: the mean is 1.184 and COV 8.2%)

3. There is no discernible effect of variations in angle between web planes beyond that incorporated in the yield line theory. The range examined included all practical values of this angle.

4. The chord wall slenderness ratio, b_0/t_0, showed no important influence on the correlation between tests and yield line theory The range of b_0/t_0 considered was 20 to 37.2, however most specimens corresponded to 26.6

5. The yield line theory incorporates the major effects of the width ratio, β. However, there is an apparent increase in test yield load compared with the theoretical load as β increases This trend is less marked in the case of the ultimate test load (corresponding to 6% b_0 deflection).

6. For the 16 DT specimens which failed in modes 1 and 2, chord wall deformations of 0 01 b_0 occurred on average when loads reached a magnitude of 61% of the theoretical yield line load

4 2 WEB MEMBER BUCKLING (DOUBLE-T JOINT TESTS)

In tests 13 to 20 web member instability was the primary failure mode Measured joint deformations showed much less ductility in these eight tests than in the other sixteen, and the maximum load reached in the test was taken as the failure load. Results are summarized in Table 4 2, in which axial loads in the web members are given.

In only three of these eight tests was the joint deformation sufficient to measure the yield load as defined in Fig 3.11. These three yield loads, after normalization, were between 88% and 99% of the theoretical yield line load, as shown in Table 3.5.

4.2.1 Comparison with Column Strength Curves

The web member compressive resistances, C_r, predicted by column strength curve No. 1 of the SSRC (Johnston 1980), are given in Table 4.2, and are based upon an assumed effective length factor of 1.0 In all of cases 13 to 20 the value is less than the measured failure load and for all other tests it was considerably greater than the test loads, suggesting that these are the only tests where web member instability was a principal factor. The ratio of maximum test load to C_r with K=1.0 varies from 1.07 to 1 51. These results

may also be expressed as corresponding to effective length factors varying between 0.96 and 0.80.

The web member support at one end closely approximated a pinned joint and, with the assumption that the SSRC column curve No. 1 is a correct measure of column resistance, these values of K less than unity can be interpreted as being related to the restraint at the joint. For elastic buckling, the restraint can be expected to relate to the relative stiffness of web member to joint. Interpreting the joint stiffness as a function of the transverse flexural stiffness of the chord wall [taken as proportional to $b_1 t_0^3/(b_0'-b_1')$], no discernible relationship was evident between the K factors and the relative stiffnesses. It is unlikely that elastic conditions existed at the joint in any of these tests in view of the high values of the test loads compared with the theoretical yield line loads.

In the three tests which exhibited some joint deformation prior to buckling (Nos. 14, 19 and 20) the calculated effective length factors included the highest as well as the lowest (0.96 and 0.80 for members pinned at one end) of all tests. No correlation with plastic joint deformations is therefore evident, and interaction between the two modes of failure does not therefore appear to be significant.

4.2.2 Effects of Principal Test Parameters

In order to make comparisons between test results related to web member instability, the measured maximum loads were normalized by multiplying the test load by the ratio of computed C_r (given by SSRC Curve No.1) based on nominal dimensions and F_y = 350 MPa, and the value of C_r calculated for actual properties of the web members. For both values of C_r, the value of K given in Table 4.2 was used, with the web member length taken as L_w' as defined in Fig. 4.7. Normalized test values are given in Table 4.2.

For similar web member slenderness ratios four test results corresponding to various α values are given in Table 4.3. No consistent variation with the angle α is evident. Virtually identical results were obtained for the planar T specimen and the DT 45° and 90° specimens.

Effects of different b_0/t_0 values can be evaluated from tests 13 and 15 ($b_0/t_0 = 26.6$) and 14 and 16 ($b_0/t_0 = 20.0$). No clear distinction is evident in the values of K or N/C_r. Any effects of different β values for Tests Nos. 19 and 17 are hidden by the effects of the different slenderness ratios

4 2.3 Conclusions

In summary, the following conclusions are drawn:

1. Effective length factors calculated from the test results, assuming SSRC column strength curve No.1, varied between 0.80 and 0.96 for web members pinned at one end. They showed no correlation with either the relative elastic stiffness between web members and joint or with the degree of joint deformation prior to web member instability.

2. No significant change of effective length factors is evident as α varies between 45° and 90°. Results for the planar T configuration are identical to those for 90° and 45° DT configurations. It is concluded that primary bending due to non-symmetric joint details, which exist when $\alpha \neq 90°$ need not be considered, and that web members may be designed as axially loaded columns

3. No variation of the web member buckling strength could be determined between results for values of b_0/t_0 of 20 and 26.6, nor for nominal β values of 0.2 and 0.4.

4 3 TESTS OF DK TRUSS SEGMENTS

The results of the tests on DT specimens described in the preceeding sections are examined here in relation to the DK truss segment tests reported in Chapter 2. The joint load-deformation curves of the DK truss segments were used to find the four test loads corresponding to the loads defined in Fig 3 11 Values of these, expressed as the component normal to the chord wall, are given in Table 4 4 Only four of the seven DK trusses failed in modes 1 or 2, and in three of these web member instability also occurred

4 3 1 Comparison with Yield Line Theory

Because of the correlation of the yield line theory with the measured loads of the DT specimens, the theory is here applied to the DK truss joints Four simple yield line mechanisms are postulated in Chapter 5, the lowest of the four yield loads giving the appropriate solution. More refined mechanisms for these trusses have been considered by Santagata (1982) These were based on the observed chord wall deformations and minimization of the yield load was not performed In most cases the simple mechanisms considered herein gave lower loads than those given by these more refined mechanisms Further refinements of the basic mechanisms for DT joints and the application of these refinements to DK joints are described in Chapter 5

The ratio of experimental yield load to theoretical value varies from 1 03 to 1.28 for the four DK trusses These results are shown in Fig 4 8, together with test values of the ultimate load Y_u. The load corresponding to deflections of 0.01 b_0 are compared with the yield line theory on Fig. 4.9. Close correspondence exists, and it can be seen that the spread between this load and that corresponding to 0.06 b_0 deflection is much smaller than for the DT specimens, i.e. the DK joints are stiffer than the DT joints.

The ratios of test load to theoretical load for the DK tests are also

shown on Figs. 4 3 to 4.5. No consistent variation with α, β or b_0/t_0 can be seen other than that predicted by the yield line theory, and the DK truss results fall within, or slightly above, the range of values obtained from the DT tests

4 3 2 Correlation between DT Joint Specimens and DK Truss Segments

The DT joint test specimens were intended to represent the main features of the compression web members in a DK or DN truss gap joint It is shown in Chapter 5 how, for a certain length of the joint gap, the yield line theory predicts the same resistance for a planar T joint as for a planar K or N joint The DK test trusses had gap lengths which were not significantly different from these theoretical values While this suggests that there may be some agreement between the yield loads of the two types of joint, other differences between them must be accounted for if a comparison is to be valid Chief among these is the magnitude of η ($=h_1/b_0$) which in the truss specimens must be adjusted to η cosecθ Other differences arise because of relatively small differences between the values of β and ξ

The expected differences due to these three parameters are eliminated in the way indicated in Table 4 5, where the ratio of DK truss yield load to adjusted DT specimen yield load is given in column (10) For DK truss 4, the differences between the β, ξ and η values of DK and DT specimens were sufficiently large that different mechanisms apply to the two cases (cols (5) and (7)) This may explain the low value of the ratio (0 801) For the other cases the ratio of DK to DT specimen loads vary from 0.95 to 1 13

4.3.3 Application of Planar Truss Joint Strength Equations

CIDECT Recommendations

The ultimate strength of K and N type planar truss joints can be predicted by the following (Wardenier 1982)

$$Y_{u1} = N_{u1} \sin\theta_1 = 7\ 7\ F_{y0}\ t_0^2 \left(\frac{b_0}{t_0}\right)^{0.5} \beta\ f(n) \qquad [4\ 2]$$

where β is now defined as $\frac{b_1 + b_2 + h_1 + h_2}{4b_0}$ and N_{u1} is the axial force in the compression web member at joint failure

In applying this equation to the DK truss joints, β is taken as

$$\beta = \frac{b_1 \sec(45^\circ - 0.5\alpha) + b_2 \sec(45^\circ - 0.5\alpha) + h_1 + h_2}{4b_0} \qquad [4\ 3]$$

in order to account for the contact width of the web members It can be seen in Table 4.6 that values based on this equation overestimate the DK truss segment test results.

Sheffield Equations

The lower bound empirical equation proposed for planar trusses by Eastwood and Wood (1970) has been used to compare with these triangular truss test results (Redwood and Bauer 1983), and gives a safe estimate of the maximum test loads. These values also are given in Table 4 6

Comment

The CIDECT planar truss joint strength equation significantly overestimates the ultimate test load of DK Trusses 1 and 4 It gives a good prediction of this load for DK Trusses 3 and 6 The Sheffield equation gives a safe estimate, with the strength underestimate varying from 0 to 61%. The yield line analysis (Chapter 5, Eqs. 5.2.24 to 5.2.33) gives a safe estimate of yield or "ultimate" loads, as defined in §3.4.2, and its variability is

much less than either the CIDECT or Sheffield predictions

4.3.4 Web Member Buckling

Compression web member buckling was observed in five of the seven truss tests, although in several cases it could not be described as a primary cause of failure For example, in Truss 5, buckling took place as the truss deformed following yield of the tension members, and in Truss 1 web member buckling took place when chord wall deformations at the joint were significant

Treating the compression web member as an axially loaded strut, the compressive resistance has been calculated according to Specification CAN3-S16.1-M84, Clause 13 3.2 Since the degree of end fixity is uncertain, values of the compressive resistance have been calculated for two effective length factors, 0.7 and 0.9, and these are given in Table 4 7 These values are based upon ϕ = 1 0, and are expressed as the shear load on the truss specimen which would produce a compressive load in the web members equal to their resistance, the analysis assuming the truss to act as a pin-jointed structure It should be noted that secondary moments in the web members arising from eccentricity have been ignored in evaluating their resistance

It can be seen that in two cases where web member buckling occurred and where chord deformations at the joints were significant (Tests 1 and 6), the ultimate load corresponded to web member buckling with an effective length factor of approximately $K \approx 0.9$. In the other two cases where joint deformations were large, one, Truss 4, did not experience web member buckling, and the other, Truss 3, had stocky compression members so that the resistance was only slightly below the squash load for the member and was therefore insensitive to variations in K.

In truss 5, in which little chord deformation occurred, web member

buckling occurred with K ≈ 0 7. In truss 2 reinforcement was added to the compression web members during the test as buckling appeared to be imminent, and one of these members buckled with an estimated K value of 0 75.

From these results it is apparent that the loss of stiffness as the joint deforms can have a significant effect on the strength of the web compression member It should also be noted that in the test trusses, the far ends of the web members were connected to a joint which was quite rigid due to attachment of the end members with overlap No yield was observed at these joints

4 3 5 Conclusions

Specific conclusions are summarized below

1. By accounting for differences in the main parameters (η, ξ, and β) between a DK and the corresponding DT specimen (i.e., same chord and web member) the DT specimens give a close prediction of the DK yield loads in three cases out of four. This suggests that the gap size is such that interaction between the adjacent members has little influence

2. The yield line theory applied to DK trusses safely predicted the measured yield loads. The ratios of test to yield line load lie within, or slightly above, the range of values obtained from the DT specimens.

3. Joint strength predictions forming the basis of current design methods for planar trusses are inferior to the yield line method given herein, when applied to the DK truss test results. The latter gives less variability than the CIDECT or Sheffield equations. The CIDECT equation for ultimate strength seriously overestimates the yield or ultimate loads of two of the DK trusses, whereas the Sheffield equation gives a generally safe prediction

4. Web member buckling is more critical in the DK truss tests than in the DT joint tests. Effective length factors of K ≈ 0.9 were observed in truss tests where joint deformations were significant, whereas values of K ≈ 0.7 were

observed in tests where joint deformations were small This suggests that the loss of stiffness as the joint deforms lowers the resistance of the compression web members in triangular trusses

Before considering design recommendations (Chapter 6), the theoretical yield line mechanisms for DT joints and triangular truss DK joints are investigated in the next chapter

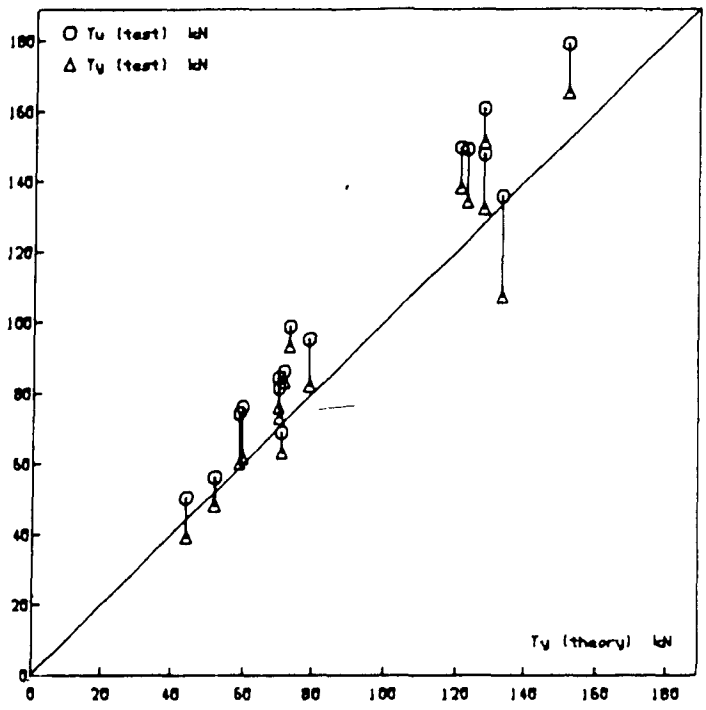

Fig. 4.1 Test values of the normal loads on the chord walls Y_u and Y_y vs. yield line theory results. Joint tests 1 to 12 and 21 to 24.

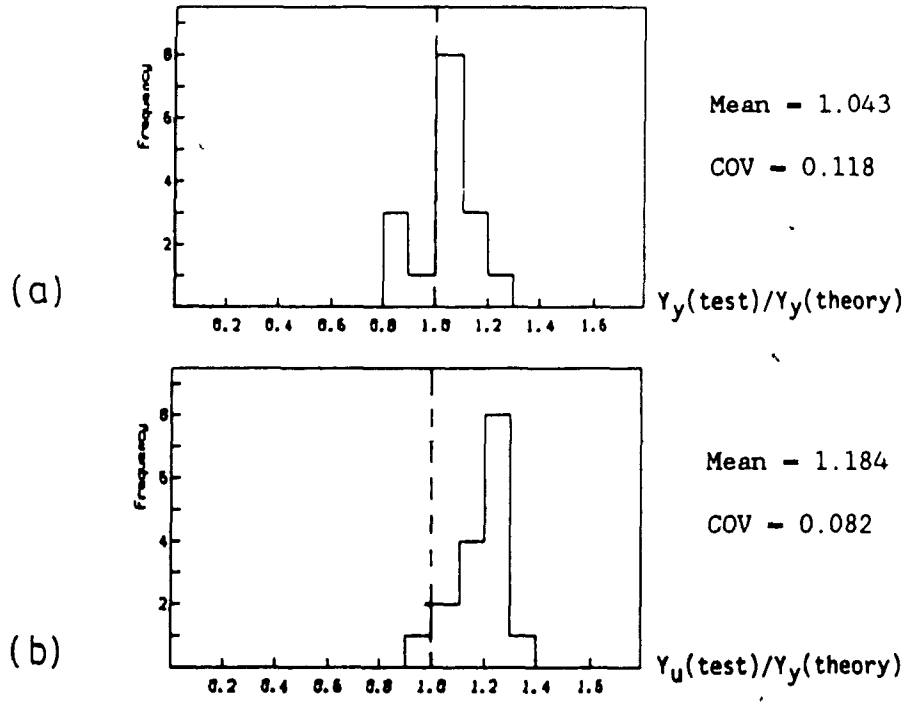

Fig. 4.2 Distribution of the ratios of test load to theoretical yield load. Joint tests 1 to 12 and 21 to 24 - (a) Test yield load vs. theoretical yield load. (b) Test ultimate load vs. theoretical yield load.

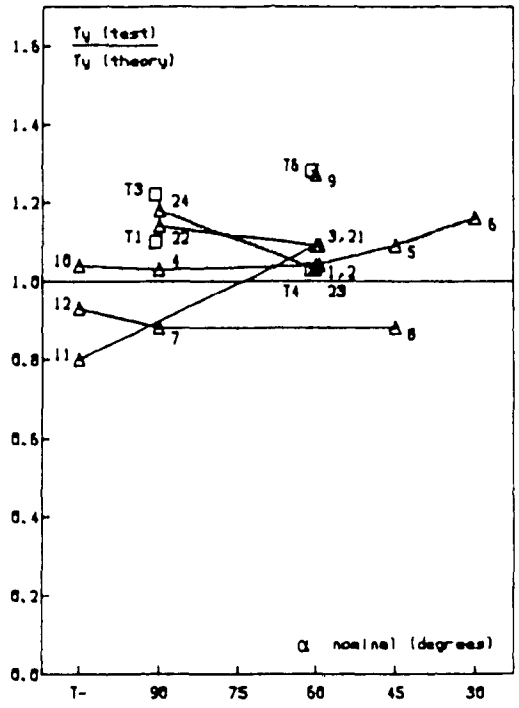

Fig. 4 3 Ratios of test yield load to theoretical yield load vs. α.

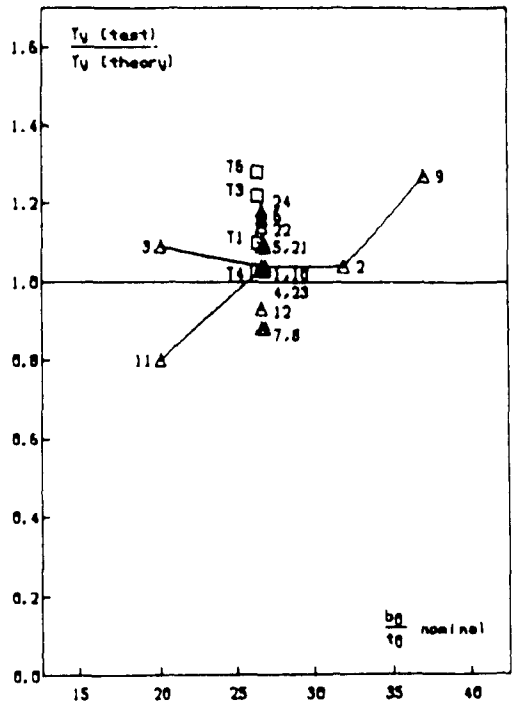

Fig 4 5 Ratios of test yield load to theoretical yield load vs. b_o/t_o

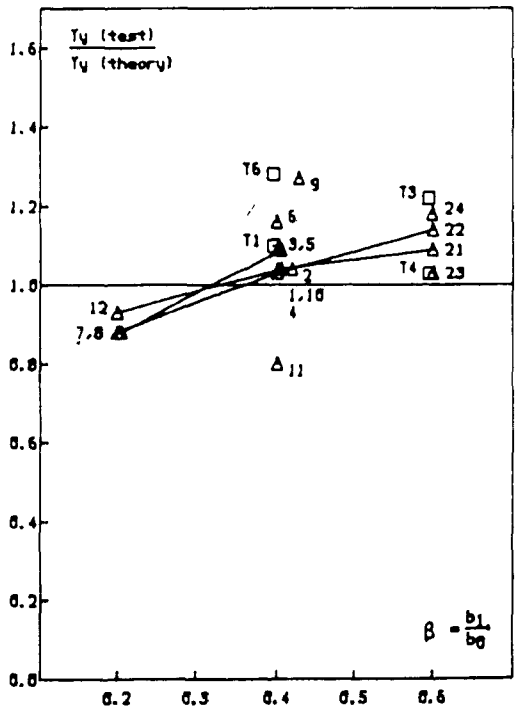

Fig. 4.4 (a) Ratios of test yield load to theoretical yield load vs. β.

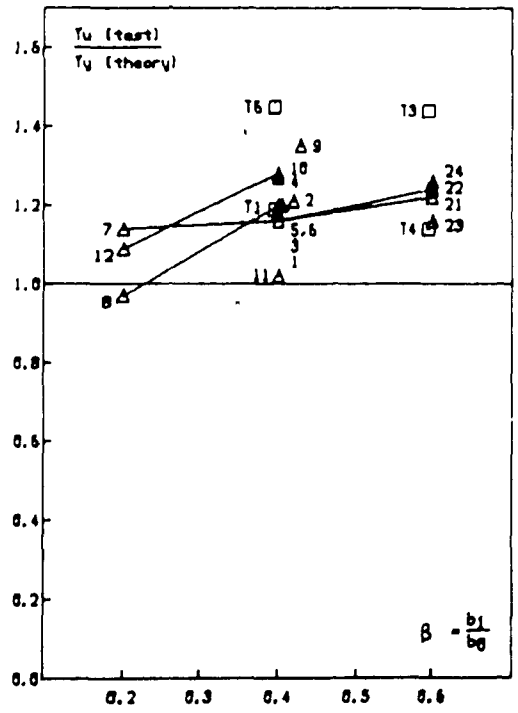

Fig. 4.4 (b) Ratios of test ultimate load to theoretical yield load vs. β.

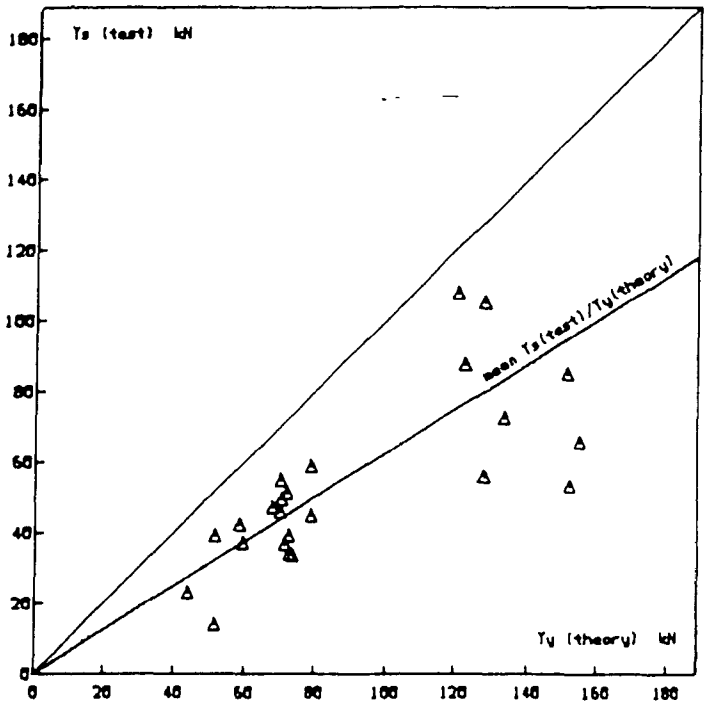

Fig 4.6 Test service loads (at a joint deformation of 1% b_0) vs. yield line theory results. Joint tests 1 to 12 and 21 to 24

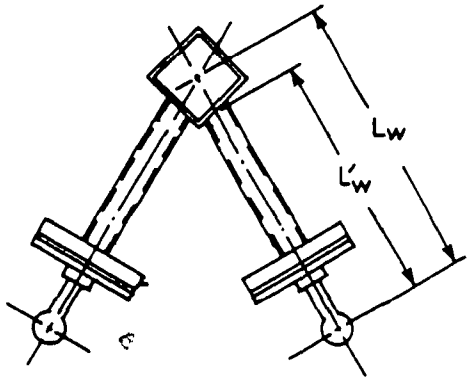

Fig. 4.7 Web member length. Joint tests.

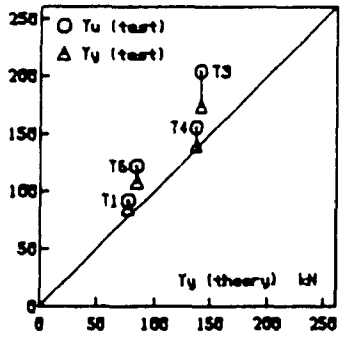

Fig. 4.8 Test yield and ultimate loads vs. theoretical yield loads. Truss tests.

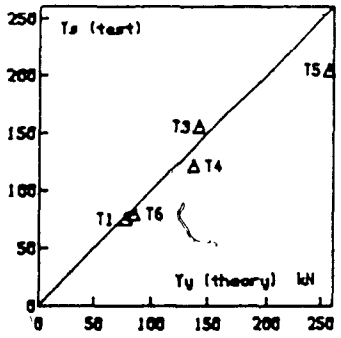

Fig. 4.9 Test service loads (at a joint deformation of 1% b_0) vs. theoretical yield loads. Truss tests.

Table 4 1 Yield loads for 90° DT and planar T specimens Joint tests

Test	α deg.	Normal Chord Loads Y_y (kN)			
		Measured in Test	Yield Line Theory Actual Properties	Yield Line Theory Nominal Properties	Test load Normalized (3)*(5)/(4)
(1)	(2)	(3)	(4)	(5)	(6)
4	90	60.0	58.4	59.3	60.9
7	90	39.0	44.1	44.1	39.0
10	T-	61.5	59.3	59.3	61.5
11	T-	107.0	133.0	113.8	91.6
12	T-	48.0	51.5	44.1	41.1
22	90	138.0	120.6	104.9	120.0
24	90	151 0	127.5	124.4	147.3

Table 4 2 Summary of results for Mode 3 failures Joint tests

Test	α (nominal) (deg.)	Measured Web Member Load at Failure N_y (kN)	C_r*	$\frac{N_{cr}}{C_r}$	Effective Length Factor + K	Normalized Web Member Test Load N_{cr} (kN)	Normalized Yield Value from Test N_y (kN)
13	60	71.4	62.1	1.15	0.92	75.6	-
14	60	142.8	133.2	1.07	0.96	124.5	115.3
15	60	62.7	54.5	1.15	0.92	64.1	-
16	60	138.0	109.9	1.26	0.88	127.6	-
17	90	67.8	50.8	1.33	0.85	72.0	-
18	45	71.5	57.4	1.25	0.88	72.9	-
19	90	64.5	42.7	1.51	0.80	55.6	43.6
20	T-	68.9	52.6	1.31	0.86	71.0	56.1

* C_r given by SSRC Column Curve No.1, using measured properties, and the length L_w' with K = 1.0 (see Fig. 4.7).

+ K is based upon length L_w'.

Table 4.3 Web member instability. Variation with α. Joint tests.

Test	α deg.	L_w'/r	Normalized Web Member Failure Load N_{cr} (kN)	Effective Length Factor K
20	T-	134	71.0	0.86
17	90	131	72.0	0.85
15	60	134	64.1	0.92
18	45	128	72.9	0.88

Table 4.4 Test and theoretical values of chord wall normal loads
Truss tests

Double-K Truss Segment Test	Load at 0.01 b_0 defn. Y_s^+	Yield Load Y_y^+	Test Value Ultimate Load 0.06 b_0 defn. Y_u^+	Maximum Load Y_{max}	Failure Mode	Yield Line Theory Y_y	$\frac{Y_y(test)}{Y_y(theory)}$
DK-1	75.3	84.9	91.6	93.1	1,3	77.0	1.10
DK-2	107.7	-	-	110.0	3	(g=0)	-
DK-3	155.6	172.9	202.9	216.0	2,3	141.2	1.22
DK-4	121.0	139.6	155.6	172.0	2	135.9	1.03
DK-5	204.1	-	-	204.1	3	255.7	-
DK-6	79.2	107.4	122.1	139.1	1,3	84.0	1.28
DK-7	-	-	-	312.4	-	975.8	-

All loads given in kN.
+ The average of values obtained from each side is given.

Table 4 5 Normalization of DT joint test results Comparison with DK truss segment tests.

Double-K Truss Segment Test	Test Y_y/m_p Double-K Truss Segment	Corresp. Double-T Joint Specimen	Test Y_y/m_p Double-T Joint Specimen	Y_y(theory)* (kN)	Col.(5) based on Eqn.:	Y_y(theory)** (kN)	Col.(7) based on Eqn.:	Normalized Double-T Joint Specimen Y_y/m_p	(2)/(9)
(1)	(2)	(3)	(4)	(5)	(6)	(7)	(8)	(9)	(10)
DK-1	38.39	4	30.30	58.4	(5.2.16)	78.15	(5.2.16)	40.54	0.947
DK-3	77.04	22	59.53	120.6	(5.2.16)	148.02	(5.2.16)	73.04	1.055
DK-4	61.16	21	61.47	122.6	(5.2.16)	152.32	(5.2.20)	76.35	0.801
DK-6	52.32	1	35.94	70.3	(5.2.20)	90.42	(5.2.20)	46.22.	1.132

* Y_y(theory) based on lower value from Eq. (5.2.16) or (5.2.20) using measured properties of double-T specimens.

** Y_y(theory) based on lower value from Eq. (5.2.16) or (5.2.20) using measured properties of corresponding double-K truss specimens.

\+ Col.(9) obtained from (4)x(7)/(5).

Table 4.6 Comparison of DK truss test results with various predictor equations.

Double-K Truss Segment Test	Test Values Y_y	Test Values Y_u	Predictor Equations: Yield Line Theory	Predictor Equations: CIDECT Eq.(4.2)	Predictor Equations: Sheffield (Eastwood and Wood 1970)
DK-1	84.9	91.6	77.0	139.5	95.2
DK-3	172.9	202.9	141.2	210.2	155.8
DK-4	139.6	155.6	135.9	215.4	155.1
DK-6	107.4	122.1	84.0	132.7	86.4

All loads given in kN.

Table 4.7 Maximum loads from tests and design equations Truss tests

Truss No.	V_{test}	$V_{chord\ face}$ +	V_{gap} +	$V_{buckling}$ + K=0.7	$V_{buckling}$ + K=0.9
DK-1*	125.9	104.1	296	153	129
DK-2	155.6	(g=0)	334	160	143
DK-3*	288.6	188.7	263	289	273
DK-4*	281.5	222.4	255	328	313
DK-5	288.6	361.6	509	281	222
DK-6*	249.4	150.6	262	307	260
DK-7	441.8	1380.0	437	811	724

Notes:

+ $V_{chord\ face}$ is calculated using Eqs. [6.1] to [6.9].
V_{gap} is calculated using Eq. [6.10].
$V_{buckling}$ is calculated using Clause 13.3.2 of CAN3-S16.1-M84.
ϕ is taken as unity since measured member properties were used in calculations.

* Significant chord wall deformation occurred in these tests.
All loads given in kN.

CHAPTER 5 YIELD LINE THEORY AND APPLICATIONS

The first section of this chapter gives a brief introduction to the yield line theory. The second section presents yield line equations that can be used for predicting the yield resistance of the simplified DT joints as well as the triangular truss DK joints The basic mechanisms on which the equations are based incorporate the off-centering of the web members typical of triangular truss joints. DK joints with different sized and off-centered tension and compression web members are treated, and hence the equations presented herein are more general than those presented by Bauer and Redwood (1985) which assumed same sized and same off-centered web members.

Refinements to the basic mechanisms for DT joints are considered in the rest of the chapter (§5.3 to 5.5). The refinements include varying the position of the end yield lines on the chord face, analysing mechanisms with fans and finally taking into account the effect of normal stresses in the chord corners. The application of these refinements to triangular truss DK joints is also discussed.

5.1 YIELD LINE THEORY

The yield line method is a simple and efficient method to calculate the plastic collapse load of flat, relatively thin, plates of rigid-perfectly plastic material when transversely loaded in bending The method was developed largely by Johansen (1943) and since then, it has been applied successfully to both concrete and steel plates (Jones and Wood 1967, Park and Gamble 1980, Jubb and Redwood 1966)

The yield line theory is briefly reviewed below. However, a basic understanding of the yield line theory is assumed in the following discussion

and the reader is referred to standard texts on the subject (see for example Johansen 1943 and Jones and Wood 1967)

The yield line method is based on the kinematic theorem of the plastic theory of structures and gives an upper bound solution for the collapse load of a plate.

In the yield line method, a plastic collapse mechanism of the plate is assumed consisting of undeformed plate segments connected by plastic hinge lines, called yield lines. The mechanism must be kinematically admissible over the whole plate and at the boundaries The bending moment distribution is not considered and, in general, the equilibrium conditions are not verified

There are two solution approaches in the yield line theory the virtual work method and the so-called equilibrium method Both methods lead to identical upper bound solutions, and it has been demonstrated that both methods represent in fact the same solution, but with a different approach (Jones and Wood 1967) The virtual work method is simpler in principle and is used for the calculations presented herein The virtual work method is outlined below.

In this method, a plastic collapse mechanism is assumed for a given plate and loading, and the collapse load P is found by equating the work done by the external load on the plate, E, to the internal work dissipated by the yield lines, D, during a small motion of the assumed collapse mechanism, viz,

$$E = D \qquad [5.1.1]$$

i.e.

$$P\delta = \sum_{j=1 \text{ no of yield lines}} m_{p,j}\theta_j l_j \qquad [5.1.2]$$

P is the applied load, acting through a virtual displacement δ. The

minimum load which would cause plastic collapse is termed the collapse or yield load P_{min}. $m_{p,j}$'s are the plastic moment resistances per unit length, θ_j's are the rotations, and l_j's are the lengths of every yield line in the assumed mechanism

Since the yield line method leads to an upper bound solution, different mechanisms as well as different dimensions for each mechanism must be tried in order to find the lowest predicted load P_{min} For simple problems, the optimum solution can be found directly by differentiation. For complex problems, a trial and error technique is faster and usually satisfactory (Jones and Wood 1967, Park and Gamble 1980)

5 2 BASIC MECHANISMS

5 2 1 DT Joints

For a DT joint in which the web members are centered on the chord face, the failure mechanism, shown in Fig 5 1, is the same as for a planar T joint For the yield line model and loading illustrated, the yield line method gives the perpendicular load on the chord wall at yielding failure of the wall as

$$\frac{Y}{m_p} = 4\ (\bar{h}_1 + 2d)\ \frac{1}{a} + \frac{4\ b_0}{d} \qquad [5\ 2\ 1]$$

where d is found by minimizing Y, i.e. by solving $\frac{dY}{dd} = 0$ leading to

$$d = \sqrt{\frac{b_0\ a}{2}} \qquad [5.2.2]$$

Substituting d from Eq. [5.2.2] into Eq [5 2.1] gives

$$\frac{Y_{min}}{m_p} = 4\ \left(\ \frac{\bar{h}_1}{a} + 2\ \sqrt{\frac{2\ b_0}{a}}\ \right) \qquad [5.2.3]$$

in which $m_p = 0.25\ t_0^2\ F_{y0}$, the plastic moment per unit width of the chord wall,

b_0 is the chord width,

$$a = \frac{(b_0 - \bar{b}_1)}{2}, \qquad [5\ 2.4]$$

and $\bar{b}_1$ and $\bar{h}_1$ are the outside contact dimensions of the web members on the chord face.

On a triangular truss tension chord, the contact dimensions of the web members are

$$\bar{b}_1 = \frac{b_1}{\cos\left(45^\circ - \frac{\alpha}{2}\right)} \quad \text{and} \quad \bar{h}_1 = \frac{h_1}{\sin\theta} \qquad [5\ 2\ 5]$$

and on a compression chord, the web members contact dimensions are

$$\bar{b}_1 = \frac{b_1}{\cos\left(\frac{\alpha}{2}\right)} \quad \text{and} \quad \bar{h}_1 = \frac{h_1}{\sin\theta} \qquad [5.2\ 6]$$

where b and h are the web member sizes. α is the angle between the web members and θ is the angle between the web members and the chord axes ($\theta = 90^\circ$ in DT joints).

To account for the weld size and the curvature at the corners of the chord, the nominal width ratio is adjusted as follows (see, for example, Kato and Nishiyama 1979), as shown in Fig. 5.2,

$$\bar{b}' = \bar{b} + 2S \qquad [5.2.7]$$

$$\bar{h}' = \bar{h} + 2S \qquad [5.2.8]$$

$$b_0' = b_0 - (4-1.5\sqrt{2})t_0 = b_0 - 1.88t_0 \qquad [5.2.9]$$

in which S = weld leg size and t_0 = wall thickness of chord.

Using an alternate notation based on unit chord width, as shown in Fig. 5.3, and defining

$$\xi = \frac{a}{b_0}, \quad \beta = \frac{\bar{b}_1}{b_0}, \quad \eta = \frac{\bar{h}_1}{b_0}, \quad \delta = \frac{d}{b_0}, \qquad [5.2.10]$$

Eq [5 2 3] can be written as

$$\frac{Y_{min}}{m_p} = 4 \left(\frac{\bar{\eta}}{\xi} + 2 \sqrt{\frac{2}{\xi}} \right) \qquad [5.2\ 11]$$

Since $a = \frac{b_0 - \bar{b}}{2}$ or $\xi = \frac{1-\bar{\beta}}{2}$, Eq. [5.2.3] can also be written as

$$\frac{Y_{min}}{m_p} = 8 \left(\frac{\bar{\eta}}{1-\bar{\beta}} + \frac{2}{\sqrt{1-\bar{\beta}}} \right) \qquad [5\ 2\ 12]$$

All the equations in this chapter can be written using this unit chord width notation if necessary

For many DT joints, the web members are not centered on the middle of the chord face in order to minimize eccentricity The essential effects of this can be determined by analysing the yield line model shown in Fig 5 4, hereafter called basic mechanism DT-1 Assuming a normal load on the chord wall, and no rotation of the web member relative to the chord, the yield load is given by

$$\frac{Y}{m_p} = 2 (\bar{h} + 2d) (\frac{1}{a} + \frac{1}{c}) + \frac{4\ b_0}{d} \qquad [5.2.13]$$

where d is found by minimizing Y, i e by solving $\frac{dY}{dd} = 0$ leading to

$$d = \sqrt{\frac{b_0}{\frac{1}{a} + \frac{1}{c}}} \qquad [5.2\ 14]$$

Substituting d from Eq. [5.2.14] into Eq. [5.2.13] gives

$$\frac{Y_{min}}{m_p} = 2\ \bar{h}\ (\frac{1}{a} + \frac{1}{c}) + 8 \sqrt{b_0}\ \sqrt{\frac{1}{a} + \frac{1}{c}} \qquad [5.2.15]$$

Using unit chord width notation, Eq. [5.2.15] can be written as

$$\frac{Y_{min}}{m_p} = 8 \left[\frac{\bar{\eta}}{4\xi \left(1 - \frac{\xi}{1-\bar{\beta}}\right)} + \frac{1}{\sqrt{\xi}\sqrt{1 - \frac{\xi}{1-\bar{\beta}}}} \right] \qquad [5.2.16]$$

in which $\xi = a/b_0$.

As before, the dimensions a, $\bar{b}_1$, $\bar{h}_1$ and b_0 can take account of the corner curvature and the weld size, and $\bar{b}_1$ accounts for the slightly wider contact width of the web member in those cases where $\alpha \neq 90^0$.

When the web member is significantly off-center, it becomes more likely that a different mechanism (from mechanism DT-1 in Fig. 5 4) involving rotation of the web member in a plane normal to the chord axis takes place. A simple representative mechanism, hereafter called basic mechanism DT-2, is shown in Fig 5.5.

Assuming that no work is done in the rotation (i.e. that the bending moment in the web member is zero), the yield load normal to the chord wall is given by

$$\frac{Y}{m_p} = \frac{2}{\frac{\bar{b} + 2c}{2(\bar{b} + c)}} \left[(\bar{h} + 2d) \left(\frac{1}{a} + \frac{1}{\bar{b} + c} \right) + \frac{2 b_0}{d} \right] \qquad [5\ 2\ 17]$$

where d is found by minimizing Y, i.e. by solving $\frac{dY}{dd} = 0$ leading to

$$d = \sqrt{\frac{b_0}{\frac{1}{a} + \frac{1}{\bar{b} + c}}} \qquad [5.2.18]$$

Substituting d from Eq. [5.2.18] into Eq. [5.2.17] gives

$$\frac{Y_{min}}{m_p} = \frac{2}{\frac{\bar{b} + 2c}{2(\bar{b} + c)}} \left[\bar{h} \left(\frac{1}{a} + \frac{1}{\bar{b} + c} \right) + 4 \sqrt{b_0} \sqrt{\frac{1}{a} + \frac{1}{\bar{b} + c}} \right] \qquad [5.2.19]$$

Alternatively, using unit chord width notation,

$$\frac{Y_{min}}{m_p} = \frac{8}{2(1-\xi) - \bar{\beta}} \left[\frac{\bar{\eta}}{2\xi} + \frac{2\sqrt{1-\xi}}{\sqrt{\xi}} \right] \qquad [5.2.20]$$

Values of Y_{min} for mechanisms DT-1 and DT-2 are given in Tables 5 1 and 5.2, respectively. The joint parameter $\bar{\beta}$ is varied from 0.2 to 0 8 and λ is varied between 0.5 and 1 0, where λ is a measure of the web member off-centering, defined as

$$\lambda = \frac{a}{a + c} = \frac{\xi}{1 - \bar{\beta}} \qquad [5\ 2\ 21]$$

Possible values of λ range from 0.5 for centered web members up to 1.0 for web members completely off-centered, that is, with one side of the web member along the corner of the chord.

For a given DT joint configuration the appropriate value of the theoretical yield load, Y_{min}, for that joint is the lower of the two upper bound solutions, Eqs [5.2 15] and [5 2.19], for mechanisms DT-1 and DT-2. These values are located above the thick line in Table 5 1 and below it in Table 5.2 For clarity, these lower values are repeated in Table 5 3 with the corresponding governing mechanism It can be seen that mechanism DT-1 governs for small values of λ and $\bar{\beta}$, while mechanism DT-2 governs for large values of these parameters.

The importance of selecting the correct mechanism is demonstrated by the percentage difference between the higher and the lower predicted loads, given on the 3rd lines in Table 5.3. For example with $\bar{\beta}$ = 0 8 and λ = 0.5, mechanism DT-1 governs and predicts a load 15% lower than mechanism DT-2 For λ = 0.9, mechanism DT-2 predicts a load 58% lower than mechanism DT-1.

5.2.2 DK Joints

Yield line analysis in its simple form has been applied to K and N planar truss joints by Davies and Roper (1975) for centered and equal sized tension and compression web members and Mouty (1977) for centered and different sized

web members. For trusses with centered and equal sized web members with equal inclinations to the chord axis, the yield line mechanism shown in Fig. 5 6 gives the following yield load normal to the chord wall

$$Y_y = 8\, m_p \left[\frac{\bar{\eta}\ \mathrm{cosec}\theta}{1-\bar{\beta}} + \frac{1}{\sqrt{1-\bar{\beta}}} + \frac{1}{4\gamma} + \frac{\gamma}{2(1-\bar{\beta})} \right] \qquad [5.2.22]$$

where $\gamma = g/b_0$ in which g is the gap dimension, and $\bar{\eta} = \bar{h}_1/b_0$, etc.

It is of relevance to note that comparison of Eqs. [5.2.12] and [5.2.22] show that the normal yield load is identical for T-joint and K-joint if the gap dimension satisfies the following:

$$\gamma = \frac{g}{b_0} = \sqrt{1-\bar{\beta}} - \bar{\eta}(\mathrm{cosec}\theta - 1) \pm \sqrt{\left[\sqrt{1-\bar{\beta}} - \bar{\eta}(\mathrm{cosec}\theta - 1)\right]^2 - \tfrac{1}{2}(1-\bar{\beta})} \qquad [5.2.23]$$

For triangular truss DK joints with web members of sizes and off-centered positions on the chord face having possibly different values for the compression and tension web members, the four yield line mechanisms DK-1, DK-2, DK-3 and DK-4, shown in Fig. 5.7, model possible modes of chord face failure. Mechanism DK-1 involves only punching in and pulling out of the web members whereas mechanism DK-2 involves also rotation of the web members These mechanisms correspond to mechanisms DT-1 and DT-2 for the DT joints. Mechanisms DK-3 and DK-4 are combinations of those two modes of deformation.

The predicted joint resistance, Y, based on the yield line mechanisms DK-1, -2, -3 and -4 is given by

$$\frac{Y}{m_p} = \frac{2}{\left(M + N\,\frac{g-x}{x}\right)} \left(K\,(\bar{h}_1+d_1+x) + L\,(\bar{h}_2+d_2+g-x)\,\frac{g-x}{x} + \frac{b_0}{d_1} + \frac{b_0}{d_2}\frac{g-x}{x} + \frac{b_0}{x} \right) \qquad [5.2.24]$$

where K, L, M, and N are defined in Table 5.4.

For each mechanism, the values of d_1, d_2 and x that minimize the load Y are found by differentiating Y with respect to d_1, d_2 and x and equating to zero

$$\frac{dY}{dd_1} = 0 \ , \quad \frac{dY}{dd_2} = 0 \ , \quad \frac{dY}{dx} = 0 \qquad [5\ 2\ 25]$$

which for all mechanisms leads to

$$d_1 = \sqrt{\frac{b_0}{K}} \ , \quad d_2 = \sqrt{\frac{b_0}{L}} \ , \qquad [5\ 2\ 26]$$

and, if the solution for x lies in the range $0 < x < g$, then the solution is

$$x = \frac{-q \pm \sqrt{q^2-4pr}}{2p} \ , \qquad [5\ 2\ 27]$$

or

$$x = -\frac{r}{q} \ , \qquad [5\ 2\ 28]$$

where

$$p = \frac{1}{g}\ (K+L)\ (M-N)$$

$$q = 2\ N\ (K+L) \qquad [5.2\ 29]$$

$$r = (\bar{h}_1+d_1)\ KN - (\bar{h}_2+d_2+g)\ LM + \frac{b_0}{d_1} N - \frac{b_0}{d_2} M - \frac{b_0}{g} (M-N) - g\ LN$$

Eq. [5.2.27] is used when $p \neq 0$ while Eq. [5 2.28] is used when $p = 0$, i.e. when $M = N$ If the value of x obtained from Eqs [5.2.27] or [5 2.28] is negative, greater than g, or imaginary, the above solution is not valid and the solutions $x = 0$ and $x = g$ must be considered as follows.

When $x = 0$, mechanisms DK-1 and DK-4 and mechanisms DK-2 and DK-3 become identical with no displacement of the compression web member, as shown in Fig. 5.8a, and Eq. [5.2.24] simplifies to

$$\frac{Y}{m_p} = \frac{2}{N} \left[L\ (\bar{h}_2+d_2+g) + \frac{b_0}{d_2} + \frac{b_0}{g} \right] \qquad [5.2.30]$$

for which Y is minimum at

$$d_2 = \sqrt{\frac{b_0}{L}} \qquad [5\ 2.31]$$

When $x = g$, mechanisms DK-1 and DK-3 and mechanisms DK-2 and DK-4 become identical with no displacement of the tension web member, as shown in Fig. 5.8b, and Eq. [5 2.24] simplifies to

$$\frac{Y}{m_p} = \frac{2}{M}\left[K\ (h_1+d_1+g) + \frac{b_0}{d_1} + \frac{b_0}{g} \right] \qquad [5.2\ 32]$$

for which Y is minimum at

$$d_1 = \sqrt{\frac{b_0}{K}} \qquad [5.2.33]$$

Note that the applied force component, normal to the chord face, of the compression web member is $Y_1 = Y$, and that of the tension web member is $Y_2 = \Lambda Y$. By using the ratio of applied force components $\Lambda = Y_2/Y_1$, the applied loads can be expressed in terms of only one unknown, as is commonly done in plastic structural analysis (Neal 1977) For tension chord joints, Λ is usually equal to 1. When the above equations are applied to compression chord joints, the value of Λ is usually $\neq 1$ because of purlin loads.

The above equations yield valid solutions even when one of the web members has the same width as the chord. When $\beta_1 = 1$ and $\beta_2 < 1$, $x = 0$ and Eq. [5.2.30] applies. When $\beta_2 = 1$ and $\beta_1 < 1$, $x = g$ and Eq. [5.2.32] applies. If both $\beta_1 = 1$ and $\beta_2 = 1$, then no solution can be obtained from the above equations. However for such a full width joint, side wall crippling or the conditions in the gap are certainly the governing failure modes (see Chapter 6).

For any DK joint configuration the correct Y_{min} for that joint is the

lowest of the minimum loads for mechanisms DK-1, -2, -3 and -4, the minimum load being, for each mechanism, the lowest of the three possible solutions, namely $0 < x < g$, $x = 0$, and $x = g$. Such values of Y_{min} and the corresponding governing mechanism (either DK-1, -2, -3 or -4) are given in Table 5.5 for the joint parameters γ ($=g/b_0$) varying between 0.1 and 0.4, $\bar{\beta}_i$ between 0 2 and 0.8, λ_i between 0.5 and 0.9, and for a ratio of the contact dimensions $\bar{h}_i/\bar{b}_i$ of the web members on the chord face equal to 1. Mechanism DK-1, involving no rotation of the web members, governs for small values of λ_i, $\bar{\beta}_i$ and γ, while mechanisms DK-2, -3 and -4 govern for large values of these parameters.

In Table 5.5, a value of $\bar{h}_i/\bar{b}_i = 1$ was chosen for simplicity This value corresponds to the case of square web members ($h_i = b_i$) connected to the chord at an angle $\alpha = 90°$ and $\theta_i = 90°$, and it corresponds also to the geometry of a simple DT joint with $h_i = b_i$, $\alpha = 90°$ and for which always $\theta_i = 90°$ However, it should be noted that Eq. [5.2 24] can be used to calculate the strength of a joint with different $\bar{h}_i$ and $\bar{b}_i$ values, for example a DK joint with $\alpha = 60°$, $\theta_i = 45°$, $h_i = 1\ 5b_i$ (rectangular web members). Hence $\bar{h}_i = 1\ 41h_i$, $\bar{b}_i = 1\ 04b_i$ and $\bar{h}_i = 2.05\bar{b}_i$, or if $h_i = \frac{b_i}{1.5}$ then $\bar{h}_i = 0.9\bar{b}_i$.

5.3 MECHANISMS WITH INCLINED END YIELD LINES

A variation of the basic mechanisms DT-1 and DT-2 for DT joints is investigated below, where the end yield lines on the chord face are permitted to make an angle other than 90° with the chord axis. These mechanisms are hereafter called DT-1-E and DT-2-E, in which 'E' stands for End yield lines.

5.3.1 Mechanism DT-1-E

A representative mechanism is shown in Fig 5 9 (the same mechanism is shown several times for different cases, as explained later). Similarly to basic mechanism DT-1, the web member is assumed not to rotate in relation to the chord. Additional yield lines now appear on each side of the web member as required for compatibility of deformations.

The mechanism is defined by 3 independent parameters, d as in basic mechanism DT-1, Ω defining the angle that the end yield lines make with the chord axis, and f locating the new yield lines.

The mechanism is shown in Fig. 5.9 for different cases of positive and negative Ω, and for $f = 0$ and $f = b_0$. These different mechanisms correspond to the different patterns in which the yield lines are hogging and sagging (hogging and sagging lines are identified as H and S in Fig. 5.9). The equations obtained for each case are different and hence should be used only with the appropriats values of Ω and f. This kind of problem where some yield lines switch from sagging to hogging or vice versa, leading to different equations, occurs in several problems and can easily be overlooked. It is not unreasonable to think that a unique equation could cover all the different cases, however such an equation was not found.

The expressions for the energy dissipated by the yield lines were derived using conventional vector addition rules for yield line calculations (see for example Johansen 1943, Wood and Jones 1967, Mills 1970). Furthermore, the yield line equations were checked against results from a numerical yield line analysis method developed by the author (Bauer 1986, Bauer and Redwood).

The yield load normal to the chord wall is

(i) for positive Ω and $f = 0$:

$$\frac{Y}{m_p} = 2\left[\bar{h}_1 + 2\,(d - b_0\tan\Omega)\right]\frac{1}{a} + 2\,(\bar{h}_1 + 2d)\,\frac{1}{c} + 4\,\frac{b_0}{(\cos^2\Omega)\,[d - (\bar{b}_1 + c)\tan\Omega]} \qquad [5.3.1]$$

(ii) for positive Ω and $0 < f \leq b_0$:

$$\frac{Y}{m_p} = 2\left[\bar{h}_1 + 2\,(d - b_0\tan\Omega)\right]\frac{1}{a} + 2\,(\bar{h}_1 + 2d)\,\frac{1}{c} + 4\,\frac{b_0 - f}{(\cos^2\Omega)\,[d - (\bar{b}_1 + c)\tan\Omega]}$$

$$+ 4\,\frac{f - c}{d - f\tan\Omega} + \frac{4}{\tan\left[\frac{\pi}{2} - \Omega - \tan^{-1}\left(\frac{c}{d}\right)\right]} \qquad [5.3.2]$$

(iii) for negative Ω and $0 \leq f < b_0$:

$$\frac{Y}{m_p} = 2\left[\bar{h}_1 + 2\,(d - b_0\tan\Omega)\right]\frac{1}{a} + 2\,(\bar{h}_1 + 2d)\,\frac{1}{c} + 4\,\frac{f}{(\cos^2\Omega)\,[d - c\,\tan\Omega]}$$

$$+ 4\,\frac{\bar{b}_1 + c - f}{d - f\tan\Omega} + \frac{4}{\tan\left[\frac{\pi}{2} + \Omega - \tan^{-1}\left(\frac{a}{d - b_0\tan\Omega}\right)\right]} \qquad [5.3.3]$$

(iv) for negative Ω and $f = b_0$:

$$\frac{Y}{m_p} = 2\left[\bar{h}_1 + 2\,(d - b_0\tan\Omega)\right]\frac{1}{a} + 2\,(\bar{h}_1 + 2d)\,\frac{1}{c} + 4\,\frac{\bar{b}_1 + c}{d}$$

$$+ \frac{4}{\tan\left[\frac{\pi}{2} + \Omega - \tan^{-1}\left(\frac{a}{d - b_0\tan\Omega}\right)\right]} \qquad [5.3.4]$$

For each of Eqs. [5.3.1] to [5.3.4] minimization of Y with respect to d, Ω and f involves searching for a solution of quite lengthy simultaneous non-linear equations. An exact closed form solution is impossible to obtain due to this complexity. An iterative numerical solution is possible. However, the simplest way to find the minimum load Y_{min} is by searching for it using Eqs. [5.3.1] to [5.3.4] over a complete range of the parameters d, Ω and f. The minimum loads found from such a search are given in Table 5.6. For

small values of λ the minimum load occurs at $\Omega = 0$, i.e. the results are the same as for the basic mechanism DT-1. For higher values of λ and as $\bar{\beta}$ increases, the minimum loads occur at decreasing (negative) values of Ω and at $f \approx 0.25$, but the minimum loads are only marginally lower than for the basic mechanism DT-1. At these values of λ and $\bar{\beta}$, basic mechanism DT-2 governs with much lower loads (see Table 5.2).

Hence mechanism DT-1-E, with inclined end yield lines, is either identical to basic mechanism DT-1, for low $\bar{\beta}$ and λ values, or does not govern, for high values of these parameters.

5.3.2 Mechanism DT-2-E

A representative mechanism is shown in Fig. 5.10. Similarly to basic mechanism DT-2, rotation of the web member is assumed in addition to punching in. The mechanism is defined by two parameters, d and Ω. There is no switching from hogging to sagging of the yield lines for any value of d and Ω. The yield load normal to the chord wall is given by

$$\frac{Y}{M_p} = \frac{2}{\frac{\bar{b}_1 + 2c}{2(\bar{b}_1 + c)}} \left[(\bar{h}_1 + 2d)\frac{1}{\bar{b}_1+c} + (\bar{h}_1+2d-2b_0\tan\Omega)\frac{1}{\bar{a}} + 2\frac{b_0}{(\cos^2\Omega)\,[d - (\bar{b}_1+c)\tan\Omega]} \right] \qquad [5\ 3.5]$$

Minimization of Y with respect to d and Ω is obtained by solving

$$\frac{dY}{dd} = 0\,, \quad \frac{dY}{d\Omega} = 0\,, \qquad [5.3.6]$$

leading to

$$\Omega = 0 \quad \text{and} \quad d = \sqrt{\frac{b_0}{\frac{1}{\bar{a}} + \frac{1}{\bar{b}_1+c}}} \qquad [5.3.7]$$

i.e., Y_{min} occurs a $\Omega = 0$, and the solution is identical to that of

basic mechanism DT-2. (Substitution of Eq. [5.3 7] into Eq [5.3.5] yields Eq. [5.2.19]).

In conclusion, the inclination of the end yield lines in DT Joints does not reduce the joint yield load for either mechanism DT-1 or DT-2 (when either mechanism governs). Because of the similarity between DT and DK joints this conclusion can be extended to DK joints. Hence the inclination of the end yield lines is not considered for DK Joints as it would produce only slight reduction, or more likely no reduction, in the joint yield load

5 4 MECHANISMS WITH FANS

Modification to basic mechanisms DT-1 and DT-2 for DT joints by incorporating fans into the mechanism are examined below Modifications are possible in many ways as shown in Fig. 5.11. However only one model is investigated herein for each basic mechanism because there is likely little difference in the joint yield load for these different modifications The mechanisms considered are called DT-1-F and DT-2-F, in which 'F' stands for Fans.

5.4.1 Mechanism DT-1-F

A typical model of mechanism DT-1 modified with fans is shown in Fig. 5.12. The configuration of the mechanism is defined by one parameter, d, with the restriction that

$$d \geq a \qquad [5.4.1]$$

for the mechanism to be possible. The joint yield load is

$$\frac{Y}{m_p} = 2 \left[\bar{h}_1 \left(\frac{1}{a} + \frac{1}{c}\right) + \frac{2\bar{b}_1}{d} + 2 \tan\left(\cos^{-1}\frac{a}{d}\right) + 2 \tan\left(\cos^{-1}\frac{c}{d}\right) \right.$$

$$\left. + 2\pi - 2 \cos^{-1}\frac{a}{d} - 2 \cos^{-1}\frac{c}{d} \right] \qquad [5\ 4\ 2]$$

Minimization of Y with respect to d leads to

$$\sqrt{\left(\frac{d}{a}\right)^2 - 1} + \sqrt{\left(\frac{d}{c}\right)^2 - 1} - \frac{\bar{b}_1}{d} = 0 \qquad [5\ 4\ 3]$$

which can be solved for d by iteration By substituting d into Eq [5 4 2], Y_{min}/m_p is found Table 5 7 shows the values of Y_{min}/m_p for a range of $\bar{\beta}$ and λ values, as well as the percentage difference compared with the minimum load for basic mechanism DT-1 For example at $\bar{\beta} = 0\ 4$ and $\lambda = 0\ 5$, Y_{min}/m_p is 12% lower than the minimum load given by basic mechanism DT-1 and, at $\lambda = 0\ 9$, Y_{min}/m_p is 22% higher

5 4 2 Mechanism DT-2-F

A typical model of mechanism DT-2 with fans is shown in Fig 5 13 Again only one parameter, d, is sufficient to define the geometry of the mechanism Restrictions on the value of d are shown in Fig 5 14 The yield load of the joint is

$$\frac{Y}{m_p} = \frac{2}{\frac{\bar{b}_1 + 2\ c}{2\ (\bar{b}_1 + c)}} \left[(\bar{h}_1 + 2d) \frac{1}{\bar{b}_1 + c} + (\bar{h}_1 + 2\ a\ \tan B) \frac{1}{a} + 2\ (\pi - A - B) \right] \qquad [5\ 4\ 4]$$

where

$$A = \tan^{-1}\left(\frac{d}{\bar{b}_1 + c}\right) \quad \text{and} \quad B = \cos^{-1}\left(\frac{a}{d} \sin A\right) \qquad [5\ 4\ 5]$$

Minimization of Y with respect to d in a closed form solution is difficult and was not attempted Instead Y_{min}/m_p was obtained from a numerical search using Eq. [5.4 4] for a wide range of d values The minimum

loads Y_{min}/m_p obtained this way are shown in Table 5.8 for the usual range of β and λ All the minimum loads in the Table were found at the minimum possible value of d, as defined in Fig 5.14. The percentage difference from the load predicted by basic mechanism DT-2 is also given in Table 5.8.

The least minimum loads Y_{min}/m_p of either mechanisms DT-1, DT-2, DT-1-F and DT-2-F are shown in Table 5 9 For most cases the mechanisms with fans govern, the largest reduction from the load predicted by the basic mechanisms being 17% for β = 0.2, 0 4 and λ = 0 5.

The importance of considering fans in DT joints is indicated by the variation in the reduction of joint strength with the off-centering ratio λ For β = 0 4, the reduction in joint strength when $\lambda > 0$ 5 is at most 5% higher than when λ = 0 5 (Table 5.9) For β = 0.6, the reduction in joint strength when λ = 0.5 is 3% higher than when λ = 0 5. For other β values the maximum reduction in joint strength occurs at values of λ = 0 5, i.e the reduction is at most equal to that in planar K truss joints

Since the design equations for planar K joints neglect the lower joint strength of mechanisms with fans (Wardenier 1982), and because the joint strength in triangular DT joints, based on mechanisms with fans, is not significantly lower than in planar K joints, it is therefore proposed to ignore the mechanisms with fans in design recommendations given subsequently

5.5 EFFECT OF NORMAL STRESSES IN CHORD CORNERS

In DT and DK joints, if the web members are shifted towards the chord upper corner, as shown in Fig. 2.4, they produce more load on this side of the chord. The effect on the chord face yield load of the normal stresses in the chord corner yield lines is investigated below. The approach to the problem

is similar to that for near full and full width T, Y and X joints (Davies et al. 1984, Szlendak and Brodka 1985). Methods of taking into account the effect of normal stresses in the plastic analysis of a structure are discussed in Appendix C.

Solutions are presented below for DT joints in which bending of the chord face is analysed using yield line mechanisms and the effect of normal stresses in the chord corner yield lines is analysed using either the static or kinematic approaches. Equilibrium solutions for bending of the chord face are not considered Hence Methods 3 and 4 presented in Appendix C are used below to investigate the DT joint behaviour

Consider the DT joints shown in Fig. 5 15b Sharing of the total normal load Y on each side of the chord, i e the values of ρ_1 and ρ_2, can be assumed in several ways. The following simple load distribution is assumed

$$\rho_1 = \frac{\bar{b}_1}{2} + c \quad \text{and} \quad \rho_2 = \frac{a + \frac{\bar{b}_1}{2}}{b_0} \qquad [5.5\ 1]$$

5 5 1 Solution N1

This solution is based on Method 3 (see Appendix C), using a kinematic approach for the bending moments in the chord face and a static approach for the normal forces assuming a uniform normal stress distribution in the chord corners.

Bending of the chord face is readily analysed based on the mechanisms shown in Figs 5 4 and 5 5 The virtual work equation is,

for mechanism DT-1-N1,

$$K_2\ Y = m_p\left[K_1(\bar{h}_1+2d) + \frac{4\ b_0}{d}\right] + \int_0^{\bar{h}_1+2d} m'_{p_1}(x)\ \frac{dx}{a} + \int_0^{\bar{h}_1+2d} m'_{p_2}(x)\ \frac{dx}{c} \qquad [5\ 5.2]$$

and for mechanism DT-2-N1,

$$K_2 Y = m_p\left[K_1(\bar{h}_1+2d) + \frac{4 b_0}{d}\right] + \int_0^{\bar{h}_1+2d} m'_{p_1}(x) \frac{dx}{a} + \int_0^{\bar{h}_1+2d} m'_{p_2}(x) \frac{dx}{\bar{b}_1+c} \qquad [5.5.3]$$

where the constants K_1 and K_2 are defined in Table 5.10. m'_{p_j} is the plastic moment resistance per unit length of chord wall j (j=1,2) reduced by the normal stress n_j which is, in general, function of the location x along the chord corner yield line. The reduced plastic moment resistance is

$$m'_{p_j}(x) = \left[1 - \left(\frac{n_j(x)}{n_p}\right)^2 \right] m_p \quad , \qquad j=1,2 \qquad [5.5.4]$$

where $n_p = \sigma_y$, the yield stress of the chord wall material

An equilibrium equation is now written for the normal forces Assuming a uniform distribution of the normal stresses along the chord corners, as shown in Fig. 5.15c, the equations of equilibrium are

on side 1

$$n_1(x) = n_1 = \frac{\rho_1 Y}{(\bar{h}_1+2d)\ t_0} \qquad [5.5.5]$$

on side 2

$$n_2(x) = n_2 = \frac{\rho_2 Y}{(\bar{h}_1+2d)\ t_0} \qquad [5.5.6]$$

Substituting Eqs. [5.5.4], [5.5.5] and [5.5.6] into either Eq [5.5.2] or [5.5.3] leads to

$$\frac{K_3}{(\bar{h}_1+2d)} \left(\frac{Y}{m_p}\right)^2 + K_2 \left(\frac{Y}{m_p}\right) - 2 K_1 (\bar{h}_1+2d) - \frac{4 b_0}{d} = 0 \qquad [5.5.7]$$

or

$$\frac{Y}{m_p} = \frac{-q+\sqrt{q^2-4pr}}{2p} \qquad [5.5.8]$$

where

$$p = \frac{K_3}{(\bar{h}_1+2d)}$$

$$q = K_2 \qquad [5.5.9]$$

$$r = -\ 2\ K_1\ (\bar{h}_1+2d)\ \frac{4\ b_0}{d}$$

where K_1, K_2 and K_3 are defined in the Table 5.10.

Finally Y/m_p has to be minimized with respect to d. Differentiating Eq. [5.5.8] with respect to d and equating to zero gives

$$S_0 + S_2 d^2 + S_3 d^3 + S_4 d^4 + S_5 d^5 + S_6 d^6 = 0 \qquad [5.5.10]$$

where

$$S_0 = 4\ K_3\ b_0\ \bar{h}_1^{\,2}$$

$$S_2 = -\ 2\ K_4\ b_0\ \bar{h}_1^{\,2}$$

$$S_3 = -\ 8\ K_5\ b_0\ \bar{h}_1$$

$$S_4 = 2\ K_1\ K_4\ \bar{h}_1^{\,2} - 8\ K_2^{\,2}\ b_0 \qquad [5.5.11]$$

$$S_5 = 8\ K_1\ K_4\ \bar{h}_1$$

$$S_6 = 8\ K_1\ K_4$$

where K_1 to K_5 are defined in Table 5.10.

Eq. [5.5.10] can readily be solved for d by iteration and substituting the value found into Eq. [5.5.8] gives the final solution Y_{min}/m_p. Such values of Y_{min}/m_p are given in Tables 5.11 and 5.12 for mechanisms DT-1-N1 and DT-2-N2, respectively, taking into account the effect of normal stresses in the chord corners, for the usual range of $\bar{\beta}$ and λ values, for $\bar{h}_1 = \bar{b}_1$, and for values of b_0/t_0 ranging from 10 to 40. The least of the Y_{min}/m_p values for either of these mechanisms is given in Table 5.13, together with the % reduction from the Y_{min}/m_p values for the basic mechanisms without normal stress effects taken into account (see Table 5.3). The % reduction is larger for low b_0/t_0 values and large $\bar{\beta}$ and λ values, with a maximum reduction of 14% for $b_0/t_0 = 10$, $\bar{\beta} = 0.8$ and $\lambda = 0.6$, and reductions lower than 5%

for $b_0/t_0 = 20$ and higher, and any value of $\bar{\beta}$ and λ.

The above solution assumes that the normal stresses n_j in the chord walls are less than the yield stress n_p. As pure squash would occur first in the chord wall on side 2, the limit of validity of the above solution is

$$\frac{n_2}{n_p} < 1$$

or

$$\frac{\rho_2 Y}{m_p} < \frac{t_0}{4}(h_1+2d) \qquad [5.5.12]$$

This limit is satisfied for all values in Tables 5.11 and 5.12, except for one case at $b_0/t_0 = 10$, $\bar{\beta} = 0.8$ and $\lambda = 0.9$ in Table 5.11. However for this case, mechanism DT-2-N1 governs with combined bending and normal stresses in the chord corners. Hence, for the range of parameters covered in Table 5.13, pure squash of the chord side walls does not limit the validity of the results given in the Table.

5.5.2 Solution N2

This solution is also based on Method 3 (see Appendix C), using a kinematic approach for the bending moments and a static approach for the normal forces.

A solution slightly different from the previous one is obtained by assuming a linearly varying normal stress distribution in the chord corner yield lines, as shown in Fig. 5.16. The virtual work equation for bending of the chord face remains as given by Eqs. [5.5.2], [5.5.3] and [5.5.4], but the equations of equilibrium are now assumed to be, on side j (j=1,2),

for $0 \le x < d$: $$n_j(x) = \frac{\rho_j Y}{(\bar{h}_1+d)t_0}\frac{x}{d} \qquad [5.5.13]$$

for $d \le x \le \bar{h}_1+d$: $$n_j(x) = n_{0_j} = \frac{\rho_j Y}{(\bar{h}_1+d)t_0} \qquad [5.5.14]$$

for $h_1+d < x < \bar{h}_1+2d$: $$n_j(x) = \frac{\rho_j Y}{(\bar{h}_1+d)\,t_0}\,\frac{(\bar{h}_1+2d)-x}{d} \qquad [5.5.15]$$

where the value of n_{0_j} is obtained from

$$\int_0^{\bar{h}_1+2d} n_j(x)\,dx = \rho_j Y \qquad [5.5.16]$$

Substituting Eqs. [5.5.13] to [5.5.16] into Eqs. [5 5.2], [5.5.3] and [5.5.4] leads to

$$K_3\,\frac{\left(\bar{h}_1+\frac{2}{3}d\right)}{(\bar{h}_1+d)^2}\left(\frac{Y}{\bar{m}_p}\right)^2 + K_2\,\frac{Y}{\bar{m}_p} - 2\,K_1\,(\bar{h}_1+2d) - \frac{4b_0}{d} = 0 \qquad [5.5.17]$$

or

$$\frac{Y}{\bar{m}_p} = \frac{-q \pm \sqrt{q^2 - 4pr}}{2p} \qquad [5.5.18]$$

where

$$p = \frac{\left(\bar{h}_1+\frac{2}{3}d\right)}{(\bar{h}_1+d)^2}\,K_3$$

$$q = K_2 \qquad [5.5.19]$$

$$r = -\,2\,K_1\,(\bar{h}_1+2d) - \frac{4b_0}{d}$$

where K_1, K_2 and K_3 are again defined in Table 5.10.

Differentiation with respect to d in Eq. [5.5.18] is difficult, so the minimization of Y is done by numerical differentiation (see for example Conte and de Boor 1980).

The values of Y_{min}/m_p from the above solution are only slightly smaller than those found in Solution N1. For mechanisms DT-1-N2 and DT-2-N2, and for the values of $\bar{\beta}$, λ and $\frac{b_0}{t_0}$ used in Tables 5.11 and 5.12, the difference between the two solutions is less than 2%.

5.5.3 Solution N3

This solution is based on Method 4.1, combining mechanisms (see Appendix C), using a kinematic approach for the bending moments and also a

kinematic approach for the normal forces.

Consider sub-mechanisms 1, 2 and 3, shown in Fig. 5.17. Sub-mechanism 1 is for the chord face bending deformations, whereas sub-mechanisms 2 and 3 are for the normal deflections along the chord corners. These sub-mechanisms, when combined, are equivalent to a complete mechanism (DT-1-N3) taking into account the normal force in the chord walls. Analysis of the 3 separate sub-mechanisms yields 3 virtual work equations with the 3 unknowns Y/m_p, n_{o_1} and n_{o_2}, which have to be solved simultaneously. The solution for Y/m_p thus obtained can then be minimized with respect to d in order to obtain the final solution Y_{min}/m_p.

The solutions are given below in terms of n_o, the normal load per unit length of chord wall, and x_p the location along the chord corners of the transition from n_o to n_p (n_p is now defined as the squash load per unit length of chord wall, $= t_0 \sigma_y$). Alternatively, the solutions could be given in terms of the parameters f and g, as in Solution N4 below (see Fig. 5.21), or in terms of the parameters δ_1 and δ_2, the maximum downward deflection along the chord corners. The reason for this is that these sets of parameters are function of one another.

It is assumed that

$$\frac{\rho_1}{\rho_2} = \frac{n_{o_1}}{n_{o_2}} = \frac{\delta_1}{\delta_2} \qquad [5.5.20]$$

Also, the normal stress distributions are assumed to correspond to the normal displacement along the chord corners, as shown in Fig. 5.17.

There are three cases to be considered, as shown in Fig. 5.18. In case 1, the yield condition along both chord corners is due to combined bending and normal stresses. In case 2, yield on side 2 of the chord is due to squash (i.e. normal stresses only). In case 3, yield is due to squash on

both sides of the chord.

The virtual work equations for sub-mechanisms 1, 2 and 3 (Fig. 5.17) for each case of yield condition (Fig. 5.18) are as follows:

Case 1, Combined Bending and Normal Stresses in Both Chord Walls

From sub-mechanism 1 (Fig. 5.17),

$$\frac{Y}{m_p} = 4\frac{b_0}{d} + 2(\bar{h}_1 + 2d)\left(\frac{1}{a} + \frac{1}{c}\right) - \left(\bar{h}_1 + \frac{2}{3}d\right)\frac{1}{a}\frac{n_{o_1}^2}{n_p^2} - \left(\bar{h}_1 + \frac{2}{3}d\right)\frac{1}{c}\frac{n_{o_2}^2}{n_p^2} \qquad [5.5.21]$$

where n_{o_1}, obtained from sub-mechanism 2, is given by

$$-\frac{m_p}{n_p^2}\frac{1}{a}\left(\bar{h}_1 + \frac{2}{3}d^2\right) n_{o_1}^2 + \left(\bar{h}_1 + \frac{2}{3}d^2\right) n_{o_1} + 2\, m_p \frac{(2a^2 + d^3 + d^2 + \bar{h}_1 d)}{ad} = 0 \qquad [5.5.22]$$

and where n_{o_2}, obtained from sub-mechanism 3, is given by

$$-\frac{m_p}{n_p^2}\frac{1}{c}\left(\bar{h}_1 + \frac{2}{3}d^2\right) n_{o_2}^2 + \left(\bar{h}_1 + \frac{2}{3}d^2\right) n_{o_2} + 2\, m_p \frac{(2c^2 + d^3 + d^2 + \bar{h}_1 d)}{cd} = 0 \qquad [5.5.23]$$

Case 2, Squash in Chord Wall Side 2

From sub-mechanism 1,

$$\frac{Y}{m_p} = 4\frac{b_0}{d} + (\bar{h}_1 + 2d)\left(\frac{2}{a} + \frac{1}{c}\right) - \left(\bar{h}_1 + \frac{2}{3}d\right)\frac{1}{a}\frac{n_{o_1}^2}{n_p^2} + \frac{4}{3}\frac{x_{p2}}{c} \qquad [5.5.24]$$

where n_{o_1}, obtained from sub-mechanism 2, is given by

$$-\frac{m_p}{n_p^2}\frac{1}{a}\left(\bar{h}_1 + \frac{2}{3}d^2\right) n_{o_1}^2 + \left(\bar{h}_1 + \frac{2}{3}d^2\right) n_{o_1} + 2\, m_p \frac{(2a^2 + d^3 + d^2 + \bar{h}_1 d)}{ad} = 0 \qquad [5.5.25]$$

and where x_{p2}, obtained from sub-mechanism 3, is given by

$$-\frac{1}{3} n_p x_{p2}^2 + m_p \frac{4}{3} \frac{d}{c} x_{p2} + m_p (\bar{h}_1 + 2d) \frac{1}{c} + m_p 4 \frac{c}{d} + \left(\bar{h}_1 + d^2\right) n_p = 0 \quad [5.5.26]$$

Case 3, Squash in Both Chord Walls

From sub-mechanism 1,

$$\frac{Y}{m_p} = 4\frac{b_0}{d} + (\bar{h}_1 + 2d)\left(\frac{1}{a} + \frac{1}{c}\right) + \frac{4}{3}\frac{x_{p1}}{a} + \frac{4}{3}\frac{x_{p2}}{c} \quad [5.5.27]$$

where x_{p1}, obtained from sub-mechanism 2, is given by

$$-\frac{1}{3} n_p x_{p1}^2 + m_p \frac{4}{3} \frac{d}{a} x_{p1} + m_p (\bar{h}_1+2d) \frac{1}{a} + m_p 4 \frac{a}{d} + \left(\bar{h}_1+d^2\right) n_p = 0 \quad [5.5.28]$$

and where x_{p2}, obtained from sub-mechanism 3, is given by

$$-\frac{1}{3} n_p x_{p2}^2 + m_p \frac{4}{3} \frac{d}{c} x_{p2} + m_p (\bar{h}_1+2d) \frac{1}{c} + m_p 4 \frac{c}{d} + \left(\bar{h}_1+d^2\right) n_p = 0 \quad [5.5.29]$$

Minimization of Y/m_p with respect to d from Eqs. [5.5.21], [5.5.24] and [5.5.27] can be done numerically and a value of Y_{min}/m_p can hence be obtained for each of cases 1, 2 and 3. The least of these three Y_{min}/m_p values is the solution for a particular DT joint, for mechanism DT-1-N3. Expressions similar to Eqs. [5.5.21] to [5.5.29] can be derived for mechanism DT-2-N3 and a Y_{min}/m_p value can be obtained in the same manner as explained above for mechanism DT-1-N3. The final solution for a DT joint is then the lowest of these solutions for mechanisms DT-1-N3 and DT-2-N3.

An explicit solution for d and Y_{min}/m_p is given below for the simple case of mechanism DT-1$\cup$N3 with $\lambda = 0.5$ and with combined bending and normal stresses in both chord walls (case 1 in Fig. 5.18).

Sub-mechanism 1 (Fig. 5.17a) simplifies to that shown in Fig. 5.19, and the virtual work equation simplifies to

$$Y.1 = m_p \left[2(\bar{h}_1+2d)\frac{1}{a} + \frac{4b_0}{d}\right] + m_p \left[1-\left(\frac{n_0}{n_p}\right)^2\right]\frac{2\bar{h}_1}{a} + \int_0^d m_p \left[1-\left(\frac{n}{n_p}\right)^2\right]\frac{4dx}{a} \qquad [5.5.30]$$

where $n_p = t_0\sigma_y$, the squash load/ unit length of chord wall, n and n_0 are normal loads/ unit length and $n = \frac{n_0 x}{d}$.

Sub-mechanisms 2 and 3 (Fig. 5.17) simplify to sub-mechanism 2 shown in Fig. 5.20. The virtual work equation is

$$Y = 4\,\frac{b_0}{d}\,m_p + n_0\,2\,\bar{h}_1 + 4\int_0^d n\,z\,dx \qquad [5.5.31]$$

where $z\ (=\frac{x}{d})$ is the displacement along the chord corners assumed in this sub-mechanism.

Solving Eq. [5.5.31] for n_o and substituting into Eq. [5.5.30] yields

$$\frac{Y}{m_p} = \frac{8}{3t_o^2}\sqrt{8\left(2a^2+3t_0^2\right)d^2 + 48\bar{h}_1\left(a^2+t_0^2\right)d + 18\bar{h}_1\left(2a^2+t_0^2\right)}$$

$$- \frac{32ad}{3t_0^2} + \frac{4b_0}{d} - \frac{16a\bar{h}_1}{t_0^2} \qquad [5.5.32]$$

Letting $\frac{d}{dd}\left(\frac{Y}{m_p}\right) = 0$ gives

$$S_0 + S_1 d + S_2 d^2 + S_3 d^3 + S_4 d^4 + S_5{}^5 + S_6 d^6 = 0 \qquad [5.5.33]$$

where

$$S_0 = -\,81\,b_0{}^2\,t_0{}^4\,\bar{h}_1{}^2\left(2a^2+t_0^2\right)$$

$$S_1 = -\,216\,b_0{}^2\,t_0{}^4\,\bar{h}_1\left(a^2+t_0^2\right)d$$

$$S_2 = -432\, a\, b_0\, t_0^2\, \bar{h}_1^2 \left(2a^2 + t_0^2\right) + 36\, b_0^2 t_0^4 \left(2a^2 + 3t_0^2\right)$$

$$S_3 = -1152\, a\, b_0\, t_0^2\, \bar{h}_1 \left(a^2 + t_0^2\right) \qquad [5.5.34]$$

$$S_4 = 1152\, \bar{h}_1 \left(a^2 + t_0^2\right)^2 - 576\, a^2 \bar{h}_1^2 \left(2a^2 + t_0^2\right) - 192\, a\, b_0\, t_0^2 \left(2a^2 + 3t_0^2\right)$$

$$S_5 = \left[\, 768\, \bar{h}_1 \left(2a^2 + 3t_0^2\right) - 1536\, a^2 \bar{h}_1 \right] \left(a^2 + t_0^2\right)$$

$$S_6 = \left[\, 128 \left(2a^2 + 3t_0^2\right) - 256\, a^2 \,\right] \left(2a^2 + 3t_0^2\right)$$

Finally to find Y_{min}/m_p, d is calculated by iteration from Eq. [5.5.33] and substituted into Eq. [5.5.32]. Equation [5.5.32] is equivalent to the function $f(\Omega^6)$ referred to by Szlendak and Brodka (1985).

5.5.4 Solution N4

This solution is based on Method 4.2, entire mechanism (see Appendix C), using a kinematic approach for both bending moments and normal forces.

Mechanisms DT-1-N4 and DT-2-N4, shown in Fig. 5.21, include the chord face bending deformations as well as, i.e. combined with, the axial deformations due to the normal stresses in the chord corner yield lines. For these 'entire' mechanisms a single virtual work equation can be written for Y/m_p in terms of f and g (or δ_1 and δ_2). Differentiation of that equation with respect to f and g provides two other equations, so that the value of Y/m_p, f and g can be found.

The virtual work equation includes terms for the energy dissipated by each yield line in the patterns shown in Fig. 5.21. These terms are readily obtained except those for the yield lines along the chord corners, which are derived below.

As in Solution N3 above, three cases of yield condition in the chord corners must be considered similar to those shown in Fig. 5.18 (case 1:

combined bending and normal stresses in both walls, case 2: squash in chord wall 2, and case 3: squash in both chord walls). These cases depend on the yield condition assumed at section AA along $\bar{h}_1$ and at section BB along d, as shown in Fig. 5.22, in each chord wall. When $0 \le f \le \frac{t_0}{2}$ (or $0 \le g \le \frac{t_0}{2}$), sections AA and BB are subjected to combined bending and normal stresses. When $\frac{t_0}{2} \le f$ (or $\frac{t_0}{2} \le g$), section AA and part of section BB are subjected to normal stresses only, the end part of section BB remaining subjected to combined stresses.

The energy dissipated in the chord corner yield lines is calculated below for these different yield conditions.

Combined bending and normal stresses ($0 \le f \le \frac{t_0}{2}$)

Refer to Fig. 5.22. At section AA,

$$\Delta = \delta_1 = \frac{f}{a+f}, \qquad \theta = \frac{1}{a+f} \qquad [5.5.35]$$

$$m'_p = m_p \left[1-\left(\frac{n}{n_p}\right)^2\right] = m_p \left[1-\left(\frac{2f}{t_0}\right)^2\right] \qquad [5.5.36]$$

$$n = n_p \frac{2e}{t_0} = 8\, m_p \frac{f}{t_0^2} \qquad [5.5.37]$$

Hence, the energy dissipated, D, along the length $\bar{h}_1$ is

$$D = \bar{h}_1 (m'_p\theta + n\Delta) = m_p \bar{h}_1 \frac{1}{a+f}\left(1- \frac{4f^2}{t_0^2} + \frac{8f^2}{t_0^2} \right) \qquad [5.5.38]$$

At section BB,

$$\Delta = \frac{z}{d}\delta_1 = \frac{z}{d}\frac{f}{a+f}, \qquad \theta = \frac{1}{a+f}, \qquad e = \frac{\Delta}{\theta} = \frac{f}{d} z \qquad [5.5.39]$$

$$m'_p = m_p \left[1 - \left(\frac{2e}{t_0}\right)^2 \right] = m_p \left[1 - \frac{4f^2}{t_0^2 d^2} z^2 \right] \qquad [5.5.40]$$

$$n = 8 \frac{e}{t_0^2} m_p = 8 \frac{f}{dt_0^2} z\, m_p \qquad [5.5.41]$$

Hence, the energy dissipated along the length d is

$$D = \int_0^d (m'_p\theta + n\Delta)\, dz = m_p \frac{1}{a+f} d \left(1 + \frac{4}{3} \frac{f^2}{t_o^2} \right) \qquad [5\ 5\ 42]$$

Squash stresses ($\frac{t_o}{2} \leq f$)

Refer to Fig 5 23 At section AA,

$$m'_p = 0 , \qquad n = n_p = 4 \frac{m_p}{t_o} , \qquad D = \bar{h}_1 (n\Delta) = 4\, m_p \frac{f}{a+f} \frac{\bar{h}_1}{t_o} \qquad [5\ 5\ 43]$$

At section BB,

$$e_o = \frac{t_o}{2} , \qquad d_o = e_o \theta , \qquad \theta = \frac{1}{a+f} \qquad [5\ 5\ 44]$$

$$d = \frac{z}{d} \frac{f}{a+f} , \qquad d_o = \frac{z_o}{d} \frac{f}{a+f} , \qquad z_o = \frac{d}{f} \frac{t_o}{2} \qquad [5\ 5\ 45]$$

Hence, the energy dissipated is

$$D = \int_0^{z_o} (m'_p\theta + n\Delta)\, dz + \int_{z_o}^{d} n\, \Delta\, dz = m_p \frac{1}{a+f} d \left(\frac{2f}{t_o} + \frac{t_o}{6f} \right) \qquad [5\ 5\ 46]$$

The virtual work equations for mechanisms DT-1-N4 and DT-2-N4 can now be written and solved for Y/m_p Then letting

$$\frac{d}{df} \left(\frac{Y}{m_p} \right) = \frac{d}{dg} \left(\frac{Y}{m_p} \right) = \frac{d}{dd} \left(\frac{Y}{m_p} \right) = 0 , \qquad [5\ 5\ 47]$$

the values of f, g and d are obtained for which Y/m_p is a minimum

These solutions are given below for the three yielding conditions in the chord walls, shown in Fig 5.18, for mechanisms DT-1-N4 and DT-2-N4 The following constants are used to shorten the expressions for Y_{min}/m_p, f, g and d.

$$L_1 = 2 + 4\left(\frac{f}{t_o}\right)^2 \qquad L_2 = 2 + \frac{4}{3}\left(\frac{f}{t_o}\right)^2$$

$$L_3 = 2 + 4\left(\frac{g}{t_o}\right)^2 \qquad L_4 = 2 + \frac{4}{3}\left(\frac{g}{t_o}\right)^2 \qquad [5\ 5\ 48]$$

$$L_5 = 1 + 4\frac{f}{t_o} \qquad L_6 = 1 + 2\frac{f}{t_o} + \frac{t_o}{6f}$$

$$L_7 = 1 + 4\frac{g}{t_o} \qquad L_8 = 1 + 2\frac{g}{t_o} + \frac{t_o}{6g}$$

Mechanism DT-1-N4

Case 1, Combined Bending and Normal Stresses in Both Chord Walls

$$\frac{Y_{min}}{m_p} = 1\left[\frac{4b_o}{d} + \frac{\bar{h}_1 L_1 + 2dL_2}{a+f} + \frac{\bar{h}_1 L_3 + 2dL_4}{c+g}\right] \qquad [5\ 5\ 49]$$

where

$$f = \sqrt{a^2 + \frac{t_o^2(\bar{h}_1+2d)}{2(\bar{h}_1+\frac{2}{3}d)}} - a \qquad [5\ 5\ 50]$$

$$g = \sqrt{c^2 + \frac{t_o^2(\bar{h}_1+2d)}{2(\bar{h}_1+\frac{2}{3}d)}} - c \qquad [5\ 5\ 51]$$

$$d = \sqrt{\frac{2b_o(a+f)(c+g)}{(c+g)L_2 + (a+f)L_4}} \qquad [5\ 5\ 52]$$

Case 2, squash in chord wall side 2

$$\frac{Y_{min}}{m_p} = 1\left[\frac{4b_o}{d} + \frac{\bar{h}_1 L_1 + 2dL_2}{a+f} + \frac{\bar{h}_1 L_7 + 2dL_8}{c+g}\right] \qquad [5\ 5\ 53]$$

where

$$f = \sqrt{a^2 + \frac{t_o^2(\bar{h}_1+2d)}{2(\bar{h}_1+\frac{2}{3}d)}} - a \qquad [5\ 5\ 54]$$

$$g = \frac{1 + \sqrt{1 + \frac{3c}{dt_o^2}\left[4c(\bar{h}_1+d) - t_o(\bar{h}_1+2d)\right]}}{\frac{3}{dt_o^2}\left[4c(\bar{h}_1+d) - t_o(\bar{h}_1+2d)\right]} \qquad [5\ 5\ 55]$$

$$d = \sqrt{\frac{2b_0(a+f)(c+g)}{(c+g)L_2 + (a+f)L_8}} \qquad [5\ 5\ 56]$$

Case 3, squash in both chord walls.

$$\frac{Y_{min}}{m_p} = 1\left[\frac{4b_0}{d} + \frac{\bar{h}_1L_5 + 2dL_6}{a+f} + \frac{\bar{h}_1L_7 + 2dL_8}{c+g}\right] \qquad [5\ 5\ 57]$$

where

$$f = \frac{1 + \sqrt{1 + \frac{3a}{dt_0^2}\left[4a(\bar{h}_1+d) - t_0(\bar{h}_1+2d)\right]}}{\frac{3}{dt_0^2}\left[4a(\bar{h}_1+d) - t_0(\bar{h}_1+2d)\right]} \qquad [5\ 5\ 58]$$

$$g = \frac{1 + \sqrt{1 + \frac{3c}{dt_0^2}\left[4c(\bar{h}_1+d) - t_0(\bar{h}_1+2d)\right]}}{\frac{3}{dt_0^2}\left[4c(\bar{h}_1+d) - t_0(\bar{h}_1+2d)\right]} \qquad [5\ 5\ 59]$$

$$d = \sqrt{\frac{2b_0(a+f)(c+g)}{(c+g)L_6 + (a+f)L_8}} \qquad [5\ 5\ 60]$$

Mechanism DT-2-N4

Case 1, Combined Bending and Normal Stresses in Both Chord Walls

$$\frac{Y_{min}}{m_p} = \frac{2(\bar{b}_1+c+g)}{(\bar{b}_1+2c+2g)}\left[\frac{4b_0}{d} + \frac{\bar{h}_1L_1 + 2dL_2}{a+f} + \frac{\bar{h}_1L_3 + 2dL_4}{\bar{b}_1+c+g}\right] \qquad [5\ 5\ 61]$$

where

$$f = \sqrt{a^2 + \frac{t_0^2(\bar{h}_1+2d)}{2(\bar{h}_1+\frac{2}{3}d)}} - a \qquad [5\ 5\ 62]$$

$$g = \sqrt{\left(\frac{\bar{b}_1+2c}{2}\right)^2 + \frac{t_0^2(\bar{h}_1+2d) + \bar{b}_1\left(\frac{t_0}{2}\right)^2 K}{2(\bar{h}_1+\frac{2}{3}d)}} - \frac{\bar{b}_1+2c}{2} \qquad [5\ 5\ 63]$$

where $K = \left[\frac{4b_0}{d} + \frac{\bar{h}_1L_1 + 2dL_2}{a+f}\right]$ [5 5 64]

$$d = \sqrt{\frac{2b_0(a+f)(\bar{b}_1+c+g)}{(\bar{b}_1+c+g)L_2 + (a+f)L_4}} \qquad [5\ 5.65]$$

Case 2, Squash in Chord Wall Side 2.

$$\frac{Y_{min}}{m_p} = \frac{2(b_1+c+g)}{(b_1+2c+2g)} \left[\frac{4b_0}{d} + \frac{\bar{h}_1 L_1 + 2dL_2}{a+f} + \frac{\bar{h}_1 L_7 + 2dL_8}{\bar{b}_1+c+g} \right] \quad [5\ 5\ 66]$$

where

$$f = \sqrt{a^2 + \frac{t_0^2(\bar{h}_1+2d)}{2(\bar{h}_1+\frac{2}{3}d)}} - a \quad [5\ 5\ 67]$$

$$g = \frac{1 + \sqrt{1 + \frac{3(\bar{b}_1+2c)}{2dt_0^2}\left[2(\bar{b}_1+2c)(\bar{h}_1+d) - t_0(\bar{h}_1+2d) - \bar{b}_1\frac{t_0}{2}K\right]}}{\frac{3}{dt_0^2}\left[2(\bar{b}_1+2c)(\bar{h}_1+d) - t_0(\bar{h}_1+2d) - \bar{b}_1\frac{t_0}{2}K\right]} \quad [5\ 5\ 68]$$

where $K = \left[\frac{4b_0}{d} + \frac{\bar{h}_1 L_1 + 2dL_2}{a+f} \right]$ [5 5 69]

$$d = \sqrt{\frac{2b_0(a+f)(\bar{b}_1+c+g)}{(\bar{b}_1+c+g)L_2 + (a+f)L_8}} \quad [5\ 5\ 70]$$

Case 3, Squash in Both Chord Walls

$$\frac{Y_{min}}{m_p} = \frac{2(b_1+c+g)}{(b_1+2c+2g)} \left[\frac{4b_0}{d} + \frac{\bar{h}_1 L_5 + 2dL_6}{a+f} + \frac{\bar{h}_1 L_7 + 2dL_8}{\bar{b}_1+c+g} \right] \quad [5\ 5\ 71]$$

where

$$f = \frac{1 + \sqrt{1 + \frac{3a}{dt_0^2}\left[4a(\bar{h}_1+d) - t_0(\bar{h}_1+2d)\right]}}{\frac{3}{dt_0^2}\left[4a(\bar{h}_1+d) - t_0(\bar{h}_1+2d)\right]} \quad [5\ 5\ 72]$$

$$g = \frac{1 + \sqrt{1 + \frac{3(\bar{b}_1+2c)}{2dt_0^2}\left[2(\bar{b}_1+2c)(\bar{h}_1+d) - t_0(\bar{h}_1+2d) - \bar{b}_1\frac{t_0}{2}K\right]}}{\frac{3}{dt_0^2}\left[2(\bar{b}_1+2c)(\bar{h}_1+d) - t_0(\bar{h}_1+2d) - \bar{b}_1\frac{t_0}{2}K\right]} \quad [5\ 5\ 73]$$

where $K = \left[\frac{4b_0}{d} + \frac{\bar{h}_1 L_5 + 2dL_6}{a+f} \right]$ [5 5 74]

$$d = \sqrt{\frac{2b_0(a+f)(\bar{b}_1+c+g)}{(\bar{b}_1+c+g)L_6 + (a+f)L_8}} \quad [5\ 5\ 75]$$

Eqs. [5.5.48] to [5.5.75] provide the complete set of solutions for a DT joint with off-centered web members. Both mechanisms DT-1-N4 and DT-2-N4 are included. Combined bending and normal stresses are assumed in the chord walls, and the cases of squashing of one or both chord walls are analysed. The correct resistance for the DT joint is the lowest value of Y/m_p calculated using Eqs. [5 5.49], [5 5 53], [5 5 57], [5 5.61], [5 5 66] and [5.5.71] and is given in Table 5.14 for the usual range of b_0/t_0, $\bar{\beta}$ and λ values, with $\bar{\eta} = \bar{\beta}$.

Pure squash of the chord wall on side 2 or of both chord walls is indicated in Table 5.14 and would occur at large values of $\bar{\beta}$. Solution N1 does not predict such pure squash stresses at these values of $\bar{\beta}$. In any case, when pure squash in the chord walls is predicted in Solution N4 the values of Y_{min}/m_p are not significantly lower than the values assuming combined bending and normal stresses.

The reduction in joint strength due to the normal stresses in the chord corners is at most 14.6% for $b_0/t_0 = 10$, $\bar{\beta} = \bar{\eta} = 0.8$ and $\lambda = 0\ 6$, and otherwise low (<10%) for $b_0/t_0 \geq 20$. Values of Y_{min}/m_p in Table 5.14 (Solution N4) are close to those in Table 5 13 (Solution N1)

5.5.5 Conclusions

Because of the different assumptions used, Solutions N1 to N4 yield slightly different results. However the differences are small, and this is expected since all the results are solutions of the same problem but using a different approach.

For the 16 DT specimens that failed in modes 1 or 2 (see Chapter 3), the effect of normal stresses in the chord corners is not large. Using Solution N1, the reduction in joint strength due to normal stresses is less than 2% for all tests. The mean ratio of test yield loads to predicted loads

is 1.05 with a coefficient of variation of 11.6%, only 0.2% better than when the effect of normal stresses in the chord corners is not taken into account (see Chapter 4)

It should be noted that the reduction in joint strength does not increase with increasing off-centering ratio λ. Hence, in triangular truss joints, the effect of normal stresses in the chord corners is maximum when the web members are centered, that is, when the joint geometry is comparable to that of planar truss joints. In planar truss joints, high normal stresses in the chord corners are of concern and included in design rules only for near full width ($\beta > 0.85$) or full width joints ($\beta = 1.0$) (Wardenier 1982) Because triangular truss joints usually have lower β ratios than planar truss joints, it is unlikely that normal stresses in the chord corners would be of concern in triangular truss joints. Therefore, it is proposed to neglect in design recommendations the mechanisms including normal stress effects for joints with values of $\beta \leq 0.85$. For the unusual cases of larger β values, and especially if the b_0/t_0 ratio is low, then one of the above solutions, N1 to N4, can be used to predict the joint strength reduced by the normal stresses perpendicular to the chord face

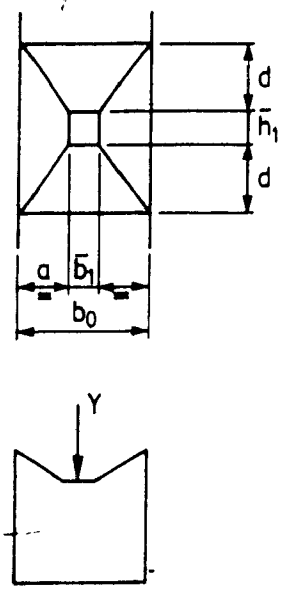

Fig. 5.1 Simple yield line model.

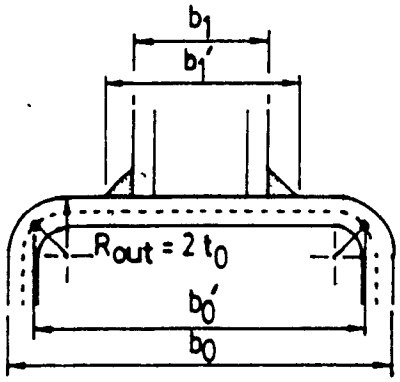

Fig. 5.2 Modification for corner curvature and welds.

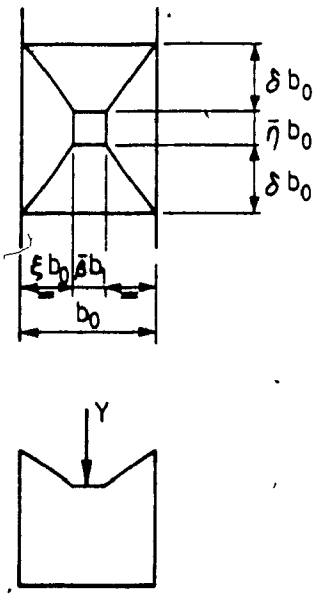

Fig. 5.3 Simple yield line model. Alternate notation.

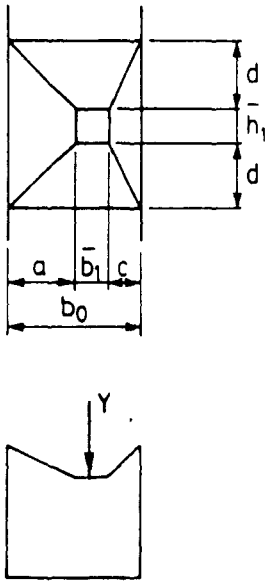

Fig. 5.4 Basic mechanism DT-1.

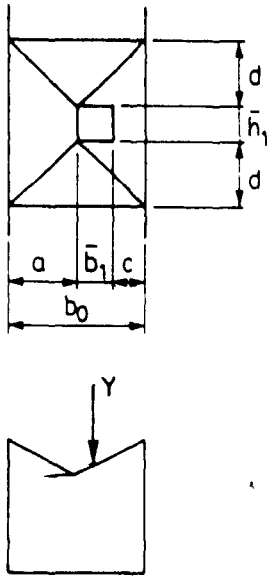

Fig. 5.5 Basic mechanism DT-2

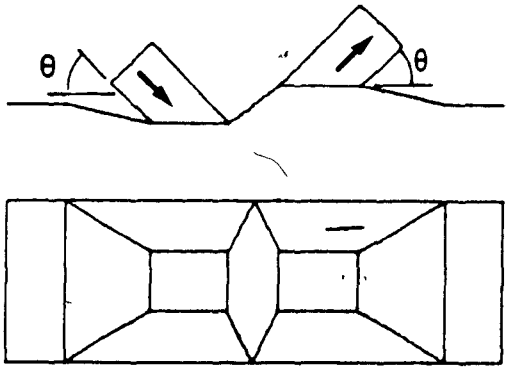

Fig. 5.6 Yield line model for planar truss joint.

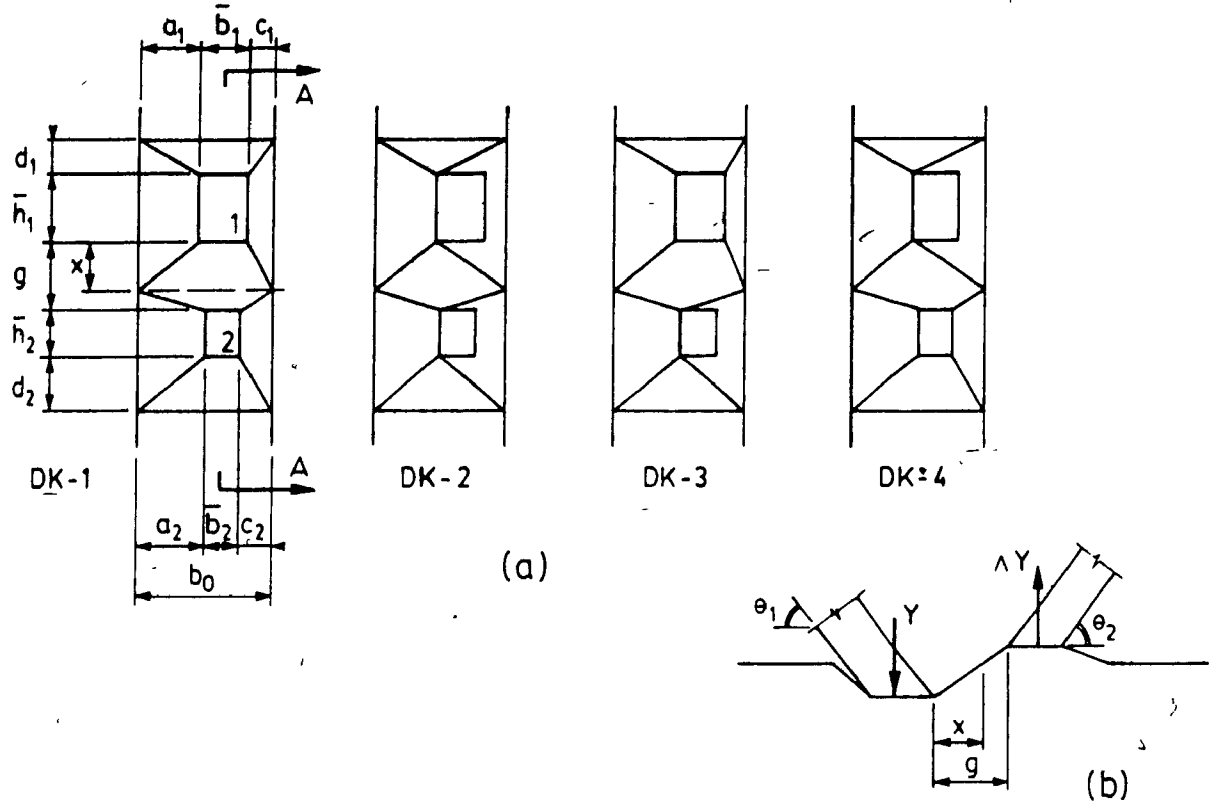

Fig. 5.7 Mechanisms DK-1, DK-2, DK-3, DK-4.
(a) Plan view of chord face. (b) Section AA.

1: compression web member
2: tension web member
Y: component of web member force normal to chord face

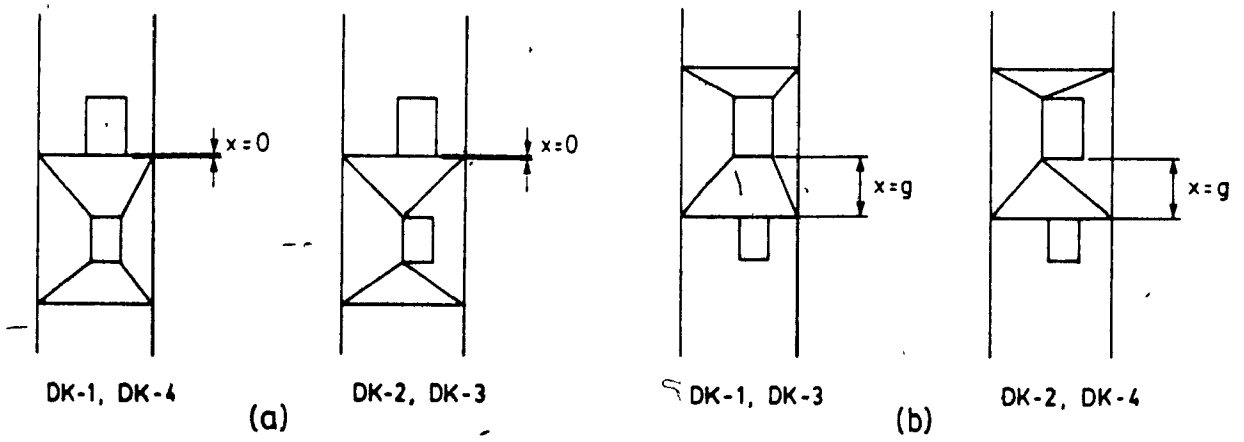

Fig. 5.8 Mecharisms DK-1, DK-2, DK-3, DK-4. Limit cases.
(a) x = 0. (b) x = g.

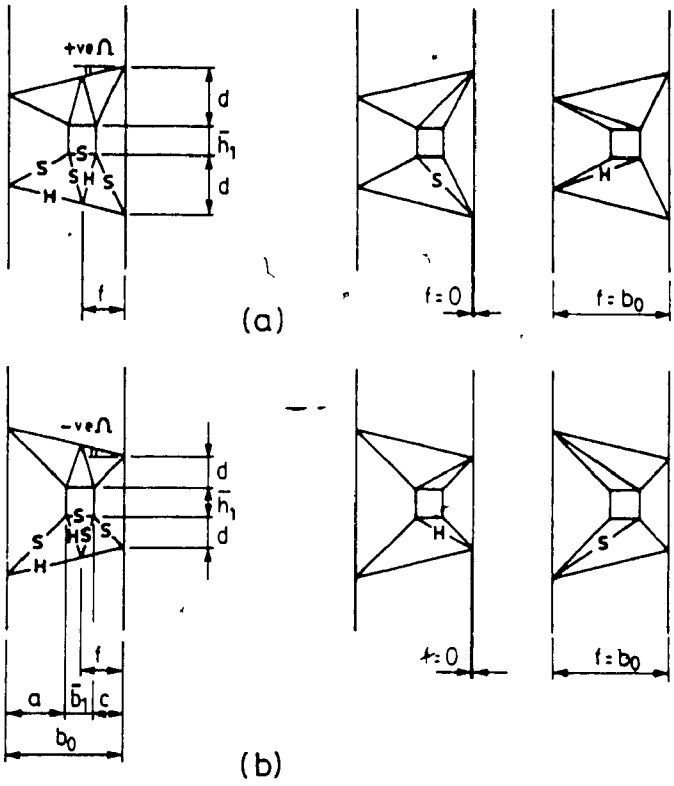

Fig. 5.9 Mechanism DT-1-E. (a) Ω positive. (b) Ω negative.
H: Hogging yield line, S: Sagging yield line

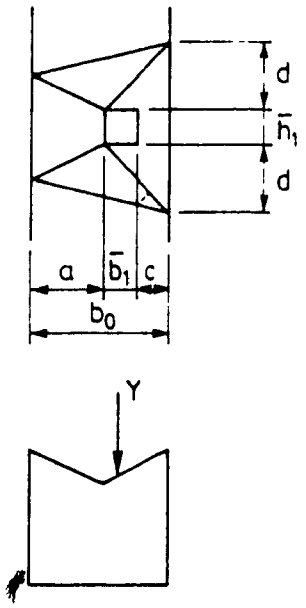

Fig. 5.10 Mechanism DT-2-E.

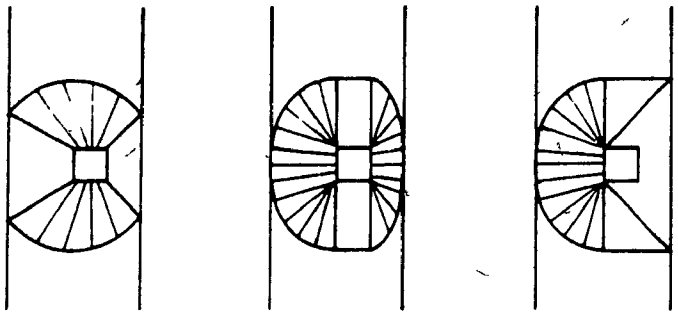

Fig. 5.11 Possible mechanisms with fans. DT joints.

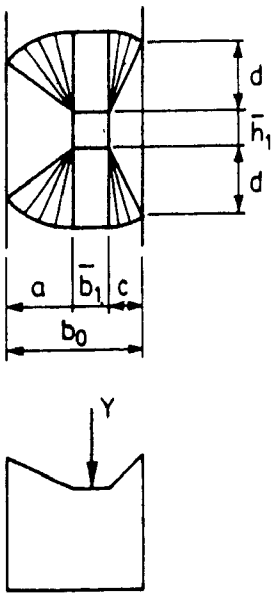

Fig. 5.12 Mechanism DT-1-F.

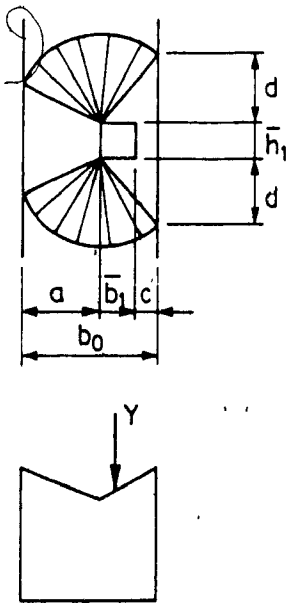

Fig. 5.13 Mechanism DT-2-F.

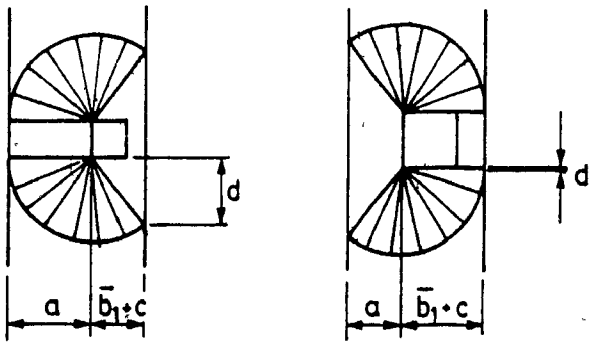

if $a \geq b_1+c$ then $d \geq \sqrt{a^2 - (b_1+c)^2}$

if $a < b_1+c$ then $d \geq 0$

Fig. 5.14 Mechanism DT-2-F. Limit cases.

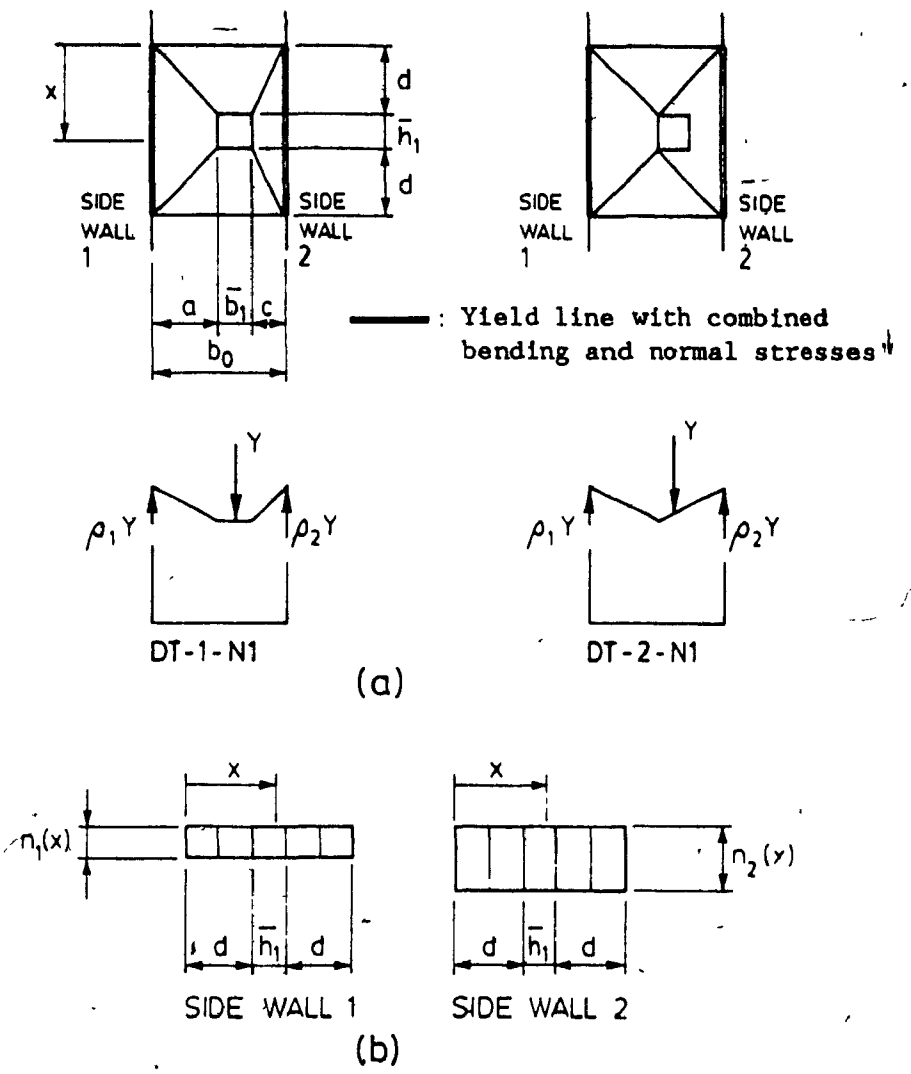

Fig. 5.15 Mechanisms DT-1-N1 and DT-2-N1.
(a) Mechanisms. (b) Normal stress distributions.

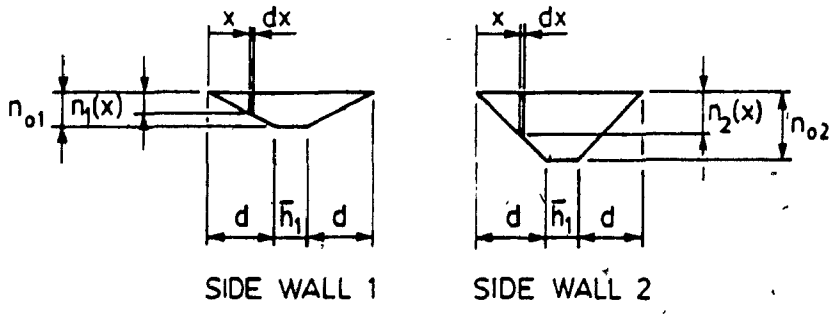

Fig. 5.16 Mechanisms DT-1-N2 and DT-2-N2.
Normal stress distribution.

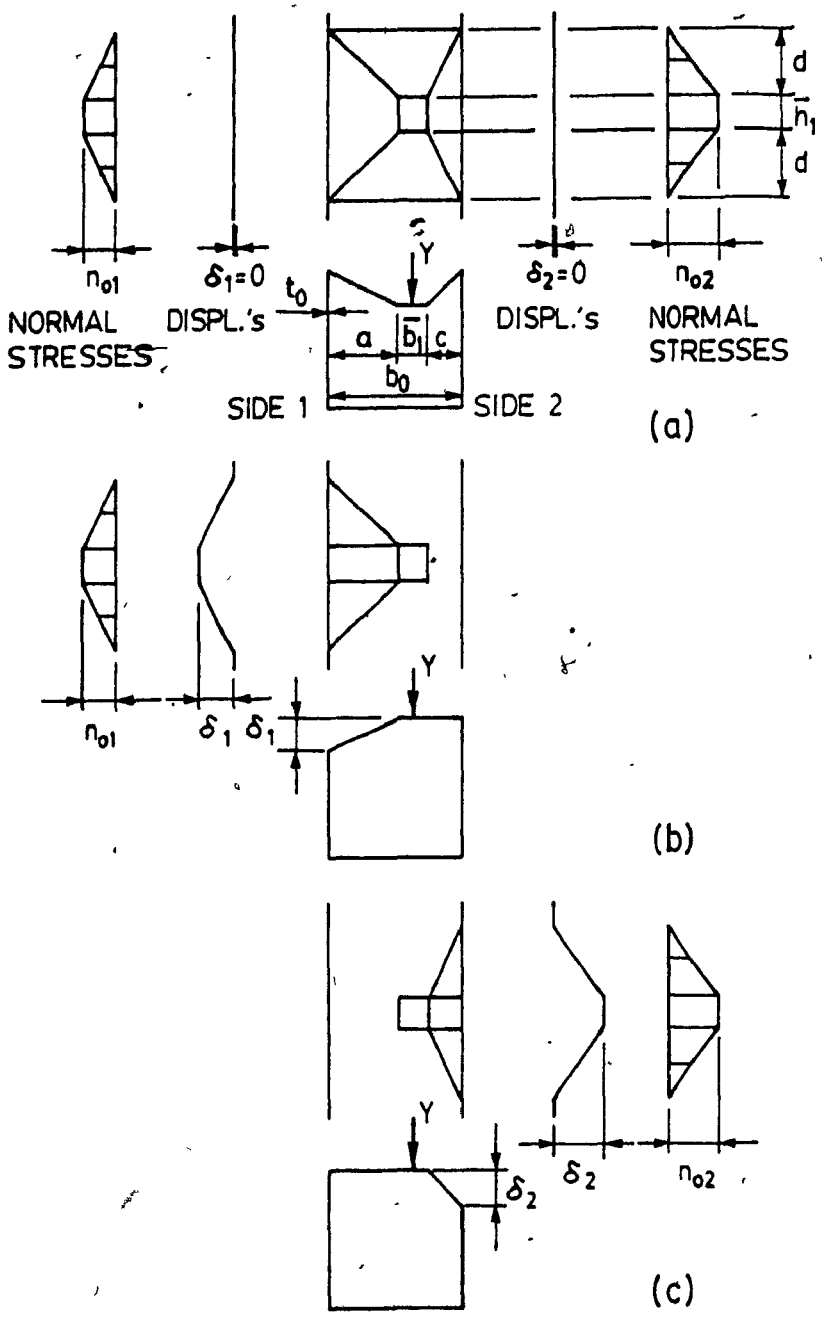

Fig. 5.17 Mechanism DT-1-N3.
(a) Sub-mechanism 1. (b) Sub-mechanism 2. (c) Sub-mechanism 3.

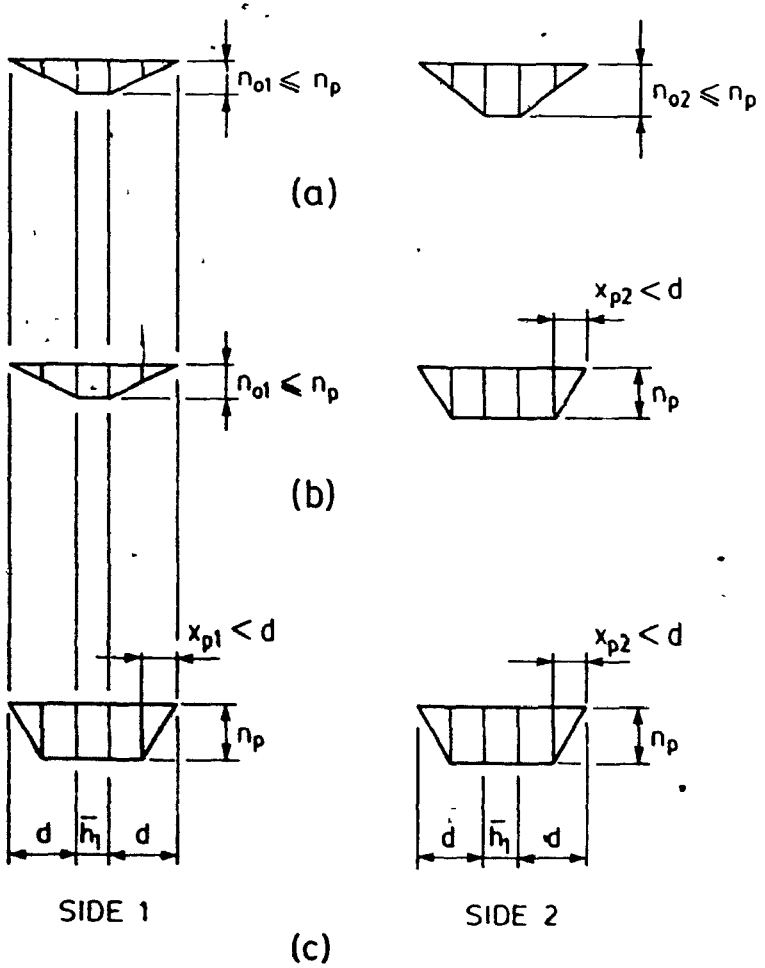

Fig. 5.18 Yield conditions along chord corners. Normal stresses.
(a) Case 1: Combined bending and normal stresses on both sides.
(b) Case 2: Pure squash on side 2.
(c) Case 3: Pure squash on both sides.

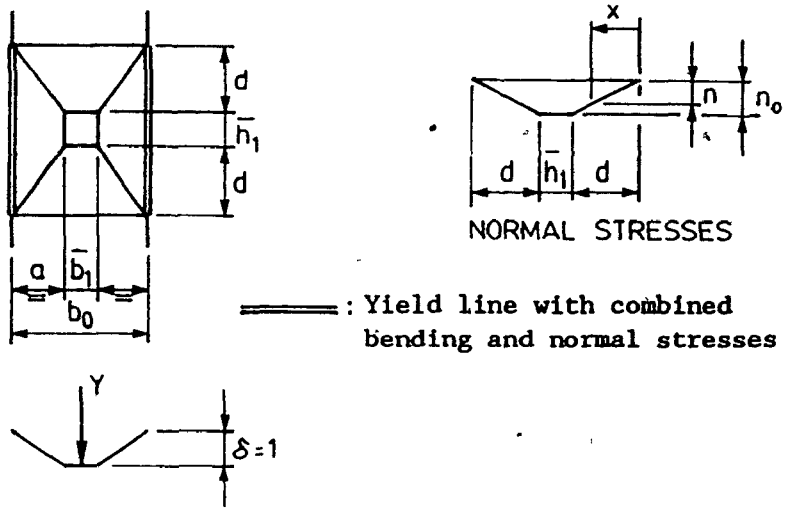

Fig. 5.19 Sub-mechanism 1. Mechanism DT-1-N3, $\lambda = 0.5$.

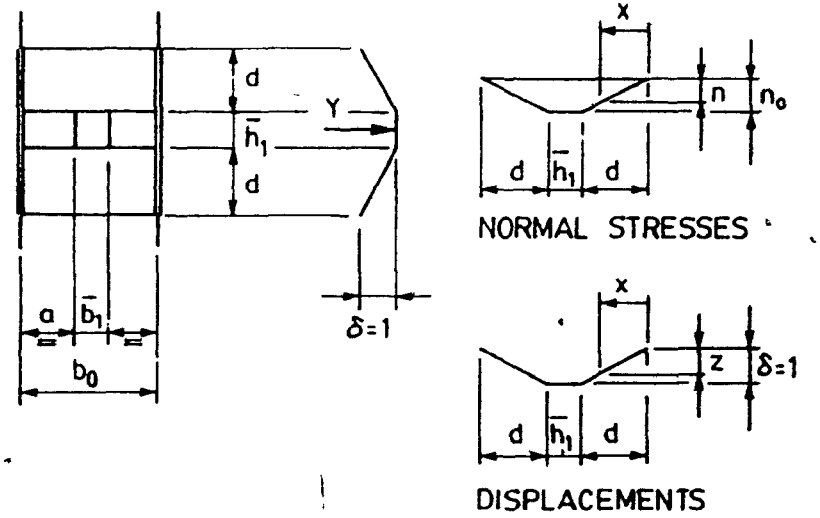

Fig. 5.20 Sub-mechanism 2. Mechanism DT-1-N3, $\lambda = 0.5$.

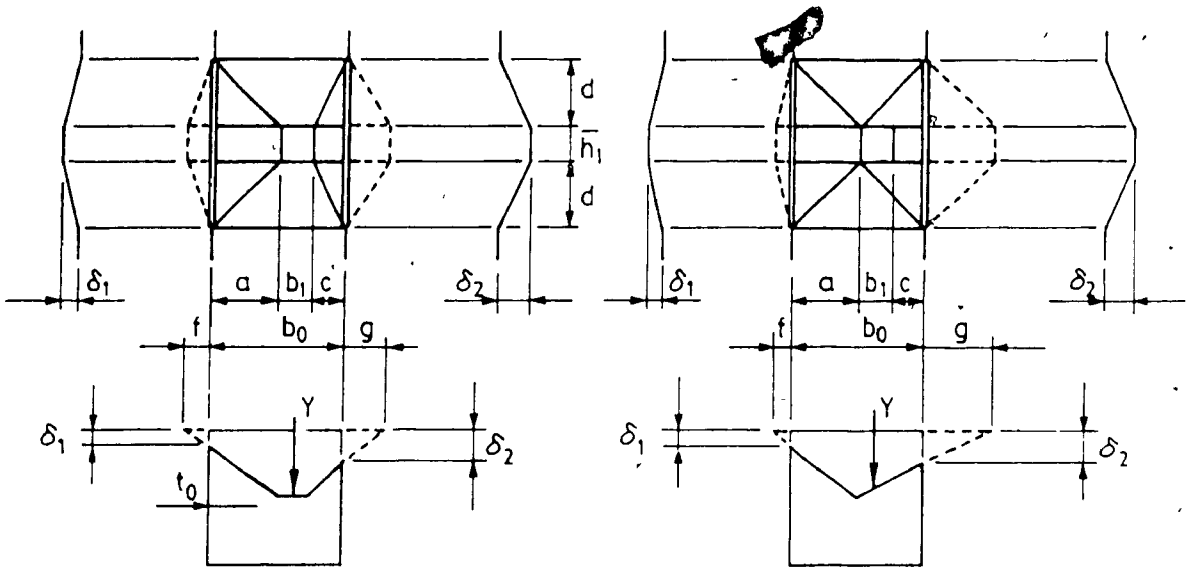

Fig 5 21 Mechanisms DT-1-N4 and DT-2-N4

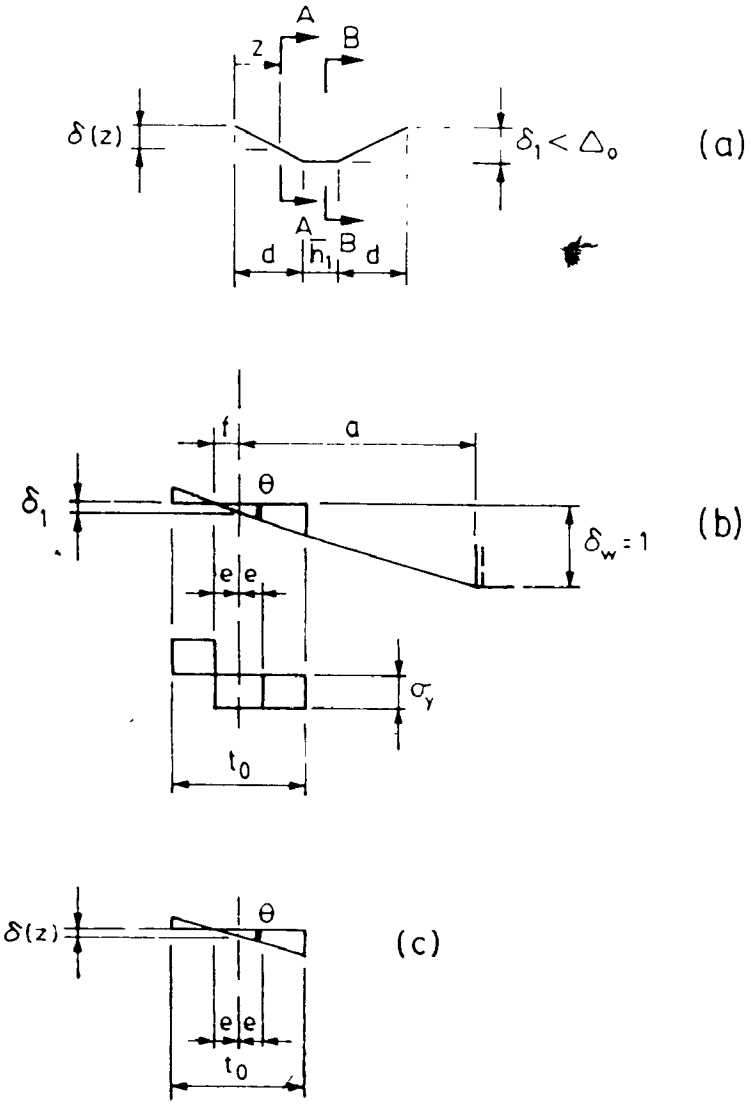

Fig 5.22 Combined stresses along chord corners Mechanisms DT-1-N4 and DT-2-N4
(a) Deflections along the chord corners
(b) Section BB. (c) Section AA.

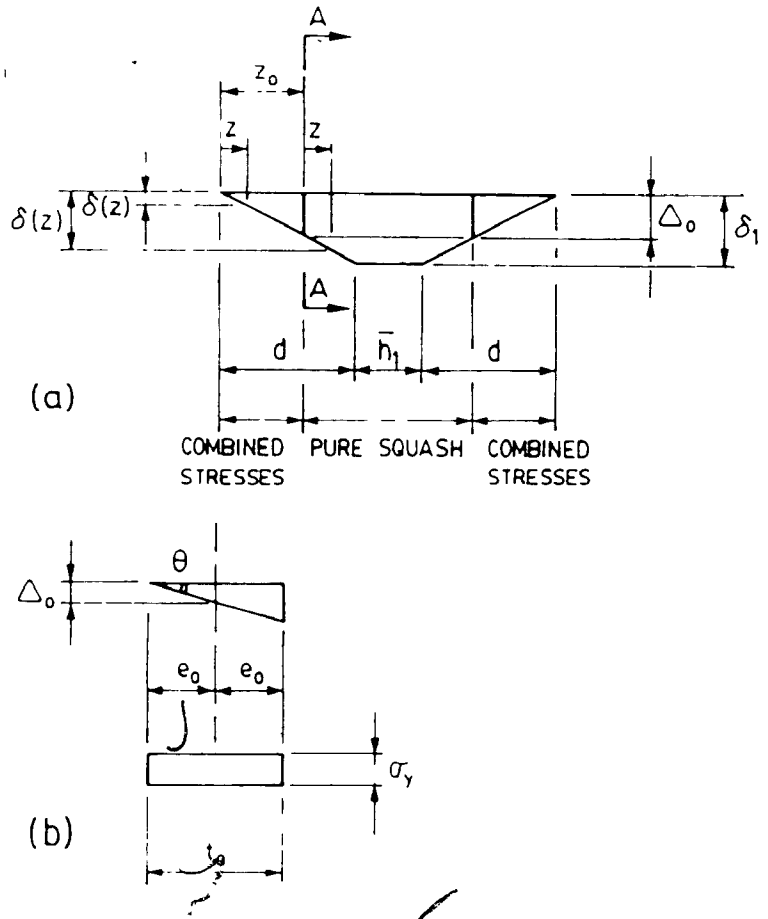

Fig 5 23 Pure squash along chord corners Mechanisms DT-1-N4 and DT-2-N4
(a) Deflections along the chord corners
(b) Section AA at $z = z_o$

Table 5.1 Y_{min}/m_p. Mechanism DT-1

λ \ β	0 2	0 4	0 6	0 8
0 5	19 89	25 99	37 30	67 78
0.6	20.34	26 64	38.32	69 85
0 7	21 90	28 89	41 89	77 13
0 8	25 49	34 15	50 37	94 72
0.9	35 37	49.24	75 50	148 52
1.0	-	-	-	-

Mechanism DT-1 governs above the solid line

Table 5 2 Y_{min}/m_p. Mechanism DT-2

λ \ β	0.2	0.4	0 6	0 8
0.5	21.60	29.77	44.00	80 00
0.6	21 81	29 29	41 82	72 91
0 7	22.96	29.75	40 75	67 95
0 8	25.48	31.23	40.56	64 39
0 9	30.80	34 10	41 18	61 82
1 0	45.00	39.33	42 66	60 00

Mechanism DT-2 governs below the solid line

Table 5 3 Y_{min}/m_p Lowest of mechanism DT-1 and DT-2.

λ \ β	0 2	0 4	0.6	0 8
0 5	19 89 DT-1 -8%	25 99 DT-1 -13%	37 30 DT-1 -15%	67 78 DT-1 -15%
0 6	20 34 DT-1 -7%	26 64 DT-1 -9%	38 32 DT-1 -8%	69 85 DT-1 -4%
0 7	21 90 DT-1 -5%	28 89 DT-1 -3%	40 75 DT-2 -3%	67 95 DT-2 -12%
0 8	25 48 DT-2 0%	31 23 DT-2 -9%	40 56 DT-2 -19%	64 39 DT-2 -32%
0 9	30 80 DT-2 -13%	34 10 DT-2 -31%	41 18 DT-2 -45%	61 82 DT-2 -58%
1 0	45 00 DT-2 -	39 33 DT-2 -	42 66 DT-2 -	60 00 DT-2 -

The 2nd line indicates governing mechanism
The 3rd line gives the reduction from higher to lower predicted load

Table 5 4 Constants used with mechanisms DK-1, DK-2, DK-3 and DK-4

Mechanism	K	L	M	N
DK-1	$\frac{1}{a_1} + \frac{1}{c_1}$	$\frac{1}{a_2} + \frac{1}{c_2}$	1	Λ
DK-2	$\frac{1}{a_1} + \frac{1}{\dot{b}_1+c_1}$	$\frac{1}{a_2} + \frac{1}{\dot{b}_2+c_2}$	$\frac{\dot{b}_1+2c_1}{2(\dot{b}_1+c_1)}$	$\Lambda \frac{\dot{b}_2+2c_2}{2(\dot{b}_2+c_2)}$
DK-3	$\frac{1}{a_1} + \frac{1}{c_1}$	$\frac{1}{a_2} + \frac{1}{\dot{b}_2+c_2}$	1	$\Lambda \frac{\dot{b}_2+2c_2}{2(\dot{b}_2+c_2)}$
DK-4	$\frac{1}{a_1} + \frac{1}{\dot{b}_1+c_1}$	$\frac{1}{a_2} + \frac{1}{c_2}$	$\frac{\dot{b}_1+2c_1}{2(\dot{b}_1+c_1)}$	Λ

Table 5.5 Y_{min}/m_p. Lowest of mechanisms DK-1, DK-2, DK-3 and DK-4
(a) $g/b_0 = 0.1$. (b) $g/b_0 = 0.2$ (c) $g/b_0 = 0.3$ (d) $g/b_0 = 0.4$.

β_2	λ_2	β_1 / λ_1	0.2			0.4		
			0.5	0.7	0.9	0.5	0.7	0.9
0.2	0.5		31.94 1	31.87 1	31.94 1	31.94 1	31.94 1	31.94 1
	0.7		31.87 1	32.74 1	33.33 1	33.33 1	33.33 1	33.33 1
	0.9		31.94 1	33.33 1	41.85 1	36.99 1	39.20 1	43.24 1
0.4	0.5		31.94 1	33.33 1	36.99 1	36.33 1	36.95 1	36.99 1
	0.7		31.94 1	33.33 1	39.20 1	36.95 1	38.41 1	39.21 1
	0.9		31.94 1	33.33 1	43.24 1	36.99 1	39.21 1	53.88 1
0.6	0.5		31.94 1	33.33 1	43.14 1	36.99 1	39.21 1	46.65 1
	0.7		31.94 1	33.33 1	43.24 1	36.99 1	39.21 1	50.44 1
	0.9		31.94 1	33.33 1	43.24 1	36.99 1	39.21 1	55.73 1
0.8	0.5		31.94 1	33.33 1	43.24 1	36.99 1	39.21 1	55.73 1
	0.7		31.94 1	33.33 1	43.24 1	36.99 1	39.21 1	55.73 1
	0.9		31.94 1	33.33 1	43.24 1	36.99 1	39.21 1	55.73 1

β_2	λ_2	β_1 / λ_1	0.6			0.8		
			0.5	0.7	0.9	0.5	0.7	0.9
0.2	0.5		31.94 1	31.94 1	31.94 1	31.94 1	31.94 1	31.94 1
	0.7		33.33 1	33.33 1	33.33 1	33.33 1	33.33 1	33.33 1
	0.9		43.14 1	43.24 1	43.24 1	43.24 1	43.24 1	43.24 1
0.4	0.5		36.99 1	36.99 1	36.99 1	36.99 1	36.99 1	36.99 1
	0.7		39.21 1	39.21 1	39.21 1	39.21 1	39.21 1	39.21 1
	0.9		46.65 1	50.44 1	55.73 1	55.73 1	55.73 1	55.73 1
0.6	0.5		45.65 1	46.63 1	46.65 1	46.65 1	46.65 1	46.65 1
	0.7		46.63 1	49.28 1	50.47 1	50.47 1	50.47 1	50.47 1
	0.9		46.65 1	50.47 1	63.95 2	64.77 2	64.77 2	64.77 2
0.8	0.5		46.65 1	50.47 1	64.77 2	71.89 1	73.89 1	73.87 4
	0.7		46.65 1	50.47 1	64.77 2	73.89 1	79.99 1	80.62 4
	0.9		46.65 1	50.47 1	64.77 2	73.87 3	80.62 3	81.86 2

(a)

β_2	λ_2	β_1 / λ_1	0.2			0.4		
			0.5	0.7	0.9	0.5	0.7	0.9
0.2	0.5		21.94 1	22.50 1	22.94 1	22.94 1	22.94 1	22.94 1
	0.7		22.50 1	23.33 1	24.52 1	24.44 1	24.52 1	24.52 1
	0.9		22.94 1	24.52 1	33.24 1	28.32 1	30.44 1	35.13 4
0.4	0.5		22.94 1	24.44 1	28.32 1	26.99 1	27.84 1	28.33 1
	0.7		22.94 1	24.52 1	30.44 1	27.84 1	29.21 1	30.79 1
	0.9		22.94 1	24.52 1	35.13 3	28.33 1	30.79 1	39.01 2
0.6	0.5		22.94 1	24.52 1	34.76 1	28.33 1	30.79 1	37.49 4
	0.7		22.94 1	24.52 1	35.59 2	28.33 1	30.79 1	39.55 4
	0.9		22.94 1	24.52 1	35.59 2	28.33 1	30.79 1	40.44 2
0.8	0.5		22.94 1	24.52 1	35.59 2	28.33 1	30.79 1	40.44 2
	0.7		22.94 1	24.52 1	35.59 2	28.33 1	30.79 1	40.44 2
	0.9		22.94 1	24.52 1	35.59 2	28.33 1	30.79 1	40.44 2

β_2	λ_2	β_1 / λ_1	0.6			0.8		
			0.5	0.7	0.9	0.5	0.7	0.9
0.2	0.5		22.94 1	22.94 1	22.94 1	22.94 1	22.94 1	22.94 1
	0.7		24.52 1	24.52 1	24.52 1	24.52 1	24.52 1	24.52 1
	0.9		34.76 1	35.59 2	35.59 2	35.59 2	35.59 2	35.59 2
0.4	0.5		28.33 1	28.33 1	28.33 1	28.33 1	28.33 1	28.33 1
	0.7		30.79 1	30.79 1	30.79 1	30.79 1	30.79 1	30.79 1
	0.9		37.49 3	39.55 3	40.44 2	40.44 2	40.44 2	40.44 2
0.6	0.5		36.65 1	38.06 1	38.60 4	38.65 1	38.65 1	38.65 1
	0.7		38.06 1	40.47 1	42.13 4	42.85 1	42.85 1	42.85 1
	0.9		38.60 3	42.13 3	45.95 2	47.58 2	47.58 2	47.58 2
0.8	0.5		38.65 1	42.85 1	47.58 2	63.89 1	65.38 4	63.55 4
	0.7		38.65 1	42.85 1	47.58 2	65.38 3	68.20 2	65.40 2
	0.9		38.65 1	42.85 1	47.58 2	63.55 3	65.40 2	63.66 2

(b)

Table 5 5 Cont'd

δ_2	λ_2	β_1 / λ_1	0.2			0.4		
			0.5	0.7	0.9	0.5	0.7	0.9
0.2	0.5		19.11 1	19.73 1	20.61 1	20.55 1	20.61 1	20.61 1
	0.7		19.73 1	20.59 1	22.37 4	21.94 1	22.29 1	22.38 1
	0.9		20.61 1	22.37 3	29.63 2	25.88 3	27.75 3	31 22 2
0.4	0.5		20.55 1	21.94 1	25.88 4	24.33 1	25.29 1	26.29 4
	0.7		20.61 1	22.29 1	27.75 4	25.29 1	26.67 1	28.63 4
	0.9		20.61 1	22.38 1	31.22 2	26.29 3	28.63 3	33.83 2
0.6	0.5		20.61 1	22.38 1	31.44 4	26.33 1	28.90 1	33.95 4
	0.7		20.61 1	22.38 1	31.94 4	26.33 1	29.05 3	35.43 4
	0.9		20.61 1	22.38 1	31.94 2	26.33 1	29.05 1	35.81 2
0.8	0.5		20.61 1	22.38 1	31.94 2	26.33 1	29.05 1	35.97 2
	0.7		20.61 1	22.38 1	31.94 2	26.33 1	29.05 1	35.97 2
	0.9		20.61 1	22.38 1	31.94 2	26.33 1	29.05 1	35.97 2

δ_2	λ_2	β_1 / λ_1	0.6			0.8		
			0.5	0.7	0.9	0.5	0.7	0.9
0.2	0.5		20.61 1	20.61 1	20.61 1	20.61 1	20.61 1	20.61 1
	0.7		22.38 1	22.38 1	22.38 1	22.38 1	22.38 1	22.38 1
	0.9		31.44 3	31.94 3	31.94 2	31.94 2	31.94 2	31.94 2
0.4	0.5		26.33 1	26.33 1	26.33 1	26.33 1	26.33 1	26.33 1
	0.7		28.90 1	29.05 4	29.05 1	29.05 1	29.05 1	29.05 1
	0.9		33.95 3	35.43 3	35.81 2	35.97 2	35.97 2	35.97 2
0.6	0.5		34.32 1	35.92 1	36.23 4	37.32 1	37.32 1	37.32 1
	0.7		35.92 1	38.33 1	39.06 4	41.90 1	41.90 1	41.89 4
	0.9		36.23 3	39.06 3	40.49 2	42.94 2	42.94 2	42.94 2
0.8	0.5		37.32 1	41.90 1	42.94 2	62.56 1	62.73 4	60.09 4
	0.7		37.32 1	41.90 1	42.94 2	62.73 3	63.52 2	60.54 2
	0.9		37.32 1	41.89 3	42.94 2	60.09 3	60.54 2	58.48 2

(c)

δ_2	λ_2	β_1 / λ_1	0.2			0.4		
			0.5	0.7	0.9	0.5	0.7	0.9
0.2	0.5		17.94 1	18 62 1	19.92 4	19.66 1	19.90 1	19.94 1
	0.7		18.62 1	19.52 1	21.64 4	21.01 1	21.53 1	21.88 4
	0.9		19.92 3	21.64 3	27.81 2	24.84 3	26.58 3	29.37 2
0.4	0.5		19.66 1	21.01 1	24.84 4	23.33 1	24.37 1	25.53 4
	0.7		19.90 1	21.53 1	26.58 4	24.37 1	25.79 1	27.67 4
	0.9		19.94 1	21.88 3	29.37 2	25.53 3	27.67 3	31.59 2
0.6	0.5		19.94 1	21.90 1	30.10 4	25.94 1	28.41 1	32.43 4
	0.7		19.94 1	21.90 1	30.67 2	25.98 3	28.67 3	33.71 2
	0.9		19.94 1	21.90 1	30.71 2	25.98 3	28.69 3	33.85 2
0.8	0.5		19.94 1	21.90 1	30.90 2	25.99 1	28.97 1	34.44 2
	0.7		19.94 1	21.90 1	30.90 2	25.99 1	28.97 1	34.44 2
	0.9		19.94 1	21.90 1	30.90 2	25.99 1	28.97 1	34.44 2

δ_2	λ_2	β_1 / λ_1	0.6			0.8		
			0.5	0.7	0.9	0.5	0.7	0.9
0.2	0.5		19.94 1	19.94 1	19.94 1	19.94 1	19.94 1	19.94 1
	0.7		21.90 1	21.90 1	21.90 1	21.90 1	21.90 1	21.90 1
	0.9		30 0 3	30.67 2	30.71 2	30.90 2	30.90 2	30.90 2
0.4	0.5		25.94 1	25.98 4	25.98 4	25.99 1	25.99 1	25.99 1
	0.7		28.41 1	28.67 4	28.69 4	28.97 1	28.97 1	28.97 1
	0.9		32.43 3	33.71 2	33.85 2	34.44 2	34.44 2	34.44 2
0.6	0.5		33.65 1	35.03 4	35.20 4	37.65 1	37.65 1	37.63 4
	0.7		35.03 3	37.45 2	37.75 4	40.85 2	40.85 2	40.85 2
	0.9		35 20 3	37.75 3	38.17 2	41.44 2	41.44 2	41.44 2
0.8	0.5		37.65 1	40.85 2	41.44 2	62.89 1	62.12 4	59.07 4
	0.7		37.65 1	40.85 2	41.44 2	62.12 3	61.96 2	58.84 2
	0.9		37.63 3	40.85 2	41.44 2	59.07 3	58.84 2	56.54 2

(d)

Notes:

1: Mechanism DK-1, 2. Mechanism DK-2, 3 Mechanism DK-3, 4 Mechanism DK-4

Square contact dimensions: $\bar{b}_1 = \bar{h}_1$ and $\bar{b}_2 = \bar{h}_2$

$m_p = 1.0$.

Table 5.6 Y_{min}/m_p Mechanism DT-1-E.

	β			
λ	0.2	0 4	0 6	0 8
0 5	*	*	*	*
0 6	*	*	*	*
0 7	*	*	*	*
0.8	*	*	50 14 0 5%	94.41 0 3%
0 9	35 27 0 3%	47.73 3.2%	<72 73 >3 8%	<145 11 >2' 3%
0 6	-	-	-	-

* P_{min}/m_p same as for basic mechanism DT-1

Table 5 7
Y_{min}/m_p Mechanism DT-1-F

λ \ β	0 2	0 4	0 6	0 8
0 5	16 55 17%	22 95 -12%	34 76 -7%	65 98 -3%
0 6	17 42 -14%	23 67 -11%	35 77 -7%	68 02 -3%
0 7	20 30 7%	26 65 -8%	39 34 -6%	75 21 2%
0 8	27 16 +7%	34 45 +1%	49 04 -3%	92 63 -2%
0 9	49 17 +39%	60 28 +22%	82 51 +9%	149 17 +0 4%
1 0	-	-	-	-

Table 5 8
Y_{min}/m_p Mechanism DT-2-F

λ \ β	0 2	0 4	0 6	0 8
0 5	18 41 -15%	28 42 -5%	48 46 +10%	108 51 +36%
0 6	17 65 19%	26 22 -10%	43 23 +3%	93 58 +28%
0 7	18 99 -17%	25 36 -15%	39 96 -2%	83 14 +22%
0 8	22 55 -11%	25 77 -17%	38 04 -6%	75 54 +17%
0 9	30 09 2%	28 38 -17%	37 20 -10%	69 87 +13%
1 0	50 57 +12%	34 02 -14%	37 35 -12%	65 57 +9%

Table 5 9 Y_{min}/m_p Lowest of mechanisms DT-1, DT-2, DT-1-F and DT-2-F

λ \ β	0 2	0 4	0 6	0 8
0 5	16 55 DT-1-F -17%	22 95 DT-1-F -12%	34 76 DT-1-F -7%	65 98 DT-1-F -3%
0 6	17 42 DT-1-F -14%	23 67 DT-1-F -11%	35 77 DT-1-F -7%	68 02 DT-1-F -3%
0 7	18 99 DT-2-F -13%	25 36 DT-2-F -12%	39 34 DT-1-F -3%	67 95 DT-2 -
0 8	22 55 DT-2-F -11%	25 77 DT-2-F -17%	38 04 DT-2-F -6%	64 39 DT-2 -
0 9	30 09 DT-2-F -2%	28.38 DT-2-F -17%	37.20 DT-2-F -10%	61 82 DT-2 -
1.0	45 00 DT-2 -	34 02 DT-2-F -14%	37.35 DT-2-F -12%	60 00 DT-2 -

The 2nd line gives the governig mechanism.
The 3rd line gives the reduction of the predicted joint load from the lowest of basic mechanisms DT-1 or DT-2.

Table 5.10 Constants used with mechanisms DT-1-N and DT-2-N

Mechanism	K_1	K_2	K_3	K_4	K_5
DT-1	$\frac{1}{a} + \frac{1}{c}$	1	$\left(\frac{\rho_1^2}{a} + \frac{\rho_2^2}{c} \right) \frac{t_0^2}{16}$	$8 K_1 K_3 + K_2^2$	$4 K_1 K_3 + K_2^2$
DT-2	$\frac{1}{a} + \frac{1}{b_1+c}$	$\frac{b_1+2c}{2(b_1+c)}$	$\left(\frac{\rho_1^2}{a} + \frac{\rho_2^2}{b_1+c} \right) \frac{t_0^2}{16}$	$8 K_1 K_3 + K_2^2$	$4 K_1 K_3 + K_2^2$

Table 5.11 Y_{min}/m_p. Mechanism DT-1-N1 (a) $b_0/t_0 = 10\ 0$ (b) $b_0/t_0 = 20\ 0$. (c) $b_0/t_0 = 30.0$. (d) $b_0/t_0 = 40.0$

(a)

		β			
		0 2	0 4	0.6	0 8
λ	0 5	19 61	25 41	35.67	58 94
	0 6	20.01	25.96	36.46	60.05
	0 7	21 33	27.80	39.08	63 58
	0 8	24 06	31 62	44 40	70 12
	0 9	29 00	38 77	53 94	79 94
	1 0	-	-	-	-

(b)

		β			
		0 2	0 4	0 6	0 8
λ	0 5	19 82	25 84	36 87	65 11
	0 6	20 26	26 46	37 82	66 84
	0 7	21 75	28 60	41 12	72 75
	0 8	25.10	33 45	48 61	85 67
	0 9	33 34	45 70	67 29	114 07
	1 0	-	-	-	-

(c)

		β			
		0 2	0 4	0 6	0 8
λ	0 5	19 86	25 92	37.10	66 54
	0 6	20 30	26 56	38 10	68 45
	0 7	21.83	28 76	41.54	75 06
	0 8	25 31	33 84	49 56	90 28
	0 9	34.42	47 55	71 41	129 06
	1 0	-	-	-	-

(d)

		β			
		0.2	0 4	0 6	0 8
λ	0.5	19.87	25 95	37 19	67 07
	0.6	20 32	26 59	38 19	69 05
	0 7	21.86	28 81	41 69	75.94
	0.8	25 39	33.97	49 91	92 12
	0.9	34.82	48 26	73.10	136 34
	1.0	-	-	-	-

Square contact dimensions: $\bar{b}_1 = \bar{h}_1$

Table 5.12 Y_{min}/m_p. Mechanism DT-2-N1. (a) $b_0/t_0 = 10.0$. (b) $b_0/t_0 = 20.0$. (c) $b_0/t_0 = 30.0$. (d) $b_0/t_0 = 40.0$.

(a)

	β			
λ	0 2	0.4	0.6	0.8
0 5	21.29	29.10	42.01	69.12
0.6	21.51	28 72	40.34	65.29
0 7	22.54	29 16	39.51	62 26
0.8	24.73	30 48	39.40	59.91
0 9	28 95	32.95	39 96	58.13
1 0	37.44	37 20	41 25	56 82

(b)

	β			
λ	0 2	0.4	0.6	0 8
0 5	21.52	29 60	43 47	76 70
0 6	21.73	29 15	41 43	70.70
0 7	22.85	29 60	40 43	66.35
0 8	25 29	31.04	40.26	63.15
0 9	30.30	33.80	40 86	60 82
1 0	42.65	38.76	42.29	59.14

(c)

	β			
λ	0 2	0.4	0 6	0.8
0.5	21 56	29.70	43 76	78 47
0 6	21.78	29.23	41 64	71.90
0.7	22 91	29.68	40 60	67.22
0.8	25 39	31.14	40 42	63 83
0 9	30.58	33.96	41.04	61 37
1 0	43.90	39.07	42.49	59 61

(d)

	β			
λ	0.2	0 4	0 6	0.8
0.5	21.58	29.73	43.87	79.13
0.6	21.79	29.26	41.72	72.33
0.7	22.93	29.71	40.67	67.54
0.8	25.43	31.18	40.48	64.07
0 9	30.67	34.02	41.10	61.56
1.0	44.37	39.18	42.57	59.78

Square contact dimensions: $\bar{b}_1 = \bar{h}_1$

Table 5.13 Y_{min}/m_p. Lowest of mechanisms DT-1-N1 and DT-2-N1.
(a) $b_0/t_0 = 10.0$. (b) $b_0/t_0 = 20.0$. (c) $b_0/t_0 = 30.0$. (d) $b_0/t_0 = 40.0$.

(a)

	β	0.2		0.4		0.6		0.8	
λ	0.5	19.61	1.39	25.41	2.22	35.67	4.36	58.94	13.04
	0.6	20.01	1.63	25.96	2.53	36.46	4.85	60.05	14.03
	0.7	21.33	2.60	27.80	3.77	39.08	4.10	62.26	8.37
	0.8	24.06	5.56	30.48	2.40	39.40	2.86	59.91	6.95
	0.9	28.95	6.03	32.95	3.35	39.96	2.95	58.13	5.98
	1.0	37.44	16.80	37.20	5.40	41.25	3.31	56.82	5.31

(b)

	β	0.2		0.4		0.6		0.8	
λ	0.5	19.82	0.35	25.84	0.57	36.87	1.16	65.11	3.94
	0.6	20.26	0.42	26.46	0.65	37.82	1.30	66.84	4.30
	0.7	21.75	0.67	28.60	0.99	40.43	0.79	66.35	2.35
	0.8	25.10	1.48	31.04	0.62	40.26	0.74	63.15	1.91
	0.9	30.30	1.62	33.80	0.87	40.86	0.77	60.82	1.62
	1.0	42.65	5.23	38.76	1.45	42.29	0.87	59.14	1.43

(c)

	β	0.2		0.4		0.6		0.8	
λ	0.5	19.86	0.16	25.92	0.25	37.10	0.52	66.54	1.82
	0.6	20.30	0.19	26.56	0.29	38.10	0.58	68.45	2.00
	0.7	21.83	0.30	28.76	0.44	40.60	0.35	67.22	1.07
	0.8	25.31	0.66	31.14	0.28	40.42	0.33	63.83	0.87
	0.9	30.58	0.73	33.96	0.39	41.04	0.34	61.37	0.73
	1.0	43.90	2.44	39.07	0.65	42.49	0.39	59.61	0.64

(d)

	β	0.2		0.4		0.6		0.8	
λ	0.5	19.87	0.09	25.95	0.14	37.19	0.29	67.07	1.04
	0.6	20.32	0.10	26.59	0.17	38.19	0.33	69.05	1.14
	0.7	21.86	0.17	28.81	0.25	40.67	0.20	67.54	0.61
	0.8	25.39	0.36	31.18	0.16	40.48	0.19	64.07	0.49
	0.9	30.67	0.41	34.02	0.22	41.10	0.19	61.56	0.41
	1.0	44.37	1.40	39.18	0.37	42.57	0.22	59.78	0.36

The 2nd numbers give the % reduction from the Y_{min}/m_p values in Table 5.3.
Square contact dimensions: $\bar{b}_1 = \bar{h}_1$.

Table 5.14 Y_{min}/m_p. Lowest of mechanisms DT-1-N4 and DT-2-N4.
(a) $b_0/t_0 = 10.0$. (b) $b_0/t_0 = 20.0$. (c) $b_0/t_0 = 30.0$. (d) $b_0/t_0 = 40.0$.

(a)

	β = 0.2		0.4		0.6		0.8	
λ = 0.5	19.71	0.92	25.56*	1.65	35.31**	5.34	58.50**	13.68
0.6	20.12	1.10	26.09*	2.04	36.06**	5.89	59.64**	14.62
0.7	21.50	1.82	27.89*	3.45	38.61**	5.24	61.51**	9.47
0.8	24.43*	4.12	30.32*	2.92	39.04**	3.73	58.95**	8.45
0.9	28.78*	6.56	32.67*	4.19	39.58**	3.87	57.06**	7.70

(b)

	β = 0.2		0.4		0.6		0.8	
λ = 0.5	19.84	0.23	25.89	0.37	36.33**	2.59	61.70**	8.97
0.6	20.28	0.28	26.52	0.45	37.20**	2.91	63.21**	9.50
0.7	21.79	0.48	28.64	0.85	40.20**	1.35	64 47**	5.12
0.8	25.20	1.10	31.01	0.71	40.13*	1.06	61.52**	4 45
0.9	30.22	1.90	33.73*	1.09	40.69*	1.19	59 39**	3.93

(c)

	β = 0.2		0.4		0.6		0 8	
λ = 0.5	19.87	0.10	25.95	0.17	36.67**	1.69	62.71**	7.48
0.6	20.31	0.13	26.58	0.20	37.57*	1 94	64.33**	7.89
0.7	21.85	0.22	28.79	0.34	40.57*	0.44	65.40**	3.75
0.8	25.36	0.49	31.13	0.32	40.38*	0.44	62.33**	3.19
0.9	30.53	0.87	33.93	0.48	40.97*	0.50	60.12**	2.75

(d)

	β = 0.2		0.4		0.6		0.8	
λ = 0.5	19.88	0.06	25.97	0.09	36.83**	1.25	63.20**	6.75
0.6	20.33	0.07	26.61	0.11	37.76*	1.46	64.88**	7.11
0.7	21.87	0.12	28.83	0.19	40.67	0.19	65.86**	3.08
0.8	25.41	0.27	31.17	0.18	40.48	0.19	62.73**	2.57
0.9	30.65	0.50	34.00	0.27	41.09	0.22	60.48**	2.17

The 2nd numbers give the % reduction from the Y_{min}/m_p values in Table 5.3.

Square contact dimensions: $b_1 = h_1$.

* : Pure squash on side 2.

** : Pure squash on both sides.

CHAPTER 6 DESIGN CONSIDERATIONS

The test programs have given some indication of the strength of the tension chord joints, and have also shown that web compression member strength is an important consideration, and interaction between joint deformations and buckling of these members is possible. In the following these features of triangular truss behaviour are discussed in greater detail, and in addition, other factors which must be considered in design are treated, including the joints to the compression chords and appropriate methods of analysis.

HSS planar truss behaviour has been the object of two decades of research effort in many different countries, with much of this attention being devoted to the behaviour of joints (Wardenier 1982) and it is only recently that agreement among researchers in these several countries has been sufficiently close for definitive design recommendations to be prepared (CIDECT). In comparison with this effort, the 7 truss tests and 24 joint tests outlined in Chapters 2 and 3 provide a very meagre base on which to establish a design procedure for triangular trusses. It is clear, however, that in addition to these test results, some of the work on planar trusses has relevance to triangular trusses. In the following discussion therefore, triangular truss behaviour will be related, when possible, to planar truss behaviour. For convenience, those features of the geometry of a triangular truss which are referenced are summarized in Appendix A.

6.1 TENSION CHORD GAP JOINT BEHAVIOUR - CHORD WALL BENDING

In the general case, an axial force N in a web member has a component, Y, normal to the wall of the chord and two components in the plane of the wall, one being a longitudinal force, X, and the other a transverse force Z, as

shown in Fig. 6 1 When the angle between web planes, α, is 90°, the Z force becomes zero, and the loading on the attached walls of the chord is then similar to the loading on the wall of a planar truss chord

Thus, for $\alpha = 90°$, if failure is associated primarily with deformations of the attached wall, then there is reason to expect the planar and triangular truss joints to behave in similar ways, as shown schematically in Fig 6 2a If the mode of failure involves the side walls as well as the attached wall, as shown in Fig 6 2b, the triangular truss joint might be slightly stiffer, since one of the side walls is also attached to web members, and these will inhibit the relevant side wall displacement

When the web planes are separated by an angle less than 90°, which will be a frequent case, the transverse in-plane forces, Z, will exist and will tend to flatten the tube cross-section under the compression web members in a shearing type of displacement shown in Fig 6 2c The stiffness of adjacent parts of the chord will resist this tendency to deform the cross-section shape and, in particular, the zone to which the tension web members are attached will be effective in doing this

The combined action of the loads Y and Z on the chord wall will result in the idealized plastic deformations of the chord cross section shown in Fig 6.2d. The three top-most plastic hinges shown in this diagram may not all exist, and in the real section, the increased strength of the material in the corner will force the hinges away from the corners These idealized models may be compared with observed cross-section deformations shown in Figs. 2.3 and 2.4

Fig. 6.2b and d show that when side wall deformation in 90° trusses takes place, the compression web members may tend to bend out of the web plane, away from the axis of symmetry of the truss For trusses with

$\alpha < 90°$, this effect will be more significant because the web members will seldom be placed centrally on the chord wall, since to do so would create a large offset between the intersection of the web member axes and the chord axis This is illustrated by the configuration of Truss No 4 in Fig 2 3

In summary, joints in 90° trusses have some basic similarities to plane truss joints and, in particular, the modes of failure in which bending of the connected chord wall predominates are similar For $\alpha < 90°$ the transverse shear on the chord wall will tend to flatten the cross section, which does not occur in planar trusses, and cross section deformations also differ

Design equations for the tension chord joints of a triangular truss are proposed based on the basic yield line mechanisms presented in Chapter 5 (Eqs [5 2 24] to [5 2 33]), and are as follows

> The joint resistance Y_r is the lowest value of the minimum resistance for mechanisms DK-1, DK-2, DK-3 and DK-4, the minimum resistance being, for each mechanism, the lowest of the following three possible resistances

if $0 < x < g$

$$Y_r = \phi \frac{2\, m_p}{\left(M + N \frac{g-x}{x} \right)} \left[K (\bar{h}_1+d_1+x) + L (\bar{h}_2+d_2+g-x) \frac{g-x}{x} + \frac{b_0}{d_1} + \frac{b_0}{d_2} \frac{g-x}{x} + \frac{b_0}{x} \right] \qquad [6\ 1]$$

if $x < 0$, $x > g$ or x is imaginary

$$Y_r = \phi \frac{2\, m_p}{N} \left[L (\bar{h}_2+d_2+g) + \frac{b_0}{d_2} + \frac{b_0}{g} \right] \qquad (\text{at } x = 0) \qquad [6.2]$$

or

$$Y_r = \phi \frac{2\, m_p}{M} \left[K (\bar{h}_1+d_1+g) + \frac{b_0}{d_1} + \frac{b_0}{g} \right] \qquad (\text{at } x = g) \qquad [6.3]$$

where

$$d_1 = \sqrt{\frac{b_0}{K}} \quad , \quad d_2 = \sqrt{\frac{b_0}{L}} \quad , \qquad [6\ 4]$$

if $p \neq 0$

$$x = \frac{-q \pm \sqrt{q^2 - 4pr}}{2p} \quad , \qquad [6\ 5]$$

if $p = 0$.

$$x = -\frac{r}{q} \quad , \qquad [6\ 6]$$

where

$$p = \frac{1}{g}(K+L)(M-N)$$

$$q = 2N(K+L) \qquad [6\ 7]$$

$$r = (\bar{h}_1+d_1)KN - (\bar{h}_2+d_2+g)LM + \frac{b_0}{d_1}N - \frac{b_0}{d_2}M - \frac{b_0}{g}(M-N) - gLN$$

where K, L, M, and N are defined in Table 5 4

If $\beta_1 = 1.0$ (and $\beta_2 < 1\ 0$), Y_r is found from Eq [6 2] If $\beta_2 = 1\ 0$ (and $\beta_1 < 1.0$), Y_r is found from Eq [6 3] If $\beta_1 = \beta_2 = 1\ 0$, none of the above solutions are valid

Note that $\bar{b}_i$ and $\bar{h}_i$ are the attached width of the web members, i e

$$\bar{b}_i = b_i \sec(45° - \frac{\alpha}{2}) \qquad [6\ 8]$$

$$\bar{h}_i = h_i \operatorname{cosec} \theta \qquad [6\ 9]$$

where b_i and h_i are the web member sizes. g is the gap dimension at the joint, as shown in Fig 5 7 The dimension a_i and c_i are also defined in the Figure.

The web member weld size and the chord corner curvature can be taken into account by replacing $\bar{b}_i$, $\bar{h}_i$ and b_0 by $\bar{b}_i'$, $\bar{h}_i'$ and b_0', respectively, as defined by Eqs [5.2.7] to [5 2.9], and adjusting the values of a_i, c_i and g in Eqs. [6.1] to [6.9] Such an interpretation of the joint geometry leads to higher predicted joint strengths

Inclusion of a performance factor, ϕ, in these equations is required for conformity with the usual format of limit state design used in Canada (CSA 1984) Using the procedure presented by Kennedy and Gad Aly (1980), Minicucci and Zafrani (1986) calculated a value of the ϕ factor equal to 0 8591 ≈ 0 86 for triangular truss tension chord joints, based on test results of the 16 DT joints that experienced chord face failure

The use of Eqs [6.1] to [6 9] outside the range of parameters examined in the tests should be treated with caution The principal parameters were limited in the truss segment tests and in the DT joint tests to those shown in Table 6 1

6 2 TENSION CHORD GAP JOINT BEHAVIOUR - CONDITIONS IN THE GAP

The ratio of average web member width to chord width, β, has a significant influence on the joint strength In order to increase the resistance of the joint when governed by failure of the connected chord wall, choice of rectangular section members (b > h) will frequently be made in order to increase β without increasing web member mass. Furthermore, for triangular trusses with $\alpha < 90^{\circ}$ the width of web member attached to the chord will exceed the nominal member width, thus leading to a higher effective β For high values of β, the chord wall deformations may become less critical than the conditions in the gap between tension and compression web members, where the chord section is loaded by high tension and shear forces as well as bending moments. For planar trusses, the whole chord cross section is considered in resisting these gap forces (Wardenier 1982), and with the same assumption, Bauer (1982) gives equations for the strength of a square chord oriented such that shear forces act across one diagonal, and bending is about the other diagonal, as shown in Fig. 6 3b. Two solutions are given

(Bauer 1982), one based on the attainment of full yield of the cross section and the other based upon assumed strain hardening of the material The latter model gives ultimate loads from 22% to 40% greater than the yield model in a number of trial cases, but its form is considerably more complex than the yield model. This yield model is therefore proposed in modified form suitable for design, as follows·

$$\frac{M_f}{M_r} + \left(\frac{T_f}{T_r}\right)^2 + \left(\frac{V_f}{V_r}\right)^2 < 1.4 \qquad [6\ 10]$$

where the right hand side has been increased from 1 0 to 1 4 to account for strain hardening This results in an increase in resistance of about 20-25%, depending on the geometry In this equation,

$$M_r = \phi\ Z_z F_y = \phi\ 0\ 943\ Z_x\ F_y$$

$$V_r = \phi\ \frac{A}{\sqrt{2}}\ \frac{F_y}{\sqrt{3}} = \phi\ 0\ 408\ A\ F_y \qquad [6\ 11]$$

$$T_r = \phi\ A\ F_y$$

and M_f, T_f and V_f are the factored bending moment, tensile force and shearing force acting in the gap. The moment M_f is a function of the eccentricity in the joint, e, and also the position of the web member on the chord wall, defined by ψ, as shown in Fig. 6 3a and b. General expressions for this moment and the other force components are given in Appendix B

For planar HSS trusses, it is recommended (Stelco 1981) that eccentricities should lie within the range $-0.5\ b_0 \le e \le 0.33\ b_0$ The corresponding range for the tension chord in a triangular truss is $-0.71\ b_0 \le e \le 0.47\ b_0$, and it is recommended that this range be adhered to, even though the gap conditions are more fully treated herein for triangular trusses.

6.3 COMPRESSION CHORD JOINTS - GENERAL

No test results related to the behaviour of compression chord joints in HSS triangular trusses are available, and therefore some caution must be exercised in their design. Overlap joints with direct transfer of some or all of the vertical and transverse loads directly between web members may be preferred, particularly if heavy concentrations of load are applied at the joints through purlins On the other hand, in lightly loaded trusses, gap joints to the compression chord are seen to be feasible when treated as discussed below This approach is by means of analysis based on conservative assumptions or on extrapolation of other available test results

A gap joint is shown in Fig 6 4 In the region of this joint, three design checks must be made which consider (i) connection of bracing members in the top plane of the truss, (ii) connection of bracing members to the compression chord, and (iii) conditions in the gap

(i) Bracing Members in Top Plane These bracing members are connected to a chord wall which is normal to the plane in which they lie, and the joint can therefore be treated as in a planar truss, or as in a triangular truss tension chord joint with $\alpha = 90°$ With N or K arrangement of bracing members, Eqs. [6.1] to [6.9] can again be used by letting $\alpha = 90°$ If only a tie member is used, with no diagonals, the resistance of the resulting T joint, expressed as the force in the tie, is given as

$$T_r = \phi \frac{2.2 t_0^2 F_y}{(1-\beta)} \left[\frac{h_3}{h_0} + 2\sqrt{1-\beta} \right] \qquad [6\ 12]$$

which is based on Eq [5.2.12]. F_y is the chord yield stress, h_0 the chord height, and h_3 the tie width (in the horizontal direction). Eq. [6.12] is limited to cases where $\beta = b_3/h_0 < 0\ 85$. For greater values of

β, appropriate design equations are given elsewhere (Wardenier 1981, 1982)

(ii) Connection of Web Members to Compression Chord. The web members transmit loads to the bottom wall of the compression chord with components Y normal to the wall, Z transverse to it, and X in the longitudinal direction as shown in Fig. 6.4. It is proposed that the normal force Y be treated using triangular truss tension chord joint equations, Eqs. [6.1] to [6.9], with $\bar{b}_1$ being now defined as

$$\bar{b}_1 = b_1 \sec(\alpha/2) \qquad [5.2\ 6] \text{ (repeated)}$$

This is based on the performance of DK trusses nos. 4 and 6 and DT joints nos 1, 2, 3, 5, 6, 8 and 21 in the tension chord joint tests, where the lateral inclination of the web members did not appear to significantly affect the joint strength It should however be recognised that the inclination to the compression chord will often exceed that existing in these tests

The increased value of $\bar{\beta}$ resulting from the inclination of the web members, together with the fact that the two compression chords will frequently be smaller sections than the tension chord (i.e., b_0 will be smaller), will in general lead to high predicted strengths of the joints, and suggests that the gap conditions, discussed below, may be of greater concern.

(iii) Conditions in the Gap. The gap in the compression chord is subjected to a complex state of stress resulting from the axial force, biaxial bending moments and shearing forces, and torsion. These loading conditions are illustrated in Fig. 6.4c. It is conservatively assumed that short chord gaps exist between the horizontal tie member and the two web members. The tie resists the out of balance Z component forces, and also develops secondary bending moments as it resists twisting of the compression chords. In the gaps loading conditions may be critical either at Section AA or Section BB as shown in Fig. 6.4a. Which of these is critical depends primarily on whether

$N_1\cos\theta_1$ is greater or less than $N_2\cos\theta_2$, although the web members positions on the wall of the chord, defined by ψ_1 and ψ_2 shown in Fig 6 4b, also have a slight influence The gap resistance must therefore be evaluated at these two sections The loads at Section AA are shown in Fig 6.4c, and expressions for these loads are given in Appendix B Moments are again dependent on eccentricity and on ψ_1 and ψ_2, and four eccentricities must be considered in the general case, as shown in Fig. 6 4b The eccentricities e'_1, e'_2, $e"_1$ and $e"_2$ can be found from geometrical considerations once the gap dimensions g_1 is known, and the relevant relationships are given in Appendix A The value of g should be selected as the minimum consistent with welding requirements The designer has little control over the values of $e"_1$ which will in general exceed the maximum value of $0.33b_0$ recommended for planar trusses Since the resulting moments are being considered explicitely the necessarily large eccentricity can be accepted The values of e'_1 on the other hand can be expected to lie within the limits given for planar trusses

The conditions in the chord gaps can be checked by using an iteraction equation representing full yield of the cross section under the combined action of the loads described above, as shown in Fig 6 4c An exact formulation treating all of these load components is not available, although biaxial bending, axial load and torque have been treated (Morris and Fenves 1969) A simplified treatment is suggested which makes use of interaction equations for biaxial bending and axial force given in the Canadian Standard CAN3-S16.1-M84 (CSA 1984) Thus for square chord sections, the gap loads should satisfy

$$\frac{1}{\sqrt{1-\bar{r}^2}}\left[\frac{C_{rg}}{C_r}+0.85\left(\frac{M_{rz}}{M_{rz}}+0.5\frac{M_{ry}}{M_{ry}}\right)\right]<1.0 \qquad [6\ 13]$$

The bracketed term is given in S16 1-M84 (CSA 1984), and in it M_{fz}/M_{rz} should be interchanged with M_{fy}/M_{ry} if $M_{fy} > M_{fz}$. The term preceeding the brackets accounts for the presence of shearing stresses due to torsion and the shearing forces In this the term $\bar{r}$ is written as follows:

$$\bar{r} = \left| \frac{M_{ft}}{M_{rt}} \right| + \frac{1}{2} \left| \frac{V_{fz}}{V_{rz}} \right| + \frac{1}{2} \left| \frac{V_{fy}}{V_{ry}} \right| \qquad [6\ 14]$$

where it is required that

$$V_{fz} \leq 0\ 5\ V_{rz} \qquad [6\ 15]$$

In the case of a rectangular section chord, the term in square brackets in Eq [6 13] should be replaced by Eq. [9a] of Clause 13 8.3 of S16 1-M84 (CSA 1984)

In the above equations, the factored resistances are given by the following.

$$C_r = \phi\ A\ F_y$$

$$M_{ry} = \phi\ Z_y\ F_y$$

$$M_{rz} = \phi\ Z_z\ F_y$$

$$V_{ry} = \phi\ 1.15\ h_0\ t_0\ F_y \qquad [6\ 16]$$

$$V_{rz} = \phi\ 1.15\ b_0\ t_0\ F_y$$

$$M_{rt} = \phi\ 1.15\ (h_0-t_0)\ (b_0-t_0)\ t_0\ F_y$$

The factored loads C_{fg}, M_{ft}, etc. are given in Appendix B

The proposed treatment of the tension and compression chord gaps in triangular trusses is considerably more detailed than the suggested treatment of planar truss chord gaps (Stelco 1981). For the latter, the extensive test data justifies the neglect of moments in the gap for small eccentricities.

With limited test results for tension chords of triangular trusses and none for compression chords, together with the fact that the geometry does not permit easy adjustment of eccentricities, which leads to quite large values in the compression chord, it is considered that the design checks proposed are justified until further information becomes available

6 4 COMPRESSION STRENGTH OF WEB MEMBERS

A recent study of the behaviour of compression members in planar trusses (de Ville de Goyet et al 1981) indicates that web members in trusses without eccentricity at the joints will usually have effective length factors less than 0 8 However, in cases where eccentricity exists it is recommended that either K be taken as unity and the bars be treated as axially loaded, or K be evaluated on the basis of available restraint from other truss members, and at the same time the secondary moments be calculated and the axial force-moment interaction be taken into account These studies considered both HSS and W-shaped members.

For planar trusses with HSS members, recommended effective length factors are 0.9 or less (Stelco 1981) At the same time joints are designed either by conservatively estimating their ultimate strength (Stelco 1981, Eastwood and Wood 1970), or by ensuring that the joint deformation remains small under the factored loads (Packer 1983, Packer and Haleem 1981)

For triangular trusses, there is less certainty that joint deformations will be small at the loads predicted by Eqs [6 1] to [6 9] Furthermore, secondary bending moments causing bending out, as well as in, the web plane arise particularly when $\alpha < 90°$. Interaction between web member buckling and joint deformations is possible, as observed in the truss segment tests For these reasons, supported by the K values obtained from the truss tests, it is

not appropriate to use effective length factors less than 0.9. It is of obvious convenience in design to treat the compression web member as axially loaded only and, if this is to be done, with the uncertainties associated with the secondary moments, together with the possible interaction of buckling with joint deformation, the appropriate K values may be greater than those for planar HSS trusses. It is suggested that the effective length factor of web members should be taken as 0.95 for both axes of bending unless it is established that the joint resistance at both ends of the member exceeds the web member resistance based on this value by at least 25% In this case values of K of 0 90 or lower would be appropriate, as long as the joint resistance still exceeds the revised web member resistance by 25% The value of 0.95 is proposed, in spite of the recommendations of de Ville de Goyet et al (1981), on the basis of the test results and established practice for planar HSS trusses

For the chords the effective length factors used in planar truss design are suggested as being appropriate The bottom chord is laterally braced by the inclined web members, and therefore out of plane buckling under reversals due to wind loads is unlikely to be critical.

6.5 OTHER CONSIDERATIONS

The following additional factors should be considered in the design of a triangular truss

1. Truss analysis - this should be carried out by treating the triangular truss as a space truss, that is, no moment continuity at joints need be considered (Bauer et al. 1983).
2. In simply supported trusses, chords will frequently have reduced cross-section areas near the supports, and, for appearance, this will normally

be achieved by maintaining the same nominal chord wall widths and reducing the wall thickness. The critical joints will therefore be near the ends of the truss where in addition, web members carry their maximum loads.

3 Notwithstanding item 2., the smaller web member forces near the centre of the truss will lead to smaller width ratios, which could result in critical joint behaviour in this region

4 In the event that the tension chord is curtailed just beyond its outermost joints, and not continued to the supports, the chord should be provided with an end plate sufficiently stiff to maintain the cross-section shape under the action of the nearby joint loads

5. Secondary moments due to joint eccentricities should be considered in the chords as in the case of planar trusses Expressions for these moments are given in Appendix B.

6. The end joints of the compression chords are at the points of bearing As far as possible eccentricities should be minimized at this point in view of the single chord which must resist secondary moments.

7 The joint strength equations [6.1] to [6 9] are proposed herein without restriction on the magnitudes of the joint parameters. For planar trusses, limits on eccentricity are specified (Stelco 1981), and recent planar joint strength equations are accompanied by specific limits on their applicability, these limits corresponding to those of the tests on which they are based (Packer 1983, Wardenier 1981, 1982). It will not be always possible to keep triangular truss joint parameters within these same limits, but they do provide guidance and should be satisfied when possible. An example where it will seldom be possible to satisfy the planar truss limit on eccentricity is in e", over which the designer has little control once the angle between web planes has been selected.

6.6 DESIGN AIDS

The design procedure proposed in this chapter can be rather long, especially if all the calculations are done by hand. To simplify the task of calculations, design aids have been investigated based on the following two approaches:

1) a graphical approach using simplified plots based on values obtained from the design equations. Simplified graphs predicting tension chord face resistance were produced and presented by Skold (1986) Further work is required to cover all design considerations based on this approach.

2) a computerized approach using spreadsheets that allow the design equations to be checked. Three programs have been used, namely, Lotus' 123, Symphony and Hewlett Packard's Executive Spreadsheet, all running on IBM PC and compatibles. The spreadsheets include calculations of truss and joint geometries, checks of the tension and compression chord face resistance and gap resistance, checks of eccentricity limits, etc. The spreadsheets also contain tables of HSS section sizes and properties that are used for the interactive selection of members. Further details about these spreadsheets are given by Minicucci and Zafrani (1986).

The next chapter presents an example of the design of a triangular truss. All the calculations in this example are given in detail and were done by hand for illustration purposes. It should be noted that the graphical aids or better the computer spreadsheets mentioned above can be used advantageously in lieu of hand calculations for the design of HSS triangular trusses.

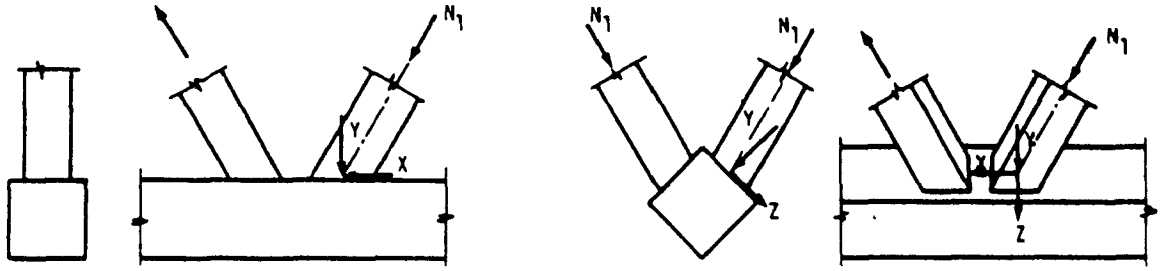

Fig. 6 1 Components of load on tension chord wall

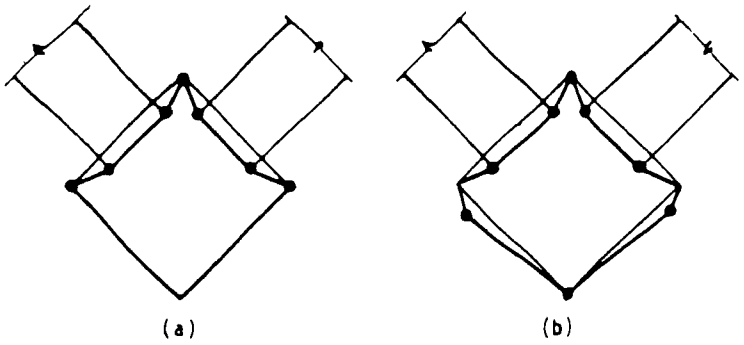

Chord deformation with $\alpha = 90°$

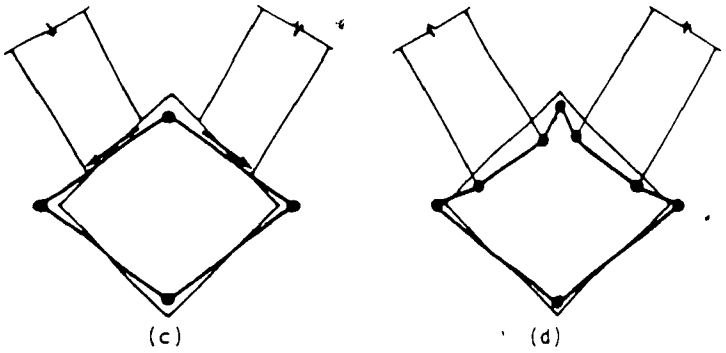

Chord deformation with $\alpha < 90°$

Fig 6 2 Idealized chord deformations under web compression members

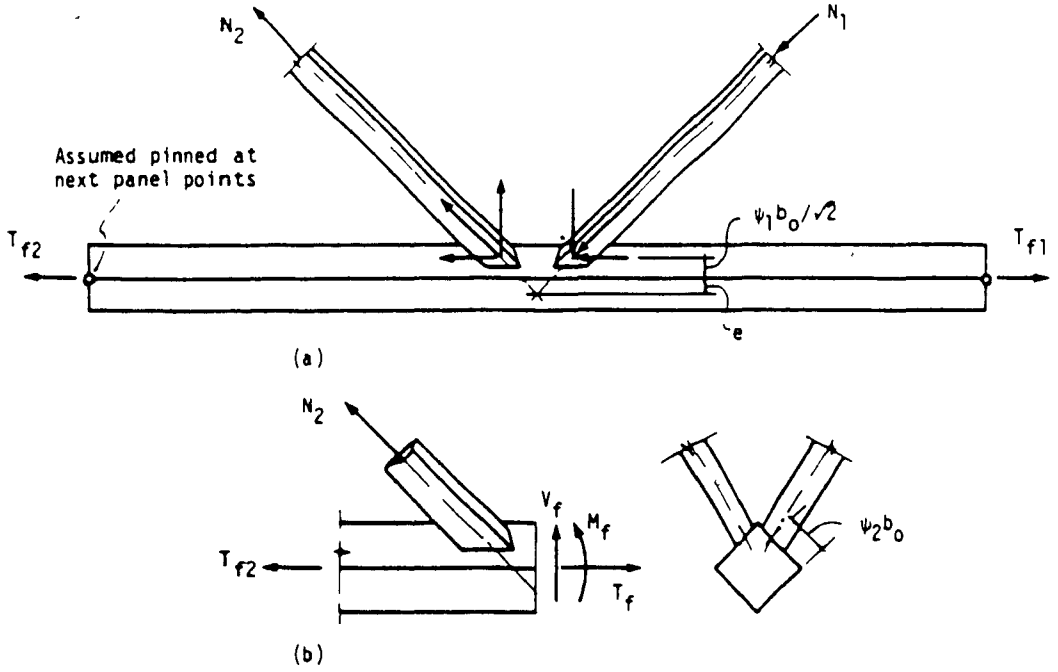

Fig 6.3 Forces in tension chord members and gap Intermediate joint
(a) Forces on tension chord. (b) Forces in the gap

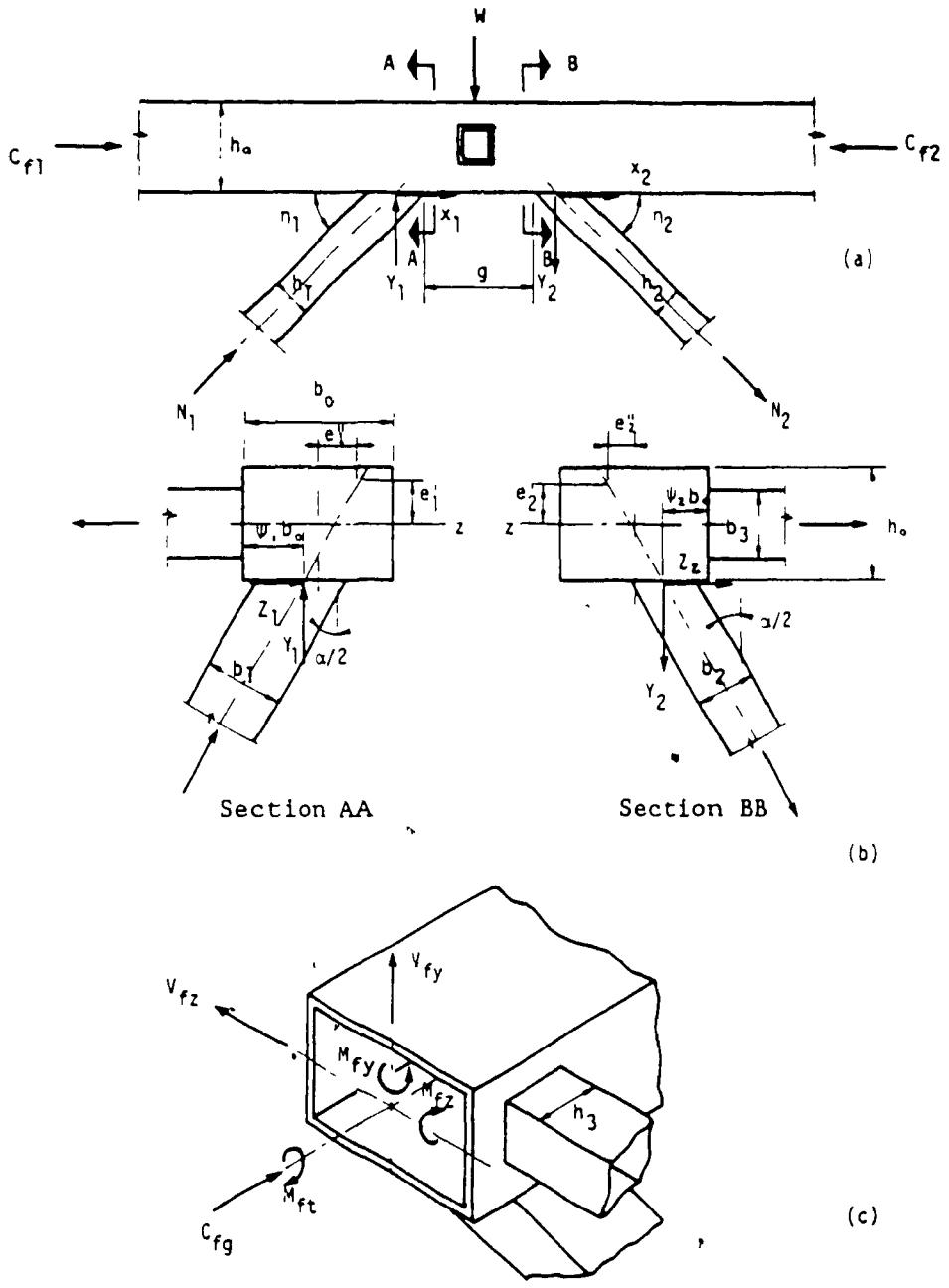

Fig 6.4 Compression chord joint

Table 6.1 Limit values of principal test parameters (a) Truss segment tests (b) DT joint tests.

$60° \leq \alpha \leq 90°$	$30° \leq \alpha \leq 90°$
$15\ 8 \leq b_o/t_o \leq 26\ 0$	$20\ 0 \leq b_o/t_o \leq 37\ 2$
$0\ 4 \leq \beta \leq 0\ 62$	$0\ 2 \leq \beta \leq 0\ 6$
$0\ 52 \leq \tilde{\beta}' \leq 0\ 77$	$0\ 286 \leq \tilde{\beta}' \leq 0\ 752$
(a)	(b)

CHAPTER 7 DESIGN EXAMPLE

In the following, some of the main features of a triangular truss design are described. The truss considered spans 22 m and is shown in Fig 7 1 Loading is assumed to be applied by purlins directly to the compression chord joints, and is considered to be applied symmetrically about the truss centre-line, resulting in no torsion of the truss These assumptions simplify the design and are made for clarity In a real truss, roof decking may be supported directly by the compression chords, and unsymmetric loading or lateral loading would lead to a requirement for shear stiffness in the top plane of the triangular truss, resulting in consideration of diaphragm action, or Vierendeel or diagonal truss action in this plane (Cases of triangular trusses subjected to unbalanced loading have been studied by Kawczak 1983) The one loading condition considered comprises factored gravity load of 32 kN/m

Emphasis is on aspects of design particular to triangular trusses Welding is not considered and for the treatment of welding details, reference should be made elsewhere (Stelco 1981), where a wide range of HSS applications is described. Other details not considered include support bearing points and purlin support details

The geometry of one panel is shown in Fig 7 2a The truss has parallel chords and a Warren arrangement of members with all web members having the same inclination, θ, to the chord axis Thus $\theta_1 = \theta_2 = \theta = 59\ 23^\circ$ At the same time web members lie in a plane which is at an angle of $45^\circ - \alpha/2$ (-15°) to the plane which is normal to the tension chord wall and which contains the chord axis, as shown in Fig 7 2b Therefore if the factored axial load in a web member is N_{t1}, the component of this force normal to the tension

chord wall (the Y_i component given in Fig 6 1), is given by

$$Y_{fi} = N_{fi} \sin\theta_i \cos(45^\circ - \alpha/2) \qquad [7\ 1]$$

For the example truss, $Y_{fi} = 0.830\ N_{fi}$ for the tension chord.

For the compression chord, the component of force normal to the chord wall (Y_i as shown in Fig 6 4) is given by

$$Y_{fi} = N_{fi} \sin\theta_i \cos(\alpha/2) \qquad [7\ 2]$$

for the example truss, this becomes $Y_{fi} = 0.744\ N_{fi}$ The length of the web members is 2688 mm in all cases, this distance being measured between points of intersection of the member axes in the idealized geometry shown in Fig 7 2a

For symmetric loading and the support conditions shown in Fig 7 1, the truss is statically determinate, and can be analysed by hand with relative ease. Alternatively a space truss analysis by computer could be used The member axial forces are shown in Fig. 7.3a, and the preliminary selection of member sizes is shown in Fig 7 3b. This selection is discussed below The material corresponds to CSA Standard G40.21-M81 Grade 350W and is Class H in accordance with CSA Standard G40 20-M81

In the example, the possibility of using gap joints will first be investigated. If unreinforced gap joints are not feasible, alternatives are discussed

7 1 PRELIMINARY MEMBER SELECTION

7.1.1 Tension Chord

Member 12-15 $T_f = 968.0$ kN

Due to probable joint eccentricities, there will be a moment in this

member, therefore select member with $T_r > T_f$

Try HSS - 101 6 x 101 6 x 9 53 $\quad T_r = 1030$ kN
$M_r = 34\ 6$ kN m
$r = 36\ 9$ mm

Max permissible factored moment

$$M_f = \left(1 - \frac{T_f}{T_r}\right) M_r = \left(1 - \frac{968}{1030}\right) 34\ 6 = 2\ 08 \text{ kN m}$$

At 15 (Eq B 1)

$$M_f = 0\ 5\ (968\text{-}907\ 5)\ e = 30\ 25\ e$$

. require $e \leq 68\ 8$ mm

This will be satisfied since e is limited to $+\sqrt{2}b_o/3 = 48$ mm

Slenderness ratio, both planes $\frac{Kl}{r} = \frac{0\ 9\ (2750)}{36\ 9} = 67 < 300$

∴ use HSS - 101 6 x 101 6 x 9 53

It may possible to reduce the chord section near the supports The next lighter section, HSS - 101 6 x 101 6 x 7 95 is adequate to carry the axial load and moment providing the following eccentricities are not exceeded

Member			
	3 - 6	e = 37.5 mm	(at joint 3)
	6 - 9	e = 36 7 mm	(at joint 6)

The choice of a lighter section section in this region is, however, influenced significantly by the joint design. The choice of section in this region will therefore be discussed later.

7 1 2 Compression Chord

The compression chord is treated as a beam-column with biaxial bending moments giver by Eqs B 7 and B 8 (Appendix B) Joint geometry must be established before the eccentricities can be determined However, preliminary selection of this chord can be made with the assumption that bending accounts for 15% of the interacting force components in the central region of the truss.

Member 10-13 C_f = 468.8 kN

Try HSS - 101 6 x 101 6 x 6.35 A = 2320 mm^2
$r_x = r_y$ = 38 4 mm

$$\frac{K l}{r} = \frac{0.9\ (2750)}{38.4} = 64.5$$

C_r = 260 (2320) 10^{-3} = 603.2 kN

$$\frac{C_f}{C_r} = \frac{468.8}{603.2} = 0\ 78 < 0\ 85$$

.. suitable as trial section

Further verification will be made after joints are considered

7 1 3 Web Member Design

All members have the same length l = 2688 mm

Take K = 0 95 Kl = 2554 mm

Compression Web Members

The following are the suitable HSS sections with the least mass, which are readily available

Member	C_f (kN)	Section	Kl/r	C_r (kN)
3-4	207.0	76.2 x 76 2 x 4 78	88.7	257
6-7	147.8	76.2 x 76.2 x 4 78	88.7	257
9-10	88.7	63.5 x 63.5 x 3.18	104 7	108
12-13	29.6	50.8 x 50.8 x 2.79	131.6	50

Tension Web Members

All members have the same length l = 2688 mm

Take K = 0.95 Min. rad. of gyration = 0 95 (2688)/300 = 8.5 mm

Member	T_f (kN)	Section	r (mm)	T_r (kN)
1-3	207.0	50.8 x 50 8 x 3 81	18 9	214
4-6	147 8	38.1 x 38.1 x 3.81	13 7	153
7-9	88.7	38.1 x 38.1 x 2.54	14.3	109*
10-12	29.6	38.1 x 38 1 x 2.54	14.3	109*

* These are not the lightest sections, but are selected in order that the value of β not be too low

Member sizes obtained in this preliminary design are shown in Fig. 7 3b

7.2 DESIGN OF JOINTS TO TENSION CHORD

The design of Joint 3 is considered in detail in the following

Data:

b_0 = 101.6 mm
t_0 = 9.53 mm
$b_1 = h_1$ = 76 2 mm
$b_2 = h_2$ = 50 8 mm
N_2 = 207.0 kN (tens)

Factored Loads (Fig 7 3a)

T_{f1} = 423 5 kN
T_{f2} = 0
V = 308 kN
N_1 = 207 0 kN (comp)

7 2 1 Joint Resistance - Chord Wall

Factored normal load on joint $Y_{f1} = 0.83(207\ 0) = 171\ 8$kN (Eq [7 1])

Assume g = 20 mm, λ_1 = 0 5 and λ_2 = 0 769 (see 'Gap Conditions' below) For simplicity and also because it is conservative, the web members weld size and the curvature at the corners of the chord are not considered

Using Eqs [6 1] to [6 9]

$$\bar{b}_1 = b_1 \sec(45°-\alpha/2) = \frac{76\ 2}{\cos(15°)} = 78\ 89 \text{ mm}$$

$$a_1 = c_1 = \frac{b_0-\bar{b}_1}{2} = \frac{101\ 6\ -\ 78\ 89}{2} = 11\ 36 \text{ mm}$$

$$\bar{h}_1 = h_1 \operatorname{cosec}(\theta) = \frac{76\ 2}{\sin(59\ 23°)} = 88\ 68 \text{ mm}$$

$$\bar{b}_2 = b_2 \sec(45°-\alpha/2) = \frac{50\ 8}{\cos(15°)} = 52\ 59 \text{ mm}$$

a_2 = 37 70 mm,

$$c_2 = b_0 - a_2 - \bar{b}_2 = 101\ 6 - 37\ 70 - 52\ 59 = 11\ 31 \text{ mm}$$

Note that

$$\lambda_2 = \frac{a_2}{a_2 + c_2} = \frac{a_2}{b_0 - \bar{b}_2} = \frac{37\ 70}{101\ 6 - 52\ 59} = 0\ 769$$

and

$$\psi_2 = \frac{a_2 + \frac{\bar{b}_2}{2}}{b_0} = \frac{37\ 70 + (52\ 59/2)}{101\ 6} = 0\ 63$$

$$\bar{h}_2 = h_2 \operatorname{cosec}(\theta) = \frac{50\ 8}{\sin(59\ 23°)} = 59\ 12 \text{ mm}$$

$$m_p = 0\ 25\ t_0^2\ F_{y0} = 0\ 25\ (9.53 \text{ mm})^2\ 0.350 \text{ N/mm}^2 = 7\ 947 \text{ kN-m/m}$$

Mechanism DK-1:

K = 0 176134, L = 0.114943, M = 1.0, N = 1 0,

d_1 = 24.017 mm, d_2 = 29.731 mm,

p = 0, q = 0.582153, r = 5.852330,

Eq. [6 6]: x = -10.053 mm ∴ x = 0 mm or 20 mm (-g)

Eq [6.2]: $Y_r = \phi$ 333 9 kN

Eq [6 3]: $Y_r = \phi$ 519 5 kN

Mechanism DK-2

K = 0.099110, L = 0 042175, M = 0 562888, N = 0 588498,

d_1 = 32 018 mm, d_2 = 49 082 mm,

p = -0.000181, q = 0 166291, r = 4.332301,

Eq [6 5]: x = -25.353 mm, 944.529 mm ∴ x = 0 mm or 20 mm (-g)

Eq. [6 2]: $Y_r = \phi$ 339 1 kN

Eq. [6.3] $Y_r = \phi$ 626 8 kN

Mechanism DK-3

K = 0.176134, L = 0 042175, M = 1 0, N = 0 588498,

d_1 = 24 017 mm, d_2 = 49 082 mm,

p = 0.004492, q = 0.256948, r = 4.107376,

Eq. [6 5]. x = imaginary ∴ x = 0 mm or 20 mm (-g)

Eq. [6.2]: $Y_r = \phi$ 339.1 kN

Eq. [6.3]. $Y_r = \phi$ 519 5 kN

Mechanism DK-4.

K = 0.099110, L = 0.114943, M = 0.562888, N = 1 0,

d_1 = 32.018 mm, d_2 = 29 731 mm,

p = -0.004678, q = 0.428105, r = 6.091046,

Eq. [6.5]: x = -12.516 mm, 104.026 mm ∴ x = 0 mm or 20 mm (-g)

Eq. [6.2] $Y_r = \phi$ 333 9 kN

Eq. [6 3] $Y_r = \phi$ 626.8 kN

Hence $Y_{r\,min} = \phi$ 333 9 kN = 287 2 kN > 171 8 kN ∴ OK

7 2 2 Joint Resistance - Gap Conditions

The loading in the gap is a function of joint eccentricity, e, and this will be evaluated by assuming a gap size sufficiently large to provide space for welding If the resulting eccentricity lies within the recommended limits, the conditions in the gap will be checked using Eq [6 10]

Gap at Joint 3

A gap dimension g = 20 mm is tried To find the corresponding eccentricity, values of ψ_1 and ψ_2 must also be known A drawing of two half sections through the chord is shown in Fig 7 2b It is evident that the 76 2 mm width of the compression web member leaves only just enough space for welds at each side, and it must therefore be centered on the chord wall. Hence ψ_1 = 0 5. The other members being only 50.8 mm wide can be shifted upwards, thus reducing the eccentricity. From Fig 7 2b, a value of ψ_2 = 0 63 is seen to be feasible

By using Eq. [A.6] given in Appendix A, or by using the graphical construction shown in Fig 7 4, the eccentricity e corresponding to g = 20 mm is found to be 35 0 mm ($< \sqrt{2}b_0/3$ = 47 9 mm) Now the gap conditions can be checked

For the chord. HSS- 101 6 x 101.6 x 9 53 $A = 3280$ mm^2

$Z_x = 110 \times 10^3$ mm^3

Resistances.

$M_{rz} = \phi$ 0 943 $Z_x F_y$ = 32.67 kN m

$V_r = \phi$ 0 408 $A F_y$ = 421.5 kN

$T_r = \phi\ A\ F_y$ = 1033.2 kN

Loading:

Eq. [B.4] $V_f = V = 308$ kN

Eq. [B.3] $T_f = 0.5\, T_{f1} = 211.8$ kN (end joint)

Eq. [B.6] $M_f = T_{f1}e + \sqrt{2}\psi_1 b_0 N_1 \cos\theta = 22.43$ kN.m

Eq [6 10]: $\frac{22.43}{32.67} + \left(\frac{211.8}{1033.2}\right)^2 + \left(\frac{308}{421.5}\right)^2 = 1.26 < 1\ 4$

Critical conditions in the gap, according to Eq. [6 10] would occur if the eccentricity was 45 6 mm, with a corresponding gap dimension of g = 36.3 mm.

7.2.3 Other Tension Chord Joints

With this chord section having $t_0 = 9\ 53$ mm, all other joints in the tension chord can be chosen as gap joints Values of e can be selected within recommended limits, and the corresponding values of g are large enough for welding

7 ? 4 Lighter Tension Chord

The tension chord 3-6, and 6-9 could have reduced wall thickness ($t_0 = 7.95$ mm). The joint design at 6 and 9 could be carried out as above, and the resulting maximum values of e and g permit practical gap joint configurations. At joint 3 however the maximum gap size shrinks to an impractical small value. In this case an overlap joint could be used.

7 3 DESIGN OF JOINTS TO COMPRESSION CHORD

In the following we consider the design of Joint 4

Data.	Chord	HSS - 101.6 x 101.6 x 6 35	
	Compression web member	HSS - 76.2 x 76.2 4 78	
	Tension web member	HSS - 38.1 x 38 1 x3 81	
	Loads	$C_{f1} = -105.9$ kN	$\theta = 59.23°$
		$C_{f2} = -287.4$ kN	$\alpha = 60°$
		$N_1 = -207.0$ kN	$\eta = 55.49°$
		$N_2 = 147.8$ kN	
	Tie member	$T_f = 25.4$ kN	

7 3 1 Joint Resistance - Chord Walls

Tie Member and its Joint T_f = 25 4 kN

Try HSS 38.1 x 38.1 x 2.54 T_r = 109 kN > 25 4 kN OK

For the joint, β = 38.1/101 6 = 0 375

Eq [6.12]. $T_r = \frac{0.9(2\ 2)(6.35)^2(350)(10^{-3})}{(1 - 0\ 375)} \left[\frac{38.1}{101\ 6} + 2\sqrt{1 - 0\ 375} \right]$

= 87 4 kN > 25 4 kN

∴ use HSS - 38 1 x 38 1 x 2 54

Web Member Joints (see Fig 6 4a)

Factored normal loads on joint

Eq [7 2]. $Y_{f1} = N_1 \sin\theta \cos(\alpha/2) = 154\ 0$ kN

$Y_{f2} = N_2 \sin\theta \cos(\alpha/2) = 110\ 0$ kN

Assume g = 15 mm, $\lambda_1 = \lambda_2 = 0\ 5$ (see 'Gap Conditions' below) If the web members weld size and the chord corners curvature are not taken into account, the predicted joint strength is equal to ϕ 160 1 kN $\not>$ 154 kN and hence not satisfactory. Assuming a weld leg size of 5 mm around the compression web member and 4 mm around the tension web member, the effect of weld sizes and corner curvature is taken into account as follows

$b_0' = b_0 - 1.88\ t_0 = 89.7$ mm

$\bar{b}_1' = b_1 \sec(\alpha/2) + 2S_1 = 98.0$ mm > b_0' ∴ $\bar{b}_1' = b_0' = 89\ 7$ mm

$a_1' = c_1' = 0$

$\bar{h}_1' = h_1 \operatorname{cosec}(\theta) + 2S_1 = 98\ 7$ mm

$\bar{b}_2' = b_2 \sec(\alpha/2) + 2S_2 = 52\ 0$ mm

$a_2' = c_2' = \frac{b_0' - \bar{b}_2'}{2} = 18\ 8$ mm

$\bar{h}_2' = h_2 \operatorname{cosec}(\theta) + 2S_2 = 52.3$ mm

$g' = g - S_1 - S_2 = 6$ mm

$m_p = 0.25\ t_0^2\ F_{y0} = 3.528$ mm

$$\Lambda = \frac{Y_{f2}}{Y_{f1}} = 0.714$$

Since $\beta_1' \geq 1.0$, $x = 0$ and Eq.[6.2] is used:

Mechanisms DK-1 and DK-4:

$L = 0.106157$, $N = 0.714$,

$d_2 = 29.1$ mm,

$Y_r = \phi\ 269.9$ kN

Mechanisms DK-2 and DK-3.

$L = 0.067197$, $N = 0.451958$,

$d_2 = 36.5$ mm,

$Y_r = \phi\ 371.1$ kN

Hence $Y_{r\ min} = \phi\ 269.9$ kN $= 232.1$ kN > 154.0 kN $\therefore$ OK.

7 3.2 Joint Resistance - Gap Conditions

When $\theta_1 = \theta_2$ the critical gap conditions will occur near the attachment of the compression web member - see Section AA in Fig. 10a. To determine the loading in the gap, the gap dimension g will be assumed and the resulting eccentricities e'_i and e''_i will be found from Eqs. [A.8] to [A.10]. The gap loading is obtained from Eqs. [B.9] to [B.15] with $i = 1$, and its resistance will be checked using Eqs. [6.13] to [6.15]. Section AA is critical.

Joint 4

Choose as small a gap as practical for welding; take $g = 15$ mm

Assume $\psi_1 = \psi_2 = 0.5$

$h_0 = 101.6$ mm
$b_1 = h_1 = 76.2$ mm
$b_2 = h_2 = 38.1$ mm

Chord: HSS - 101.6 x 101.6 x 6.35
$A = 2320$ mm^2
$Z_y = 81.4 \times 10^3$ mm^3

Eq. [A.10] $e' = 0.5\cos 30° \left[15\tan 59.23° + \frac{76.2 + 38.1}{2\cos 59.23°} + \frac{76.2 + 38.1}{2} \tan 30° \right]$
$- 0.5(101.6)$
$= 22.8$ mm

Eq. [A.9] $e''_1 = e''_2 = e'' = [\ 0.5(101.6) + 22.8\ ] \tan 30°$
$= 42.5$ mm

Note that $e'' > 0.33 b_0 = 34$ mm as will frequently be the case.

On the other hand $e' < 0.33\ h_0 = 34$ mm

A graphical construction for the joint with g = 15 mm is shown in Fig 7 5

Loading

(Section AA)
$X_1 = 207\ 0 \cos 59\ 23°$
$= 105\ 9$ kN
$Y_1 = 154.0$ kN
$Z_1 = 207.0 \sin 59\ 23° \sin 30°$
$= 88.9$ kN
$W = 44$ kN

Eqs [B.9]
$C_{fg} = 105.9 + 105\ 9 = 211.8$ kN
$V_{fy} = 154.0$ kN
$M_{ft} = 0.5(88.9)(101.6)10^{-3} = 4\ 52$ kN.m
$M_{fy} = 0\ 5(287.4\text{-}105.9)(42.5)10^{-3} = 3\ 86$ kN m
$M_{fz} = 0\ 5\left[\ (105.9+75.6)22.8\ \right] + 0\ 5(101.6)(105\ 9)$
$= 7.45$ kN.m

Resistances

Eqs. [6.16]
$C_{rz} = 0.9(2320)(350)10^{-3} = 730.8$ kN
$M_{rz} = M_{ry} = 0.9(81.4)10^3(350)10^{-3} = 4.52$ kN.m
$V_{rz} = V_{ry} = 0.9(1.15)(101.6)(6.35)(350)10^{-3} = 233\ 7$ kN
$M_{rt} = 0.9(1\ 15)(95.25)^2(6.35)(350)10^{-6} = 20\ 87$ kN m

Interaction Equation

Eq [6.14]: $\bar{r} = \frac{4.52}{20.87} + 0\ 5\ \frac{88.9}{233\ 7} + 0\ 5\ \frac{154\ 0}{233\ 7}$

$= 0.736$

Eq. [6.13]: $\frac{1}{\sqrt{1 - (0.736)^2}} \left[\frac{221.8}{730\ 8} + 0.85 \left(\frac{7.45}{25\ 64} + 0\ 5 \frac{3.86}{25.64} \right) \right] = 0.887 < 1.0$

Eq. [6.15]: $V_{fz} = 88.9 < 0.5(233.7) = 116.9$ kN OK

The gap resistance in Joint 4 is therefore adequate.

7 3 3 Other Compression Chord Joints

Choice of the same gap dimension of 15 mm leads to satisfactory gap strength at all other intermediate joints in the compression chords Joint 4, considered above, is the most critical of all these joints

7 4 VERIFICATION OF COMPRESSION CHORD

Member 10-13 HSS - 101 6 x 101 6 x 6 35

At 10 $b_1 = h_1 = 63\ 5$, $b_2 = h_2 = 38\ 1$, $\psi_1 = \psi_2 = 0\ 5$

Assume $g = 15$ mm

Eq [A 10] $$e' = 0\ 5\cos 30^\circ \left[15\tan 59\ 23^\circ + \frac{101\ 6}{2\cos 59\ 23^\circ} + \frac{101\ 6}{2}\tan 30^\circ \right] - \frac{101\ 6}{2}$$

$= 15\ 8$ mm

Eq [A 9] $e'' = 38\ 5$ mm

$N_1\cos\theta_1 + N_2\cos\theta_2 = C_{f2} - C_{f1} = 60.4$ kN

At 10

Eq [B 14] $M_{fy} = 0\ 5(60\ 4)(38\ 5)10^{-3} = 1\ 16$ kN m

Eq [B 15] $M_{fz} = 0\ 5(60\ 4)(15.8)10^{-3} = 0\ 48$ kN.m

At 13 $M_{fy} = M_{fz} = 0$

Taking $K = 0\ 9$, $\omega_x = \omega_y = 0\ 6$, the section chosen at the preliminary design stage can be checked using the equations of §F3 of Appendix F of CAN3-S16 1-M84 (CSA 1984), and is found to be satisfactory Similar checks would show that the other sections of the compression chord are satisfactory

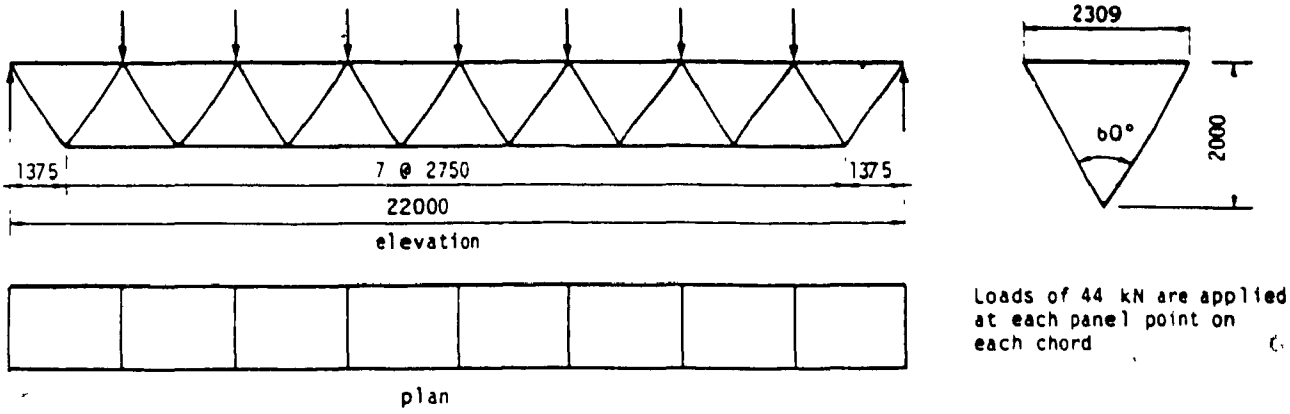

Fig 7 1 Design example Truss dimensions and loading

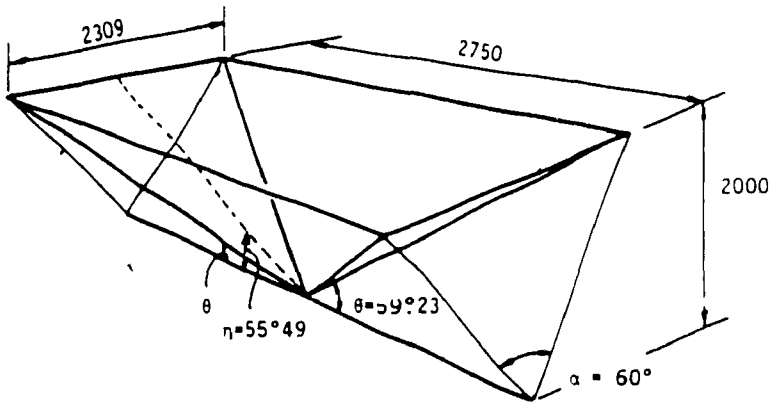

(a)

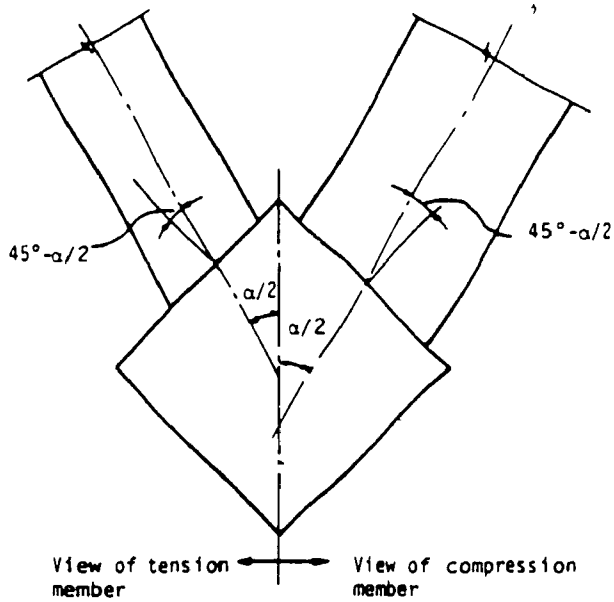

(b)

Fig. 7.2 Design example. (a) Panel geometry - (b) Tension chord cross section.

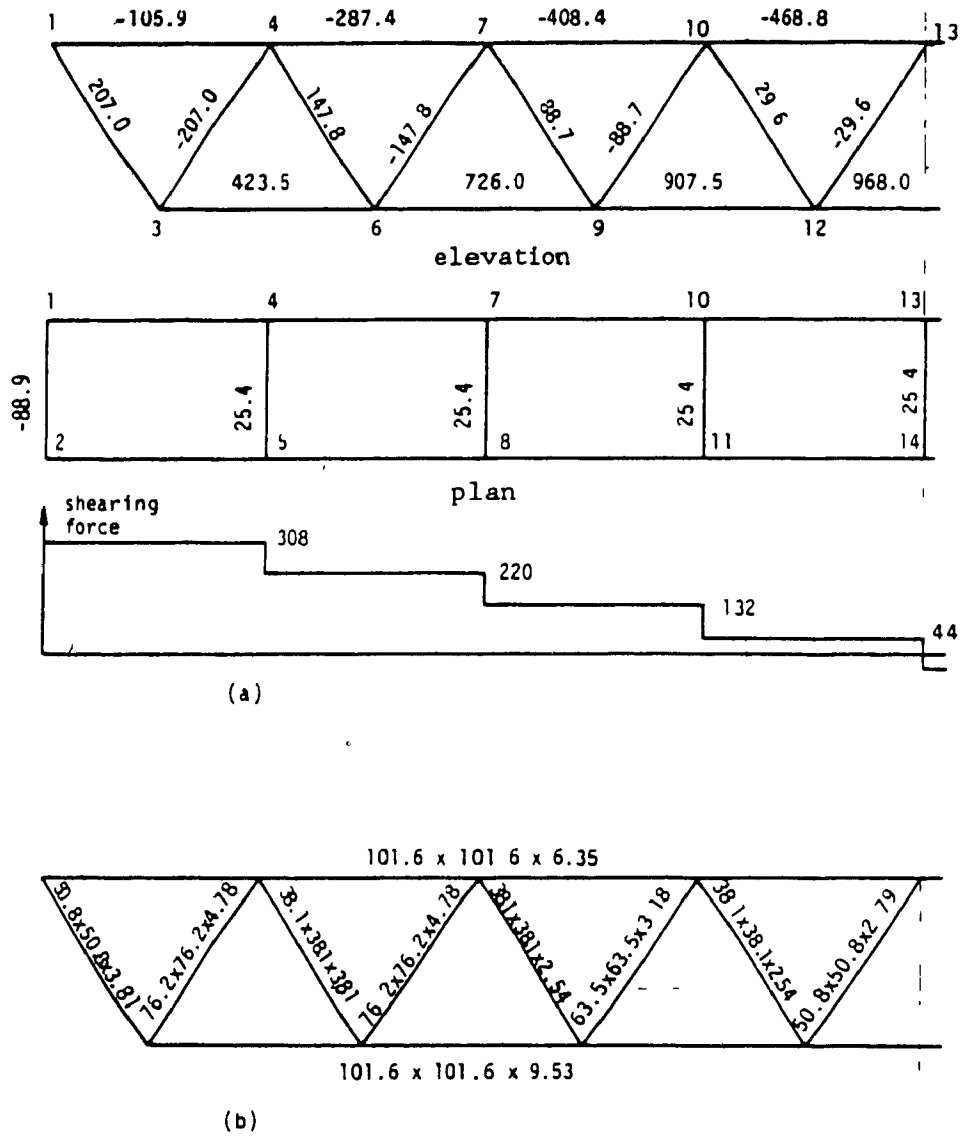

Fig. 7.3 Design example. Analysis and member sizes
(a) Member forces and shearing force on truss.
(all forces in kN)
(b) Preliminary member selection.

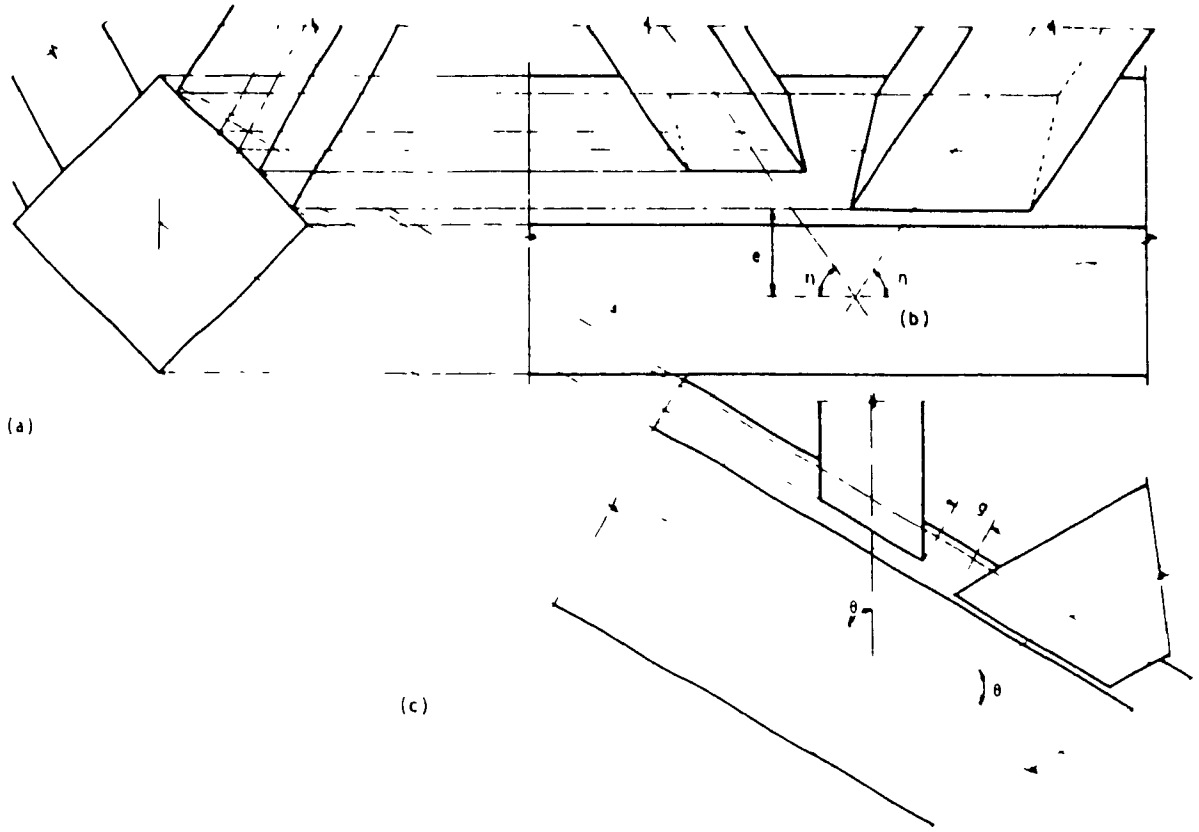

Fig 7 4 Tension chord joint configuration.
(a) Cross-section (b) Projection showing side view
(c) Projection showing view normal to web plane

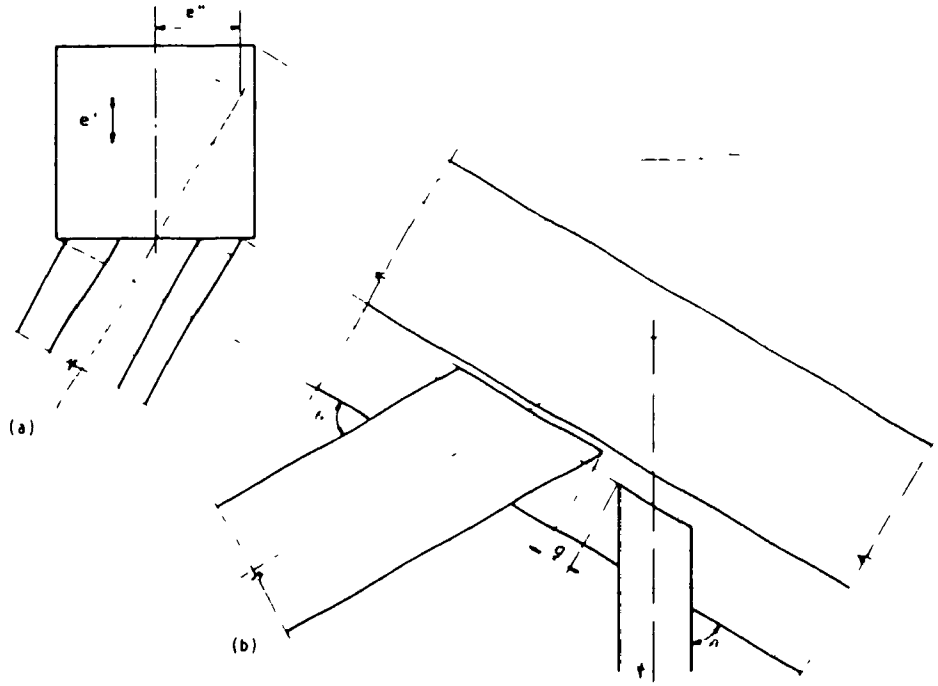

Fig. 7.5 Compression chord joint configuration.
(a) Cross-section.
(b) Projection showing view normal to web plane.

CHAPTER 8 CONCLUSIONS

The experimental research programs described herein were of limited scope. Seven DK truss segments and twenty-four DT specimens were tested in an attempt to determine joint stiffnesses and strength, and at the same time to determine if any significant trends were evident due to variation of several major parameters (α, β, g, b_0/t_0 and L_w/r).

Clearly, no general design approaches can be developed based only on such limited empirical results, and it is unlikely that the frequency of construction of triangular trusses can justify a sufficiently comprehensive test program to do this It has been demonstrated however, that the yield line theory provides an excellent correlation with the test results, and can provide a basis for the development of design rules for joints to the single chord of a triangular truss.

Proposed yield line mechanisms on which the theoretical results have been based are of very simple form. Refined models have been studied including mechanisms with inclined end yield lines, with yield line fans and mechanisms that take into account the normal stresses in the chord corners. However, better correlation does not occur with such refined models and the upper bound results do not improve. Past experience with planar truss joints also suggests that resulting improvements to simple models are relatively minor.

On the basis of the very limited number of triangular truss test results available, previous methods of planar truss joint strength prediction do seem to have some relevance to triangular trusses. However, the yield line method is superior to these because of its lower variability This probably arises because the yield line method incorporates the effect of off-centre attachment of web members. This off-centering is desirable to reduce eccentricity in the

joint and has the effect of increasing the joint resistance.

The principal features of triangular trusses which differentiate them from planar trusses have been described herein. The test results show that gap joints to the tension chord are feasible and that their resistance may be estimated by using equations based on the yield line theory It has also been shown that web member buckling may be more critical in triangular trusses than in planar trusses, and higher effective length factors are proposed if the web member strength is close to the joint strength

Emphasis in the tests was on gap joints to the tension chord, and little test information is available related directly to overlap joints or to joints to the compression chord. In an overlap joint a significant proportion of load is transferred directly from one web member to the other, and the chord is consequently not as heavily loaded as in a corresponding gap joint. For this reason, and because of the good performance of the triangular truss chords in the gap joint tests, the same procedures recommended for overlap joints in planar trusses may be used (Stelco 1981 for example)

The suggested treatment of compression chord gap joints comprises two checks, which relate to the gap conditions and the chord wall deformation respectively. The treatment of the former is considered to be conservative since it is based on a lower bound solution for a perfectly plastic material. However Eq [6.13] is based on stress resultants in the gap, and does not account for the possibility of high localized strains One check of localized conditions is made of shear stresses in the bottom wall of the compression chord through use of Eq. [6 15] The chord wall deformation has been checked based again on the yield line theory and experimental confirmation of the applicability of these to triangular truss compression chords is desirable.

The design procedures described herein result in a rather more complex treatment than is customary for planar trusses, and this particularly concerns

gap joints and the analysis of conditions in the gap Moments in the gap are considered explicitly whereas they are usually ignored in planar trusses on the basis of good performance in tests. Further experimental study of triangular truss gap joints may lead to simplification of these procedures Biaxial bending in the compression chords due to joint eccentricities is a further feature which must be treated and which is not present in planar trusses.

As in planar HSS truss design, the design of members cannot be treated in isolation from the design of joints The design procedure for triangular trusses can follow the same sequence as for planar trusses, for example as outlined by Stelco (1981) Preliminary member selection should allow for the secondary forces which will result if joints have eccentricities; joints to the tension chord should be treated before the compression chord, and web member sizes selected to suit tension chord joint requirements, compression chord joints can then be detailed and their resistance determined, and finally, with the eccentricities known, secondary forces can be used in the final check of member sizes

APPENDIX A GEOMETRICAL RELATIONSHIPS

In the following, general equations are given for a number of geometrical and loading relationships which are needed in the design of a triangular truss The relationships apply to trusses in which the angle between the chord and tension web members may be different from that between chord and compression web members, as shown in Fig A 1 Furthermore, the compression and tension web members may be attached to the chord walls at different positions relative to the centreline of the chord walls, as shown in Figs 6 3 and 6 4

A 1 TRUSS GEOMETRY

For $i = 1,2$

$$l_{wi} = \sqrt{p_i^2 + s^2} \qquad [A\ 1]$$

$$\eta_i = \tan^{-1}\left(\frac{d}{p_i}\right) \qquad [A\ 2]$$

$$\theta_i = \tan^{-1}\left(\frac{s}{p_i}\right) \qquad [A\ 3]$$

$$w = 2d\ \tan\frac{\alpha}{2} \qquad [A\ 4]$$

A 2 TENSION CHORD ECCENTRICITY (see Fig 6 3)

$$e = \frac{\tan\theta_1\tan\theta_2}{\tan\theta_1+\tan\theta_2}\cos(\alpha/2)\left[g + \frac{h_1}{2\sin\theta_1} + \frac{h_2}{2\sin\theta_2} + \tan(45°-\alpha/2)\left(\frac{b_1}{2\tan\theta_1} + \frac{b_2}{2\tan\theta_2}\right) - \frac{b_0}{\sqrt{2}\cos(\alpha/2)}\left(\frac{\psi_1}{\tan\theta_1} + \frac{\psi_2}{\tan\theta_2} \right)\right] \qquad [A\ 5]$$

For the regular Warren truss with $\theta_1 = \theta_2 = \theta$ this becomes

$$e = 0.5\tan\theta\cos(\alpha/2)\left[g + \frac{h_1+h_2}{2\sin\theta} + \frac{b_1+b_2}{2\tan\theta}\tan(45-\alpha/2) \right] - \frac{b_0}{2\sqrt{2}}(\psi_1+\psi_2) \qquad [A\ 6]$$

A 3 COMPRESSION CHORD ECCENTRICITY (see Fig 6 4)

$$e_1' = \frac{\tan\theta_1\tan\theta_2}{\tan\theta_1 + \tan\theta_2}\cos(\alpha/2)\left[g + \frac{h_1}{2\sin\theta_1} + \frac{h_2}{2\sin\theta_2} + \tan(\alpha/2)\left(\frac{b_1}{2\tan\theta_1} + \frac{b_2}{2\tan\theta_2}\right) - (\psi_2-\psi_1)b_0\frac{\sin(\alpha/2)}{\tan\theta_2}\right] - 0\ 5h_0 \qquad [A\ 7]$$

$$e'_2 = e'_1 + (\psi_2-\psi_1)b_0\cos(\alpha/2)\sin(\alpha/2) \qquad [A\ 8]$$

$$e''_i = (0\ 5h_0+e'_i)\tan(\alpha/2) - b_0(\psi_i-0\ 5) \qquad i=1,2 \qquad [A\ 9]$$

For the regular Warren truss, with $\theta_1 = \theta_2 = \theta$, Eqs [A 8] and [A 9] are unchanged, and Eq [A 7] becomes

$$e'_1 = 0\ 5\cos(\alpha/2)\left[g\tan\theta + \frac{h_1+h_2}{2\cos\theta} + \frac{b_1+b_2}{2}\tan(\alpha/2) - (\psi_1-\psi_2)b_0\sin(\alpha/2)\right] - 0.5h_0 \qquad [A\ 10]$$

Note that if $\psi_1 = \psi_2$, then $e'_1 = e'_2$ and $e''_1 = e''_2$

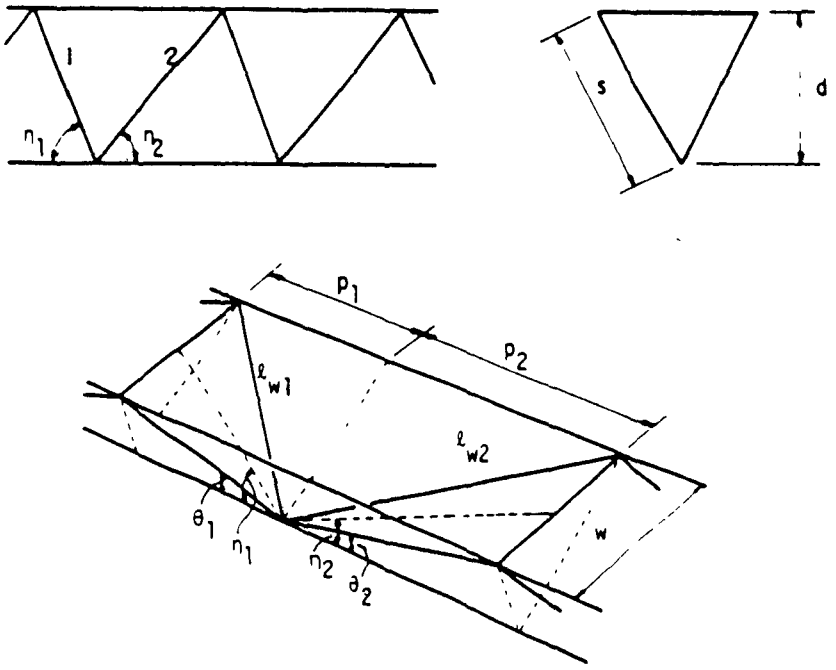

Fig. A 1 Geometry of one panel

APPENDIX B LOADS IN CHORDS

Secondary moments are induced in the clear spans of the chords as a result of joint eccentricities, and in the chord gap regions as a result of both eccentricity and of the attachment of web members to the walls of the chords, that is, offset from the chord axes In the following, the forces which must be resisted in the members and in the gaps are considered In deriving these formulae, due account has been taken of signs and therefore positive values of forces should be used in the equations given

B 1 TENSION CHORD

The secondary moment on the joint due to eccentricity is assumed to be resisted by the chords only, and the far ends of the chords are assumed to be pinned for the purpose of this calculation The distribution of bending moment in the gap and adjacent chord members is shown in Fig B.1, and the forces applied to the members are shown in Fig. 6 3a

B.1 1 Secondary Bending Moments in Chord (outside gap)

At an intermediate joint

$$M_{f1} = \frac{I_{ci}}{I_{c1}+I_{c2}} (T_{f1}-T_{f2})e \qquad i = 1,2 \qquad [B\ 1]$$

At an end joint, if the chord is curtailed beyond the tension web member connection,

$$M_{f1} = T_{f1}\, e \qquad [B.2]$$

B 1 2 Gap Forces - Tension Chord

Axial Force

$$T_{fg} = T_{f1} - 2N_1\cos\theta_1 = T_{f2} + 2N_2\cos\theta_2 \qquad [B.3]$$

At an end joint beyond which the chord carried no axial load, this becomes

$$T_{fg} = 0.5\ T_{f1}$$

Shearing Force

$V_f = V$ the shearing force carried by the truss, where [B 4]

$$V = 2N_1\sin\theta_1\cos(\alpha/2) = 2N_2\sin\theta_2\cos(\alpha/2)$$

Maximum Bending Moments

At an intermediate joint, the maximum of M_{f1} and M_{f2} where

$$M_{fi} = \frac{I_{ci}}{I_{c1}+I_{c2}}(T_{f1}-T_{f2}) + \sqrt{2}\ \psi_1 b_0 N_i\cos\theta_i \qquad i = 1,2 \qquad [B\ 5]$$

At an end joint if the chord is curtailed beyond the tension web member connection

$$M_{f1} = T_{f1}e + \sqrt{2}\ \psi_1 b_0 N_1\cos\theta_1 \qquad [B\ 6]$$

B 2 COMPRESSION CHORD

The forces acting on a compression chord joint are shown in Fig. 6.4 and the bending moment distributions are similar to those for the tension chord shown in Fig. B.1.

B.2.1 Secondary Bending Moments in Chord (outside gap)

Vertical Bending (about the z-z axis)

$$M_{fzi} = \frac{I_{ci}}{I_{c1}+I_{c2}} (N_1\cos\theta_1 e'_1 + N_2\cos\theta_2 e'_2) \qquad i = 1,2 \qquad [B\ 7]$$

Horizontal Bending (about the y-y axis)

$$M_{fyi} = \frac{I_{ci}}{I_{c1}+I_{c2}} (N_1\cos\theta_1 e''_1 + N_2\cos\theta_2 e''_2) \qquad i = 1,2 \qquad [B\ 8]$$

B 2.2 Gap Forces - Compression Chord

The subscript i = 1 relates to the web compression member and to the forces in the gap near Section AA (Fig. 6 4a), and subscript i = 2 relates to the gap near Section BB.

Axial Force

$$C_{fg1} = C_{fg2}$$

where

$$C_{fg1} = C_{f1} + N_1\cos\theta_1 \qquad [B\ 9]$$

and

$$C_{fg2} = C_{f2} + N_2\cos\theta_2 \qquad [B\ 10]$$

Shearing Forces

$$V_{fyi} = Y_i = N_i\sin\theta_i\cos(\alpha/2) \qquad i = 1,2 \qquad [B,11]$$

$$V_{fzi} = Z_i = N_i\sin\theta_i\sin(\alpha/2) \qquad i = 1,2 \qquad [B.12]$$

Twisting Moments

$$M_{fti} = N_i\sin\theta_i \left[0.5h_0\sin(\alpha/2) - (\psi_i - 0.5)b_0\cos(\alpha/2) \right] \qquad i = 1,2 \qquad [B.13]$$

Maximum Bending Moments in Gap

$$M_{fyi} = \frac{I_{ci}}{I_{c1}+I_{c2}} \left[\sum_{i=1}^{2} N_i \cos\theta_i e''_i \right] + (\psi_i - 0.5) b_0 N_i \cos\theta_i \quad i = 1,2 \qquad [B.14]$$

$$M_{fzi} = \frac{I_{ci}}{I_{c1}+I_{c2}} \left[\sum_{i=1}^{2} N_i \cos\theta_i e'_i \right] + 0.5\, h_0 N_i \cos\theta_i \quad i = 1,2 \qquad [B.15]$$

For a regular Warren truss, with $\theta_1 = \theta_2$ the gap near the compression web member, i.e., Section AA, will be the critical section and only this section need be checked. Due to the large angle ($\alpha/2$) between the web members and the normal to the bottom wall of the compression chord, it will frequently not be feasible to attach these members off centre. In this case, with $\psi_1 = \psi_2 = 0.5$, many of the above equations are simplified, and $e'_1 = e'_2$, $e''_1 = e''_2$

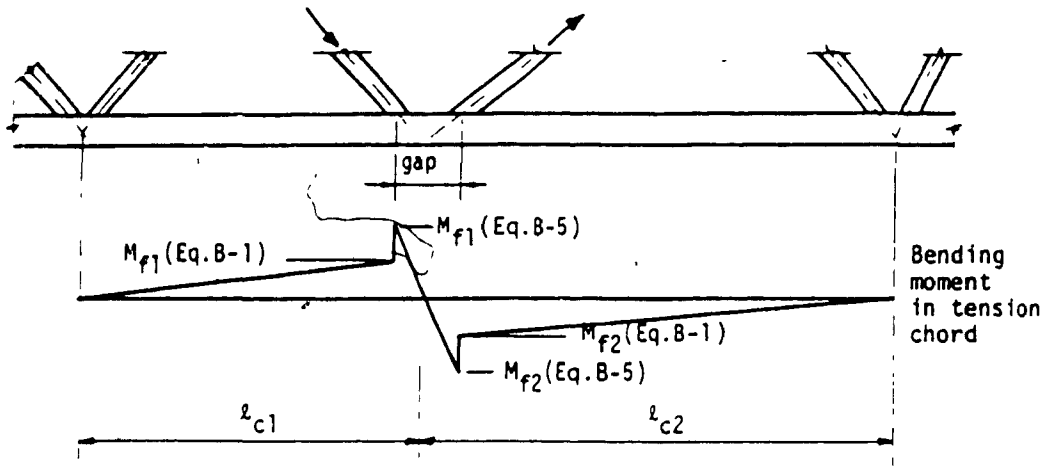

Fig. B.1 Bending moments in tension chord

APPENDIX C EFFECT OF NORMAL STRESSES

C 1 EFFECT OF NORMAL STRESSES ON A CROSS SECTION, i e YIELD CONDITION

Consider a cross section of unit width and of height t_0 subjected to a bending moment M and a normal force N, Fig C 1a In resisting these loads, full yielding over the entire cross section is assumed Depending on the relative value of M and N, the cross section may form either an ordinary plastic hinge, a complex plastic hinge, or a squashed cross section These different yield conditions are examined below

C 1 1 Ordinary Plastic Hinge (e = 0)

If N=0, pure bending exists and the resistance of the section is

$M = M_p$, or

$$\frac{M}{M_p} = 1 \quad \text{and} \quad \frac{N}{N_p} = 0 \qquad [C\ 1]$$

where M_p, the full plastic moment resistance of the section, is

$$M_p = \frac{t_0^2\ \sigma_y}{4} \qquad [C\ 2]$$

and N_p, the squash load of the section, is

$$N_p = t_0\ \sigma_y \qquad [C\ 3]$$

The stress distribution and the displacements at the section are shown in Fig C.1b Such a cross section is usually called an ordinary plastic hinge.

Referring to Fig. C.1c, note also that

$$e = \frac{\Delta}{\theta} = 0 \qquad [C\ 4]$$

where e is the distance from the centroid to the neutral axis, Δ is the axial

displacement at the centroid and θ is the rotation at the plastic-hinge cross section

C 1.2 Complex Plastic Hinge ($0 \leq e \leq \frac{t_0}{2}$)

For combined bending and normal force

$$\frac{M}{M_p} + \left(\frac{N}{N_p}\right)^2 = 1 \qquad \text{or} \qquad M = M'_p = M_p \left[1 - \left(\frac{N}{N_p}\right)^2 \right] \qquad [C.5]$$

M'_p is the plastic-moment resistance of the cross section reduced by the effect of the normal force N. (Similarly, N'_p (=N) could be defined as the squash resistance of the section reduced by the effect of the bending moment M)

Also from Fig C 1c

$$e = \frac{\Delta}{\theta} = \frac{N}{2\sigma_y} = \frac{t_0}{2} \frac{N}{N_p} \qquad [C\ 6]$$

The stress distribution and the displacements are shown in Fig C 1c The cross section forms a complex plastic hinge, as termed by Neal (1977)

C.1 3 Squashed Cross Section ($\frac{t_0}{2} \leq e$)

For normal force only

$$\frac{M}{M_p} = 0 \quad \text{and} \quad \frac{N}{N_p} = 1 \qquad [C\ 7]$$

and $e = \frac{\Delta}{\theta}$ is indeterminate, [C.8]

that is, e may take any value in the range $|e| \geq \frac{t_0}{2}$, as shown in Fig C.1d

The value of $e = \frac{t_0}{2}$ corresponds to the limit between a complex hinge and a squashed cross section, as shown in Fig. C.1e.

If $\theta = 0$ ($e = \infty$), Fig. C.1f, only the normal displacement Δ takes place and the cross section forms what may be called a 'purely-squashed cross-

section mechanism', i e the cross section deforms axially and it does not rotate. The cross section works as a 'push-button', as opposed to working as a 'hinge' for an ordinary plastic hinge Such purely-squashed cross-section mechanisms are required in the kinematic analysis of structures subjected to combined bending and normal forces, as presented in the following section

The relation between M/M_p and N/N_p is the interaction between M and N which share the resistance of the cross section This relation defines the yield surface for the plastic-hinge cross section, as shown in Fig C.2 A normality condition for the yield surface defines the relation between the ratio Δ/θ and the yield surface (Heyman 1971) This normality condition is also defined by Eqs. [C 4], [C 6] and [C 8]

The overall effect on a structure of the combined bending and normal stresses, as opposed to the effect on a cross section presented above, is now discussed

C 2 EFFECT OF NORMAL STRESSES ON A STRUCTURE

The two fundamental approaches to plasticity problems are the lower bound static approach and the upper bound kinematic approach. In the static approach, equations of equilibrium are derived directly for the structure under study. In the kinematic approach, mechanisms of deformations are assumed and the principle of virtual work is used to obtain equations equivalent to equilibrium equations These two approaches are commonly used to deal with bending effects in a structure, and can be used similarly to treat the effect of normal stresses. In the static approach, equations of equilibrium are written directly for the normal forces, and in the kinematic approach, mechanisms involving axial deformations are assumed and equations for the normal forces are obtained using the virtual work principle.

For structures analysed for both bending and normal force, each of the bending moment and normal force effects can be analysed with either the static or kinematic approaches. Hence four different methods can be used, as shown in Table C.1. In each method, two independent sets of equations are obtained, one set for bending moments and one set for normal forces. These sets of equations are then solved simultaneously to obtain a solution.

In Method 1 (see Table C.1), equilibrium equations are written for bending moments and normal forces and then solved simultaneously The usefulness of the method depends on how readily the equations of equilibrium can be obtained. For example, it may be difficult to use this method with plate bending problems in which the equations of equilibrium generally lead to complex differential equations.

In Method 2, equilibrium equations are written for the effect of bending moments, whereas equations for the normal forces are obtained using the virtual work principle, based on an axial deformation mechanism Both sets of equations are then solved simultaneously

In Method 3, a mechanism for bending deformations is assumed and equations for bending moments are obtained using the virtual work principle The effect of normal forces is treated by writing equations of equilibrium for the normal forces. The two sets of equations are then solved simultaneously. This method is often used with plane frame problems and the solution is usually carried out by iteration (Horne 1979, Heyman 1971).

Method 4.1 may lead to easier solutions than Method 3 in certain problems. In this method, two mechanisms are assumed, one for the bending effects and one for the axial force effects. Two sets of equations are obtained using the virtual work principle and then solved simultaneously.

Method 4.2 is an alternative to Method 4.1. It consists of assuming only one mechanism which includes both bending and axial deformations. In this

case, only one set of equations is obtained containing two unknowns, the internal bending moments and the internal normal forces However, since the equations represent an upper bound solution of the applied loads, minimization can be done with respect to either one of the unknowns, internal bending moment or axial force, giving another set of equations and hence a solution can be found

In Method 4 1, different mechanisms are combined as in the method of combining mechanisms for the plastic analysis of frames subjected to bending only (Neal 1977), also called the method of combined mechanisms (Horne 1979). Hence, Method 4.1 can be referred to as a 'method of combining mechanisms'

Method 4.2 corresponds to the trial-and-error method of plastic frame analysis (Neal 1977) However, the name 'method of entire mechanism' is suggested herein since the method involves a mechanism that includes directly all deformations

Methods 1 to 4 1 involve breaking down a complete problem into separate sub-problems The normal and bending stress values assumed in these separate sub-problems are not valid if these sub-problems are considered as truly separate and independent problems However, the stress values are indeed valid when considering their combined effect in the original complete problem

For example in a sub-problem for the bending effects, a section carrying maximum bending moment (equilibrium approach) or an ordinary plastic hinge (kinematic approach) must be assumed to carry only a reduced plastic moment M'_p instead of the full M_p, if this section or hinge is combined to a section carrying maximum normal stress (equilibrium approach) or to a fully-squashed cross-section mechanism (kinematic approach) in another sub-problem for normal force effects. Similarly in the second sub-problem, the section carrying maximum normal stresses or the fully-squashed cross-section mechanism

must be assumed to carry a reduced normal load N instead of the full N_p. Combining the two sub-problems leads to the correct interaction relationship for combined bending and normal stresses at the cross section considered in the original complete problem.

The four methods just described are illustrated below by two examples. For the simple problems considered, it will be found that solutions from Methods 1, 2, 3 and 4 1 are identical and that the solution from Method 4.2 is numerically equivalent to the other solutions However in more complex problems, such as in plate bending problems, the four methods will yield slightly different solutions. Method 1 uses lower bound equations for both bending and normal force effects, and the solution will be a lower bound. Methods 4.1 and 4.2 use only upper bound equations, and the solution will be an upper bound. Methods 2 and 3 use both upper and lower bound equations, and whether the solution will be too high or too low cannot be predicted in general.

C.3 EXAMPLE 1

Consider a plastic hinge, representing a simple structure, subjected to externally applied moment M and force P, as shown in Fig. C 3a. As usually the case in plasticity problems, the applied loads must be written in terms of only one unknown This is achieved by replacing M and P by a single force P shifted away by a distance 'a' such that $P\,a = M$.

C.3.1 Method 1

Refer to Table C.1 and to Fig. C.3b. The equations of equilibrium are written directly for both bending and normal force effects. Equilibrium of moments ($\Sigma M = 0$) gives

Applied Moment - Internal Moment

$$P\,a = M'_p \qquad [C\ 9]$$

where $M'_p = M_p \left[1 - \left(\frac{N}{N_p}\right)^2 \right]$ and M_p and N_p are defined in Eqs [C 2] and [C.3].

Equilibrium of forces ($\Sigma F = 0$) gives

Applied Force - Internal Force

$$P = N \qquad [C\ 10]$$

The solution for P is obtained by solving simultaneously Eqs [C 9] and [C 10]. Hence, substituting Eq [C 10] into Eq [C.9] gives

$$\frac{P}{M_p} = \frac{8}{t_0^2} \left[\sqrt{\frac{t_0^2}{4} + a^2} - a \right] \qquad [C\ 11]$$

C 3 2 Method 2

The equation of equilibrium for bending is obtained in the same way as in Method 1 and is

$$P\,a = M'_p = M_p \left[1 - \left(\frac{N}{N_p}\right)^2 \right] \qquad [C\ 12]$$

The normal force is treated by assuming a mechanism involving axial deformations only, as shown in Fig. C 3c The virtual work equation for this mechanism is

$$P\,\delta = N\,\Delta \qquad [C.13]$$

where δ is the displacement at the load P and $\delta = \Delta$, hence

$$P = N \qquad [C.14]$$

which is identical to Eq. [C 10] in Method 1. Solving simultaneously Eqs. [C.12] and [C.14] yields the same solution as that of Method 1, i.e.

Eq. [C.11].

C.3.3 Method 3

A mechanism for bending deformations is assumed as shown in Fig C.3d The virtual work equation is

$$P\,\theta\,a = M'_p\,\theta \qquad [C.15]$$

or, cancelling θ's,

$$P\,a = M_p\left[\,1 - \left(\frac{N}{N_p}\right)^2\,\right] \qquad [C.16]$$

The equilibrium equation for normal force is

$$P = N \qquad [C\ 17]$$

Eqs. [C 16] and [C 17] are identical to Eqs [C.9] and [C 10] and simultaneous solution leads to the same answer as before

C 3 4 Method 4.1

Refer to Fig C 3e. For the bending moment, the same mechanism as in Method 3 is assumed and leads to Eq. [C.16]

For the normal force, the same mechanism as in Method 2 is assumed and leads to Eq. [C.14].

Again, the simultaneous solution of these equations is identical to the previous solutions.

C.3.5 Method 4.2

A mechanism combining both bending and axial deformations is assumed as shown in Fig. C.3f. The virtual work equation for this mechanism is

$$P\,\delta = M'_p\,\theta + N\,\Delta \qquad [C.18]$$

or

$$P\ (\Delta + a\ \theta) = M_p \left[\ 1 - \left(\frac{N}{N_p}\right)^2\ \right] \theta + N\ \Delta \qquad [C.19]$$

Dividing by θ and using Eqs. [C.2], [C 3] and [C 6], Eq. [C.19] can be simplified to

$$\frac{P}{M_p} = \frac{\frac{t_0^2}{16}\left(\frac{N}{N_p}\right)^2 + 1}{\frac{t_0^2}{8}\left(\frac{N}{N_p}\right) + a} \qquad [C.20]$$

Minimization of P with respect to N is done by solving

$$\frac{dP}{dN} = 0 \qquad [C.21]$$

which leads to

$$\frac{N}{M_p} = \frac{8}{t_0^2}\left[\ \sqrt{\frac{t_0^2}{4} + a^2}\ - a\ \right] \qquad [C\ 22]$$

Substituting this value of N into Eq [C 20] gives the solution for P. This solution cannot be simplified to an equation similar to Eq [C.11] However, it can be shown to give answers numerically identical to those obtained from Eq. [C 11], i e the solution is the same as in the other methods.

In connection with Eq [C.21], note that P is the load applied to the structure whereas N is the internal normal force resistance at the plastic-hinge cross section. (N could also be called N'_p) The applied load P is minimized with respect to N in the same way that minimization is done with respect to a geometric parameter in an ordinary kinematic plastic analysis when no normal force effect is considered. The minimization could in fact be done with respect to M'_p or e since N, M'_p and e are all directly related.

Also, the interaction equations and the normality relationship at the

plastic-hinge cross section, Eqs [C.1] to [C 8], are satisfied for any assumed value of N Letting $\frac{dP}{dN} = 0$ leads to the particular value of N that minimizes P (upper bound solution).

C 4 EXAMPLE 2

Consider the frame shown in Fig. C.4a. With span b_0, and beam and column sizes t_0, the frame may also represent a simple two-dimensional model of an HSS joint An analysis of the frame for bending effects only using either the static or kinematic approach gives the following solution

$$\frac{P}{M_p} = \frac{8}{b_0} \qquad [C\ 23]$$

The effect of the normal force in the columns is now analysed using Methods 1 to 4.2

C.4.1 Method 1

Refer to Fig C 4b The equation of equilibrium for bending is

$$\frac{PL}{4} = M_p + M'_p \qquad [C.24]$$

where, as before, $M'_p = M_p \left[1 - \left(\frac{N}{N_p}\right)^2 \right]$, $M_p = \frac{t_0^2}{4} \sigma_y$, and $N_p = t_0 \sigma_y$

The equation of equilibrium for the normal force in the columns is

$$\frac{P}{2} = N \qquad [C\ 25]$$

Substituting Eq. [C.25] into Eq. [C.24], solving for P and simplifying leads to

$$\frac{P}{M_p} = \frac{8}{t_0} \left[\sqrt{\left(\frac{b_0}{t_0}\right)^2 + 2} - \frac{b_0}{t_0} \right] \qquad [C.26]$$

C 4.2 Method 2

Refer to Fig. C 4b The equation of equilibrium for bending is again

$$\frac{PL}{4} = M_p + M'_p \qquad [C.27]$$

The virtual work equation for the axial deformation mechanism is

$$P\,\delta = 2\,N\,\Delta \qquad [C\ 28]$$

Eqs [C 27] and [C.28] are identical to Eqs [C 24] and [C 25] and the solution is identical to that of Method 1

Note that in the axial deformation mechanism, purely-squashed cross-section mechanisms are used in the columns These cross-section mechanisms are assumed to carry only a reduced squash load N

C 4 3 Method 3

Refer to Fig C 4d The virtual work equation for the bending mechanism is

$$P\,\frac{\theta b_o}{2} = 2\theta M_p + 2\theta M_p \left[\ 1 - \left(\frac{N}{N_p}\right)^2\ \right] \qquad [C\ 29]$$

The equation of equilibrium for the normal forces is

$$\frac{P}{2} = N \qquad [C.30]$$

Again, the solution is the same as before

Note that in the bending deformation mechanism, an ordinary plastic hinge carrying the full plastic moment M_p is used at mid-span of the beam, while ordinary plastic hinges carrying a reduced moment M'_p are used in the columns

C.4.4 Method 4.1

Refer to Fig C.4e The virtual work equation for the mechanism with bending deformations is

$$P \frac{\theta b_0}{2} = 2\theta M_p + 2\theta M_p \left[1 - \left(\frac{N}{N_p}\right)^2 \right] \qquad [C.31]$$

The virtual work equation for the mechanism with axial deformations is

$$P \delta = 2 N \Delta \qquad [C.32]$$

Again, the solution is the same as before

C.4.5 Method 4.2

The mechanism shown in Fig C.4f combines both bending and axial deformations. The virtual work equation for this mechanism is

$$P \left(\frac{\theta b_0}{2} + \Delta \right) = 2\theta M_p + 2\theta M'_p + 2\Delta N \qquad [C.33]$$

Minimization of P with respect to N, i.e. letting $\frac{dP}{dN} = 0$, leads to

$$\frac{N}{M_p} = \frac{4}{3t_0} \left[\sqrt{\left(\frac{b_0}{t_0}\right)^2 + 6} - \frac{b_0}{t_0} \right] \qquad [C.34]$$

Substituting Eq. [C.34] into Eq. [C.33], solving for P and simplifying leads to

$$\frac{P}{M_p} = \frac{8}{3\sqrt{b_0^2+6t_0^2} + 6b_0} \left[\left(\frac{b_0}{t_0}\right)^2 + 12 - \frac{b_0}{t_0} \sqrt{\left(\frac{b_0}{t_0}\right)^2 + 6} \right] \qquad [C.35]$$

This solution cannot be simplified to Eq. [C.26]. However, it gives identical numerical results.

Note that in the mechanism shown in Fig. C.4f, complex plastic hinges carrying a reduced moment M'_p and a reduced normal load N are used in the

columns

Values of P/M_p from Eqs. [C.26] or [C.35] are given in Table C.2 for $t_0 = 0$ and $b_0 = 10$, 5 and 2. The percentage reduction from the solution for bending only, Eq. [C 23], increases as the span b_0 decreases

Note that while the above solutions assume failure due to both bending and normal forces, another mechanism is possible due to pure squashing of the columns. From equilibrium, or considering a mechanism with purely-squashed cross sections in the columns, the following equation is obtained

$$P_{squash} = 2\ N_p \qquad [C.36]$$

or

$$\frac{P_{squash}}{M_p} = \frac{8}{t_0} \qquad [C.37]$$

Hence, this failure mechanism sets a limit to Eq [C 26], or Eq [C.35], and governs for values of $b_0 \leq 0.5$ (with $t_0 = 1$) However, this situation occurs for very short spans, i.e. when the load is applied almost directly above the columns. A similar situation may arise in the tension chord joints of HSS triangular trusses when the web members are connected much off-centered on the chord faces, and hence one side of the web member is almost directly over a side wall of the chord.

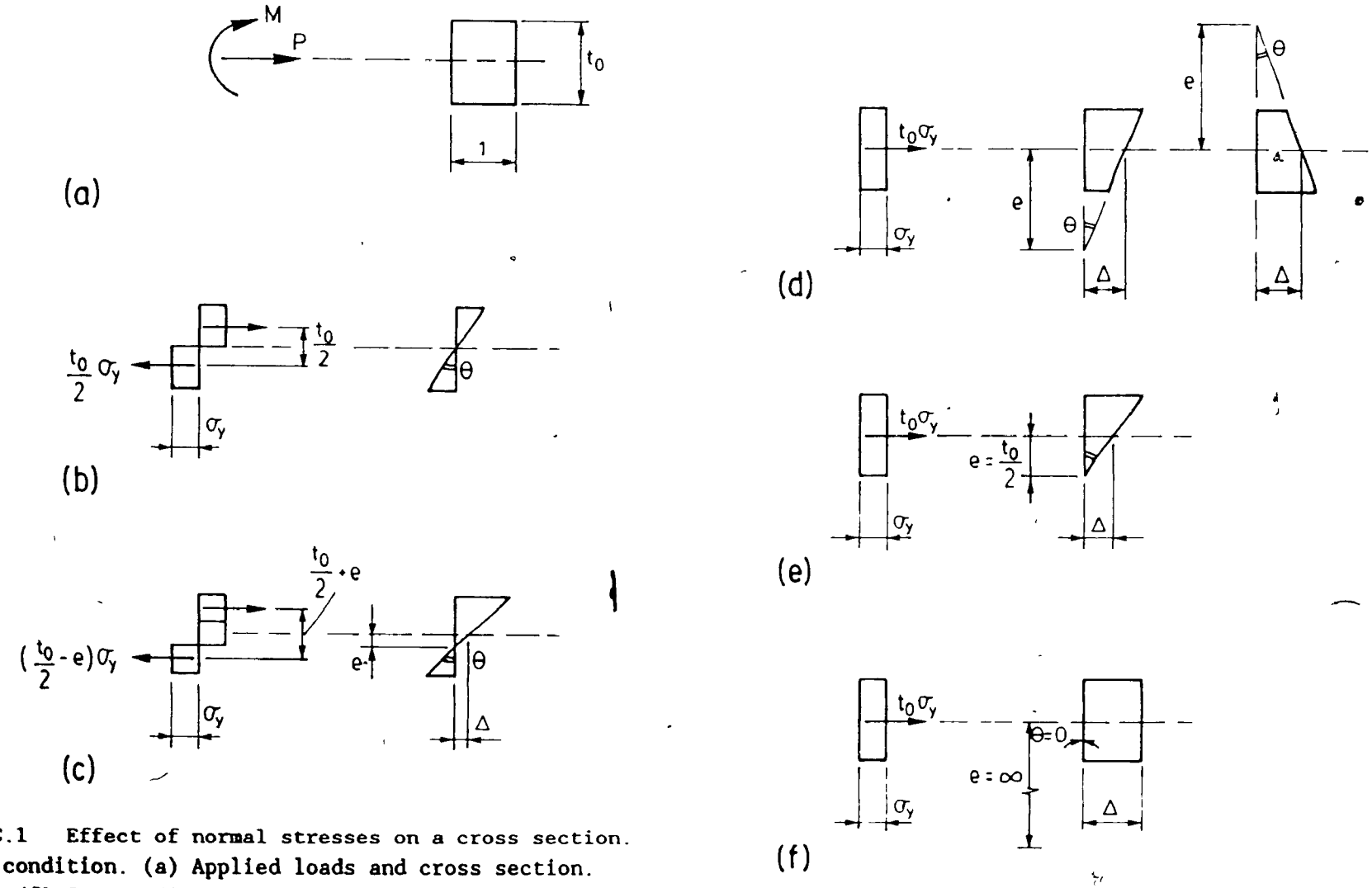

Fig. C.1 Effect of normal stresses on a cross section. Yield condition. (a) Applied loads and cross section. (b) to (f) Stress distribution and displacements: (b) Ordinary plastic hinge. (c) Complex plastic hinge. (d) Squashed cross section. (e) Limit case between (c) and (d) (f) Purely squashed cross-section.

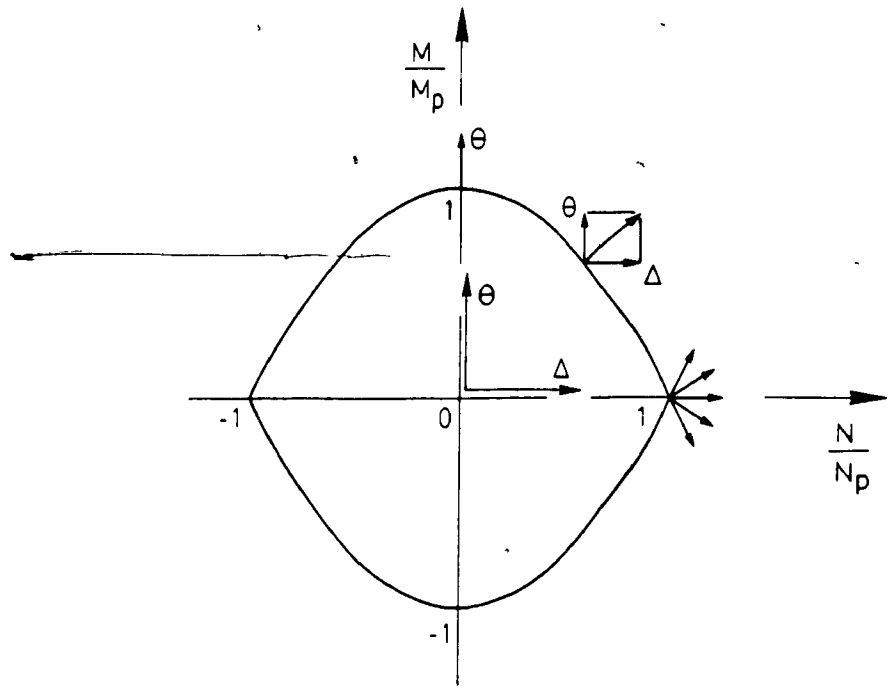

Fig. C.2 Yield surface, interaction equation and normality condition Combined bending and normal forces.

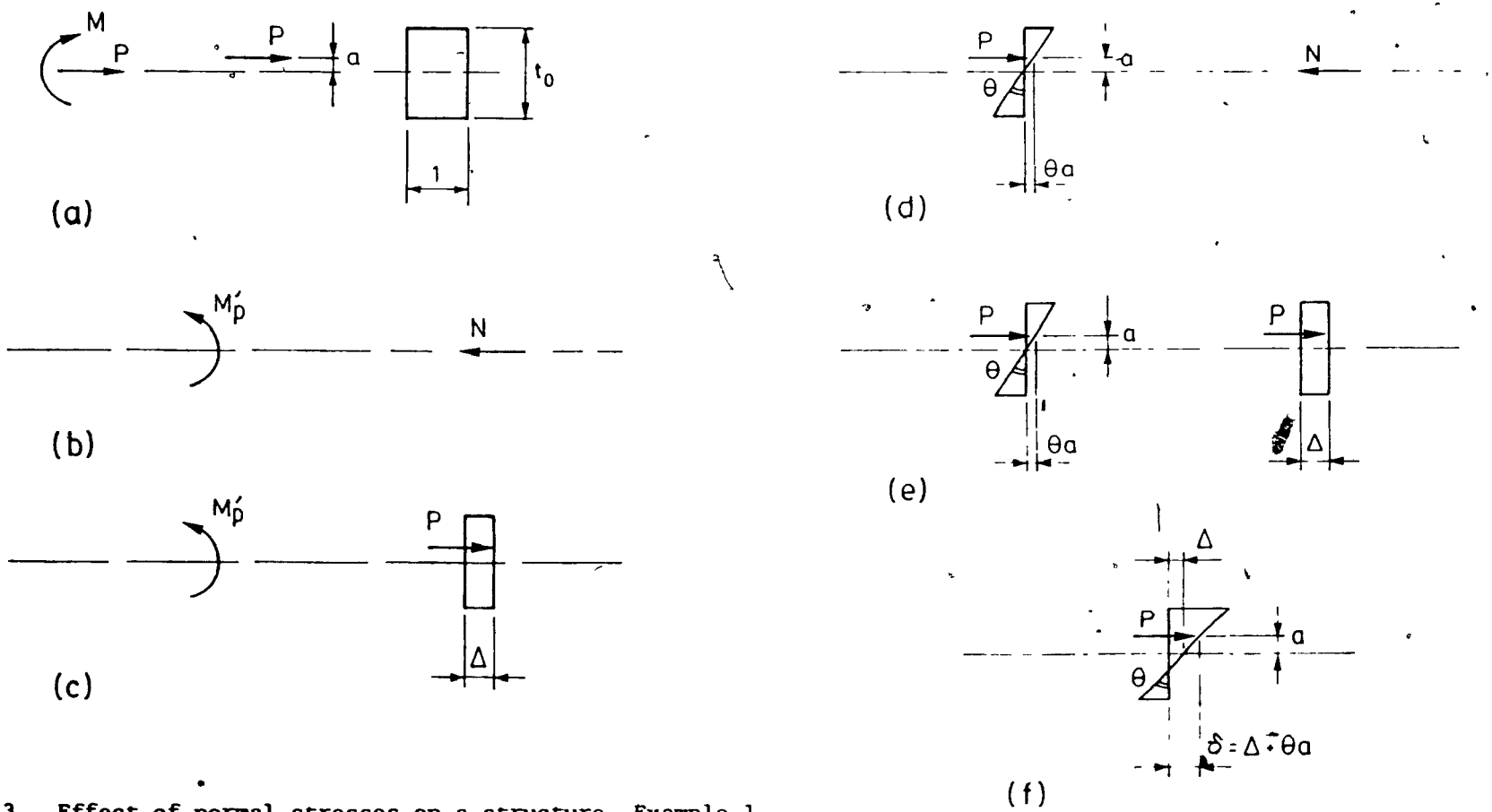

Fig. C.3 Effect of normal stresses on a structure. Example 1
(a) Applied loads and cross section.
(b) Method 1. Internal bending moment and internal normal force
(c) Method 2. Internal bending moment and normal mechanism.
(d) Method 3. Bending mechanism and internal normal force.
(e) Method 4-1. Bending mechanism and normal mechanism.
(f) Method 4-2. Mechanism with combined bending and normal deformations

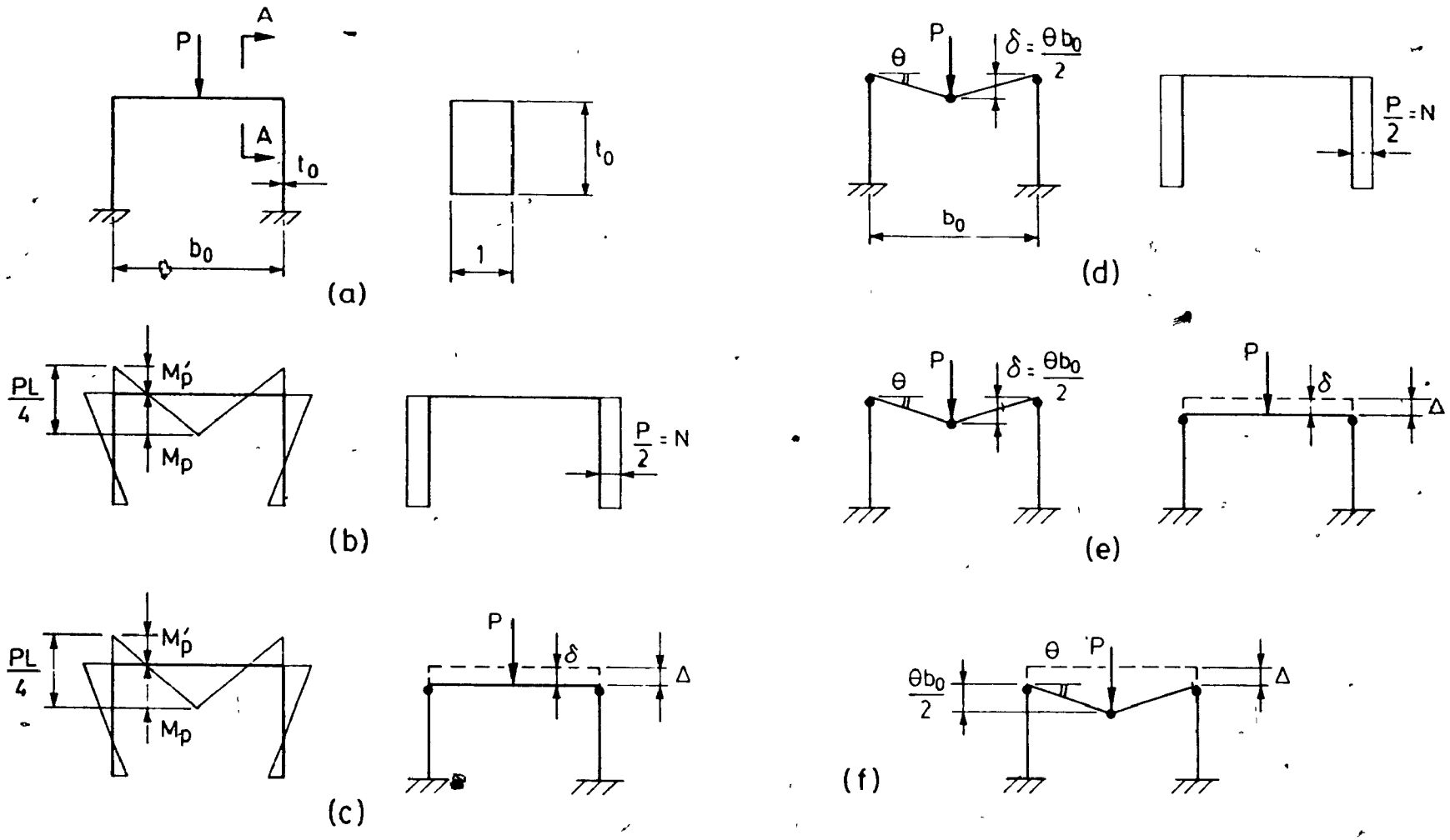

Fig. C.4 Effect of normal stresses on a structure. Example 2.

(a) Structure and cross section.
(b) Method 1. Bending moments and normal forces.
(c) Method 2. Bending moments and normal mechanism.
(d) Method 3. Bending mechanism and normal forces.
(e) Method 4-1. Bending mechanism and normal mechanism.
(f) Method 4-2. Mechanism with both bending and normal deformations.

Table C.1 Solution methods of plastic analysis for combined bending and normal force effects.

Solution Method	Bending Moments	Normal Forces
1	Static	Static
2	Static	Kinematic
3	Kinematic	Static
4 1, 4 2	Kinematic	Kinematic

Table C.2 Effect of normal stresses. Example 2.

b_0	P/m_p Eq [C.23] bending only	P/m_p Eqs [C.26] or [C 35] bending and normal forces	% reduction $\frac{\text{Col.(2)-Col.(3)}}{\text{Col.(2)}} \times 100$
(1)	(2)	(3)	(4)
10	0.8	0.796	0.5
5	1.6	1.569	1 9
2	4	3.596	10 1

Notes: $t_0 = 1$, $m_p = 1$

REFERENCES

Bauer, D. (1981)
"Tests of HSS Triangular Truss Segments", McGill University, Structural Engineering Series, Report 81-1, Master of Engineering Thesis. January 1981. 266 pp.

Bauer, D. (1982)
"Shear Strength of Tension Chords in HSS Triangular Trusses", Structural Engineering Series Report No. 82-6, McGill University. November 1982. 34 pp.

Bauer, D., Glebe, M., Redwood, R.G., and Harris, P.J. (1983)
"Tests of HSS Triangular Truss Segments", Proc. Struct. Division, CSCE Annual Conference, Ottawa, June 1983, pp.203-220.

Bauer, D., and Redwood, R.G. (1984)
"Tests of HSS Double T-Joints", Report No. 5W/2-84/3-E, CIDECT, Structural Engineering Series Report No.84-2. McGill University. August 1984. 51 pp.

Bauer, D., and Redwood, R.G. (1985)
"Welded Joints for HSS Triangular Trusses". International Symposium on Structural Steel Design and Construction. Singapore. July 1985. pp.59-82.

Bauer, D., and Redwood, R.G. (1985)
"Joints for Triangular Trusses using Rectangular Tubes". ASCE Structural Engineering Congress. Chicago. September 1985. pp.13-1 to 13-12.

Bauer, D., and Redwood, R.G.
"Triangular Truss Joints using Rectangular Tubes". ASCE Journal. Submitted for publication.

Bauer, D. (1986)
"Yield Lines, a Numerical Yield Lines Analysis Program - User's Manual", Structural Engineering Series Report No.86-3. McGill University. November 1986. 89 pp.

Bauer, D., and Redwood, R.G.
"Numerical Yield Line Analysis". Computers and Structures. Pergamon Press. To be published.

CIDECT
"The Strength and Behaviour of Statically Loaded Welded Connections in Structural Hollow Sections". Monograph 6. CIDECT, Paris, France. To be published.

Conte, S.D., and de Boor, C. (1980)
"Elementary Numerical Analysis". 3rd Ed. McGraw-Hill. New-York. 1980. pp.432.

Cran, J.A. (1982)
"HSS Warren and Pratt Truss Connections - Weld Gap and Overlap Joints", presented to the Montreal Structural Engineers, February 1982, 27pp.

CSA (1984)
"Steel Structures for Buildings - Limit State Design", CAN3-S16.1-M84, Canadian Standards Association, Rexdale, Ontario.

Davies, G., Packer, J.A., and Coutie, M.g. (1984)
"The Behaviour of Full Width RHS Cross Joints". Proc. of the 2nd Int'l Conf. on Welding of Tubular Structures. Boston. July 1984.

Davies, G., and Roper, C.G. (1975)
"Gap Joints with Tubular Members - a Yield Line Approach", Building Science, Vol. 10, Oct. 1975.

de Ville de Goyet, V., Frey, F., and Massonet, Ch. (1981)
"Ultimate Load of Trusses Buckling in Their Plane", Proc. IABSE, P47/81. November 1981. pp.141-164.

Eastwood, W., and Wood, A.A. (1970)
"Welded Joints in Tubular Structures Involving Rectangular Sections", Conf. on Joints in Structures, University of Sheffield, U.K., Sept. 1970.

Eastwood, W., and Wood, A.A. (1970)
"Recent Research on Joints in Tubular Structures", Proceedings, 2nd Canadian Structural Engineering Conference, CISC, Toronto, 1970.

Glebe, M. (1980)
"Behaviour and Strength of Chord Joints of Triangular Trusses Made of Hollow Structural Sections", Master of Engineering Thesis, Structural Engineering Series Report 80-2. McGill University. September 1980. 121 pp.

Heyman, J. (1971)
"Plastic Design of Frames. Volume 2 - Applications". Cambridge University Press. 292 pp.

Horne, M.R. (1979)
"Plastic Theory of Structures", 2nd ed., (SI Units). Pergamon Press. England. 179 pp.

Johansen, K.W. (1943)
Brudlinieteorier, Jul. Gjellerups Forlag, Copenhagen, 1943, 191 pp. ("Yield Line Theory", translated by Cement and Concrete Association, London, 1962, 181 pp.)

Johnston, B.G., Ed. (1976)
"Guide to Stability Design Criteria for Metal Structures", 3rd ed., Wiley, 1976, 616 pp.

Jones, L.L., and Wood, R.H. (1967)
"Yield-Line Analysis of Slabs". American Elsevier. New-York. 405 pp.

. Jubb, J.E.M., and Redwood, R.G. (1966)
"Design of Joints to Box Sections", Proc. Conf. on Industrialized Building and the Structural Engineer, Inst. Struct. Eng., 1966, pp.51-58.

. Kato, B., and Nishiyama, I. (1979)
"The Static Strength of R.R.-Joints with Large b/B Ratio", Dept. of Architecture, Faculty of Engineering, University of Tokyo, Japan, August 1979.

. Kawczak, M. (1983)
"Investigation of Triangular Trusses Made of Hollow Structural Sections". Master of Engineering Project Report. McGill University. March 1983, 96 pp.

. Kennedy, D.J.L., and Gad Aly, M.G. (1980)
"Limit States Design of Steel Structures - Performance Factor". Canadian Journal of Civil Engineering, Volume 7, no.1, March 1980, pp. 45-77.

. Mills, G.M. (1970)
"The Yield-Line Theory: a Programmed Text". Concrete Publications Ltd., Cement and Concrete Association, London, 1970, 96 pp.

. Minicucci, F., and Zafrani, D. (1986)
"Computer Design Aid for Joints Found in HSS Triangular Trusses" Undergraduate Project Report. Department of Civil Engineering. McGill University. December 1986. 120 pp.

. Morris, G.A., and Fenves, S.J. (1969)
"Approximate Yield Surface Equations". Journal of the Engineering Mechanics Division, Proc. ASCE, Vol.95, No.EM4, Aug. 1969.

. Mouty, J. (1977)
"Theoretical Prediction of Welded Joint Strength", Proc. Intl. Symposium on Hollow Structural Sections, CIDECT, Toronto, May 1977, 41 pp.

. Neal, B.G. (1977)
"The Plastic Methods of Structural Analysis". First published 1956. 3rd ed. (SI). Sciences Paperbacks. Chapman and Hall, London. 1977. 205 pp.

. Packer, J.A., and Haleem, A.S. (1981)
"Ultimate Strength Formulae for Statically Loaded Welded HSS Joints in Lattice Girders with RHS Chords", Proc. 1981 CSCE Conference, Fredericton, N.B., May 1981, pp.331-343.

. Packer, J.A., and Birkemoe, P.C. (1982)
"Gap and Lap Joints". Proceedings of the Canadian Symposium on Hollow Structural Sections, Steel Company of Canada, April-May 1982..

. Packer, J.A. (1983)
"Developments in the Design of Welded HSS Truss Joints with RHS Chords". Canadian Journal of Civil Engineering, March 1983.

. Park, R., and Gamble, W.L. (1980)
"Reinforced Concrete Slabs". Wiley Interscience. U.S.A. 618 pp.

Redwood, R.G., and Harris, P.J. (1981)
"Welded Joints for Triangular Trusses", Report on CIDECT Project 5W/1, McGill University, Structural Engineering Series, Report 81-2, January 1981. 59 pp.

Redwood, R.G., and Bauer, D. (1983)
"Behaviour of HSS Triangular Trusses and Design Considerations", Proc. Canadian Sym. on HSS, April-May, 1983, CIDECT, 40 pp.

Santagata, P. (1982)
Undergrad ate Technical Paper, McGill University, Department of Civil Engineering and Applied Mechanics, Sept. 1982, 52 pp.

Skold, T. (1986)
"Graphical Design Aid for Tension Chord Joints in Triangular Trusses". IAESTE Summer Project Report. Department of Civil Engineering. McGill University. 46 pp.

Stelco (1971)
(edited by Cran, J.A., Gibson, E.B., Stadnyckyj, S.)
"Hollow Structural Sections - Design Manual for Connections" Stelco Inc., Hamilton, Ontario. 73 pp.

Stelco (1981)
(edited by Cran, J.A., and Keen, R.G.)
"Hollow Structural Sections - Design Manual for Connections", 2nd edition, Stelco Inc., Hamilton, Ontario, September 1981. 144 pp.

Szlendak, J., and Brodka, J. (1985)
"Yield and Buckling Strength of T, Y and X Joints in Rectangular Section Trusses". Proc. Instn Civ. Engrs, Part 2, 1985, 79, Mar., pp.167-180.

Wardenier, J. (1977)
"Testing and Analysis of Truss Joints Made from Rectangular HSS", International Symposium on Hollow Structural Sections. Proceedings, Toronto, May 1977.

Wardenier, J., and Davies, G. (1981)
"Design Recommendations for Hollow Section Joints - Predominantly Statically Loaded", Int. Inst. of Welding, Commission XV, Oporto, 1981, IIW Doc. XV-491-81.

Wardenier, J., and Davies, G. (1981)
"The Strength of Predominantly Statically Loaded Joints with a Square or Rectangular Hollow Section Chord". Int. Inst. Welding, Annual Assembly 1981, Oporto, IIW Doc. VX-492-81.

Wardenier, J. (1982)
"Hollow Section Joints", Delft University Press, 1982, 544 pp.

Wood, R.H., and Jones, L.L. (1967)
"Yield Line Analysis of Slabs", Thames and Hudson, Chatto & Windus, London, 1967, 400 pp.